Hydrogeology and Groundwater Quality in the San Agustin Basin, New Mexico, 1975–2019

Scientific Investigations Report 2022–5029

U.S. Department of the Interior
U.S. Geological Survey

Cover. U.S. Geological Survey scientist Hal Nelson wades in a stock tank to install a fitting on the discharge pipe of a groundwater well to facilitate water quality sampling in the western San Agustin Basin, New Mexico. Photograph by Jeff Pepin, U.S. Geological Survey, April 4, 2019.

Hydrogeology and Groundwater Quality in the San Agustin Basin, New Mexico, 1975–2019

By Jeff D. Pepin, Rebecca E. Travis, Johanna M. Blake, Alex Rinehart, and Daniel Koning

Scientific Investigations Report 2022–5029

U.S. Department of the Interior
U.S. Geological Survey

U.S. Geological Survey, Reston, Virginia: 2022

Acknowledgments

Contents

Figures

Tables

Conversion Factors

U.S. customary units to International System of Units

Multiply	By	To obtain
Length		
inch (in.)	2.54	centimeter (cm)
inch (in.)	25.4	millimeter (mm)
foot (ft)	0.3048	meter (m)
mile (mi)	1.609	kilometer (km)
Area		
acre	4,047	square meter (m^2)
acre	0.004047	square kilometer (km^2)
square foot (ft^2)	0.09290	square meter (m^2)
square mile (mi^2)	2.590	square kilometer (km^2)
Volume		
gallon (gal)	3.785	liter (L)
gallon (gal)	0.003785	cubic meter (m^3)
acre-foot (acre-ft)	1,233	cubic meter (m^3)
Flow rate		
gallon per minute (gal/min)	0.06309	liter per second (L/s)
Radioactivity		
picocurie per liter (pCi/L)	0.037	becquerel per liter (Bq/L)
Specific capacity		
gallon per minute per foot ([gal/min]/ft)	0.2070	liter per second per meter ([L/s]/m)
Hydraulic gradient		
foot per mile (ft/mi)	0.1894	meter per kilometer (m/km)
Transmissivity		
foot squared per day (ft^2/d)	0.09290	meter squared per day (m^2/d)

International System of Units to U.S. customary units

Multiply	By	To obtain
Length		
meter (m)	3.281	foot (ft)
meter (m)	1.094	yard (yd)
Volume		
liter (L)	33.81402	ounce, fluid (fl. oz)
liter (L)	2.113	pint (pt)
liter (L)	1.057	quart (qt)
liter (L)	0.2642	gallon (gal)
liter (L)	61.02	cubic inch (in^3)
Mass		
gram (g)	0.03527	ounce, avoirdupois (oz)

Temperature in degrees Celsius (°C) may be converted to degrees Fahrenheit (°F) as follows:

°F = (1.8 × °C) + 32.

Temperature in degrees Fahrenheit (°F) may be converted to degrees Celsius (°C) as follows:

°C = (°F − 32)/1.8.

Datum

Vertical coordinate information is referenced to the North American Vertical Datum of 1988 (NAVD 88).

Horizontal coordinate information is referenced to the North American Datum of 1983 (NAD 83).

Elevation, as used in this report, refers to distance above the vertical datum.

Supplemental Information

Specific conductance is given in microsiemens per centimeter at 25 degrees Celsius (µS/cm at 25 °C).

Concentrations of chemical constituents in water are given in either milligrams per liter (mg/L) or micrograms per liter (µg/L). Activities for radioactive constituents in water are given in picocuries per liter (pCi/L).

Tritium (^{3}H) concentrations are given in units of picocuries per liter (pCi/L).

The conversion of picocuries per liter (pCi/L) to tritium units (TU), based on a tritium half-life of 12.32 years (Lucas and Unterweger, 2000), is 1 TU = 3.22 pCi/L.

Median annual gradient (groundwater elevation change over time) is given in feet per year (ft/yr).

Abbreviations

δ^2H	delta hydrogen-2/hydrogen-1
$\delta^{18}O$	delta oxygen-18/oxygen-16
ARPD	absolute relative percent difference
EPA	U.S. Environmental Protection Agency
GMWL	global meteoric water line
ICP-MS	inductively coupled plasma-mass spectrometry
ICP-OES	inductively coupled plasma optical emission spectrophotometry
IQR	interquartile range
LMWL	local meteoric water line
LOOCV	leave-one-out cross validation
MCL	maximum contaminant level
NA	not available
NAVD 88	North American Vertical Datum of 1988
NC	not computed
NMBGMR	New Mexico Bureau of Geology and Mineral Resources
NWIS	National Water Information System
p-value	probability value
PC	principal component
PCA	principal component analysis
pmC	percent modern carbon
RMSE	root-mean-square error
SMCL	secondary maximum contaminant level
TDS	total dissolved solids
USGS	U.S. Geological Survey

Hydrogeology and Groundwater Quality in the San Agustin Basin, New Mexico, 1975–2019

By Jeff D. Pepin,[1] Rebecca E. Travis,[1] Johanna M. Blake,[1] Alex Rinehart,[2,3] and Daniel Koning[3]

Abstract

This report describes the findings of a U.S. Geological Survey study, completed in cooperation with the Bureau of Land Management, focused on better understanding the present-day (1975–2019) hydrogeology and groundwater quality of the San Agustin Basin in west-central New Mexico to support sustainable groundwater resource management. The basin hosts a relatively undeveloped basin-fill and alluvium aquifer system and is topographically divided into east and west subbasins by the McClure Hills. Groundwater chemistry and groundwater elevation data were compiled, collected, and interpreted in the context of groundwater flow and quality. The analyses presented in this report consider groundwater chemistry data collected within the last decade (2010–19) and groundwater elevation data collected from 1975 through 2019 to provide insight into present-day conditions. Groundwater elevations show that groundwater typically moves from the highlands to the lowlands, with a prominent east to west regional trend. Groundwater elevations were lowest in the southwestern portion of the west subbasin, where estimated flow directions suggest underflow through the local highlands into the northern East Fork Gila River watershed, which is further supported by historical groundwater elevation data from the northern East Fork Gila River watershed. Gradual groundwater elevation gradients (about 2 feet per mile) near the east and west subbasin divide suggest that groundwater slowly flows from the east subbasin to the west subbasin.

Quantitative analyses of groundwater chemistry data show that groundwater in both subbasins has similar chemical characteristics. A systematic east to west groundwater evolution in water chemistry was not observed despite evidenced subbasin connectivity. The absence of this pattern suggests that groundwater mixing is regionally prevalent, sediment reactivity is low and variable, and (or) recharge conditions are comparable in both subbasins. Groundwater chemistry was generally independent of aquifer type, suggesting that the aquifers are hydrologically well connected. Corrected carbon-14 groundwater age estimates in the basin ranged from 232 to 13,916 years before present with a median of 5,409 years. A wide range of groundwater ages is therefore present in the basin, with waters commonly being thousands of years old, thereby supporting generally slow regional groundwater movement. A component of relatively young groundwater, for which estimated ages could not be accurately computed, is also present in the basin, and it may commonly mix with older waters. The spatial distribution of categorical and quantitative groundwater ages indicates that most recharge likely occurs in the highlands through mountain-block recharge and as focused recharge within arroyos, although evidence of modern (1953 and after) groundwater was minimal at sampled sites.

Median annual gradients (groundwater elevation change over time) indicate that most groundwater elevations in the lowlands changed little (−0.2 to 0.2 foot per year) from 1975 through 2019. Groundwater elevations in the highlands varied more annually, which is likely due to recharge from precipitation events. These more variable groundwater elevations in the highlands compared with the lowlands, along with groundwater ages, provide further evidence that most groundwater recharge takes place in the highlands, with minimal recharge in the lowlands. Median groundwater elevation change for all sites was −0.05 foot per year. Temporal consistency of lowland groundwater elevations suggests that regional groundwater dynamics have been more or less stable through time under current climate and development conditions, although median annual gradients indicate that groundwater elevations may have slightly declined on average between 1975 and 2019.

Introduction

The San Agustin Basin is composed of intermontane sediment filled subbasins in west-central New Mexico and hosts a relatively undeveloped basin-fill and alluvium aquifer system (fig. 1). This rural region is mainly utilized for ranching and recreation, with some irrigated agriculture (Homer and others, 2020). Interest in developing local groundwater resources has increased in recent years. This interest

---

[1]U.S. Geological Survey

[2]Earth and Environmental Science Department, New Mexico Institute of Mining and Technology, Socorro, New Mexico

[3]New Mexico Bureau of Geology and Mineral Resources, New Mexico Institute of Mining and Technology, Socorro, New Mexico

has been met with concern about potential adverse impacts of substantial development and with protest by local, State, Tribal, and Federal entities (Turner, 2019).

The U.S. Geological Survey (USGS) in cooperation with the Bureau of Land Management performed this study to improve the understanding of present-day (1975–2019) hydrogeology and groundwater quality of the basin to support sustainable groundwater resource management. This work included the compilation and collection of groundwater chemistry (major ions, trace elements, stable isotopes, and groundwater age tracers) and groundwater elevation data along with the interpretation of these data in the context of groundwater flow and quality. Groundwater elevation analyses included construction of a groundwater elevation map and assessment of the time dependence of groundwater elevations to estimate the dynamics of groundwater flow. The general character and spatial variation of groundwater chemistry were also evaluated to further understand the quality and movement of basin groundwater.

Purpose and Scope

The purpose of this report is to present interpretative results associated with groundwater elevation and groundwater chemistry analyses for the basin. This report serves to enhance the understanding of the region's groundwater resources and allow interested parties to better evaluate the potential impacts of future groundwater development scenarios. The study area and subbasin boundaries considered in this report were delineated on the basis of surface water hydrologic units derived by the USGS (1999) because groundwater boundaries were not well known. The analyses included in this report considered groundwater chemistry data collected within the last decade (2010–19) and groundwater elevation data collected from 1975 through 2019; the longer time span for groundwater elevation data was used in order to address prevalent data gaps in data collected over the last decade. Data collection efforts were subject to land access, groundwater well availability, and funding and do not comprehensively address all data gaps. Only data collected and compiled by the USGS and the New Mexico Bureau of Geology and Mineral Resources (NMBGMR) were considered in the analyses in order to utilize data that were collected while following similar procedures. Overall, this report aims to provide a broad overview of present-day (1975–2019) hydrogeology and groundwater quality for the basin to support sustainable groundwater resource management.

Description of Study Area

Physiography and Geologic History

San Agustin Basin covers approximately 1,990 square miles (mi^2) within the northern portion of the Mogollon-Datil volcanic field in west-central New Mexico (fig. 1). The Mogollon-Datil volcanic field is a transitional zone between the Colorado Plateau in northwest New Mexico and the Basin and Range Province in southwest New Mexico (Basabilvazo, 1997). This volcanic province contains abundant mid-Tertiary (43–21 million years ago) volcanic rocks and features such as dikes, vents, and pyroclastic flows (Myers and others, 1994; Chapin and others, 2004).

The basin is a graben that formed because of Neogene extension along the Rio Grande rift that traverses central New Mexico (Phillips and others, 1992; Myers and others, 1994) (fig. 1). The south and west extents of the basin are bound by the Continental Divide in the Luera and Tularosa Mountains. The northern basin boundary is formed by the Mangas, Datil, and Gallinas Mountains, whereas the Gallinas and San Mateo Mountains constrain the basin in the east. The basin is split into the east and west San Agustin subbasins by the McClure Hills (Rinehart and others, 2017). The west San Agustin subbasin (west subbasin) is the larger of the two subbasins, spanning 1,180 mi^2 or 59 percent of the basin. The east San Agustin subbasin (east subbasin) covers an area of 810 mi^2 or 41 percent of the basin. Faults further break the east subbasin into the C-N, White Lake, and North grabens (Rinehart and others, 2017). Elevation ranges from 6,892 to 9,538 feet (ft) in the east subbasin and is between 6,772 and 10,228 ft in the west subbasin, thereby yielding 3,456 ft of topographic relief across the basin.

Climate and Vegetation

Local climate is semiarid with temperatures, precipitation, and vegetation being largely dependent on elevation (Phillips and others, 1992; Myers and others, 1994). Temperature and precipitation weather station data collected in the lowlands of the east subbasin spanning from April 19, 1926, through December 31, 2019, are presented in figure 2. Lowland daily mean temperatures typically vary between 0 and 80 degrees Fahrenheit and have increased on average since the late 1970s, which is consistent with global temperature trends (Intergovernmental Panel on Climate Change, 2014). The majority of precipitation is often in the form of summer monsoonal rain and annually averages a total amount between about 10 inches (in.) in the lowlands and 30 in. in the surrounding highlands, whereas a smaller proportion of the precipitation occurs as winter snowfall (Phillips and others, 1992; Myers and others, 1994; Rinehart and others, 2017). Daily lowland precipitation historically varies between 0 and 2.5 in., with notable periods of relative dryness in the 1930s and between about 1945 and 1975 and a relatively wet period in the 1990s (fig. 2). Vegetation consists of grasses in the lowlands, pinyon pine (*Pinus* spp.) and juniper (*Juniperus* spp.) forests in the foothills, and Douglas fir (*Pseudotsuga menziesii*) forests at higher elevations (Potter, 1957; Phillips and others, 1992; Homer and others, 2020).
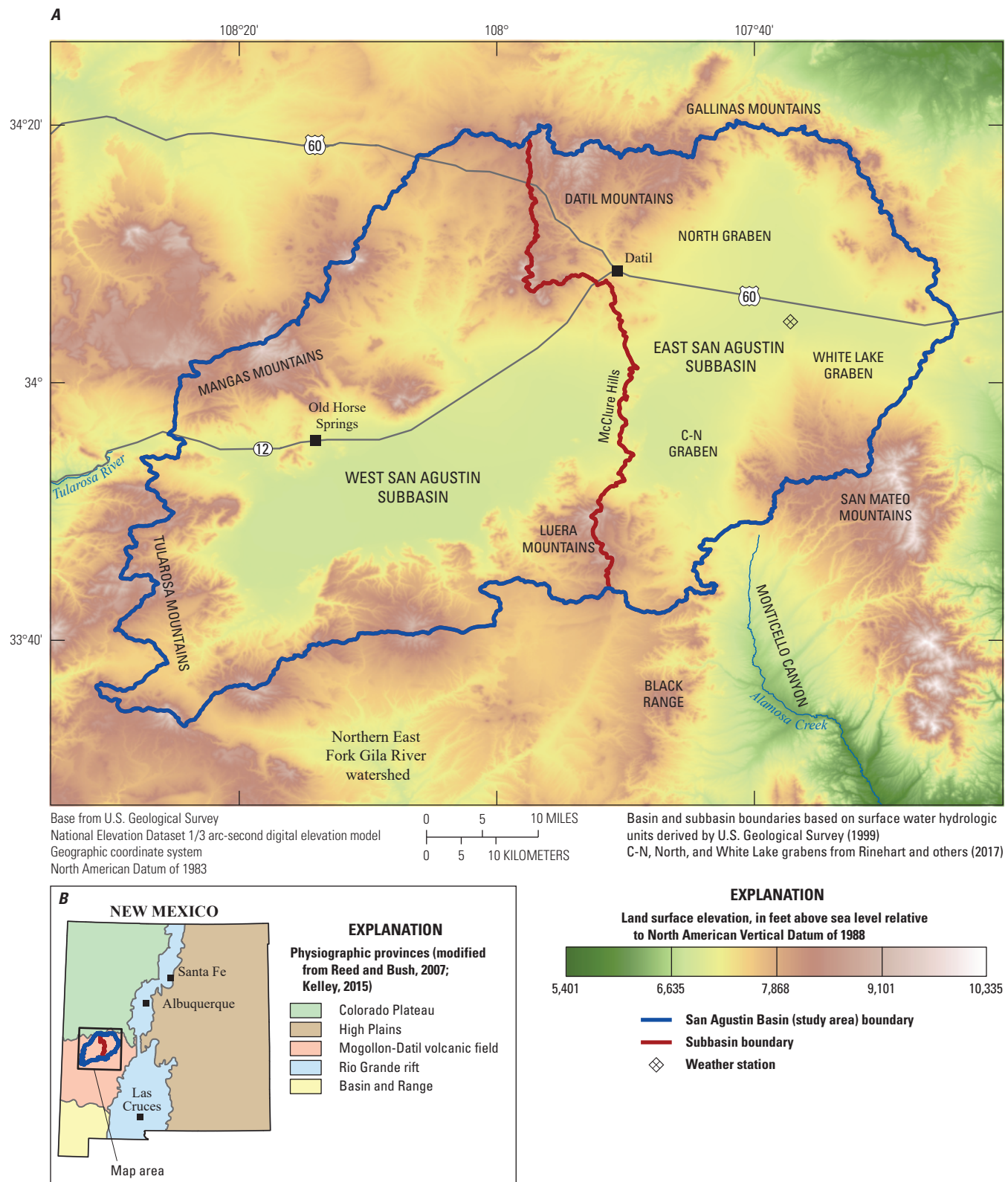
Figure 1. *A*, Study area location in the San Agustin Basin, west-central New Mexico, with land surface elevation and local key landmarks indicated and *B*, physiographic provinces of New Mexico.
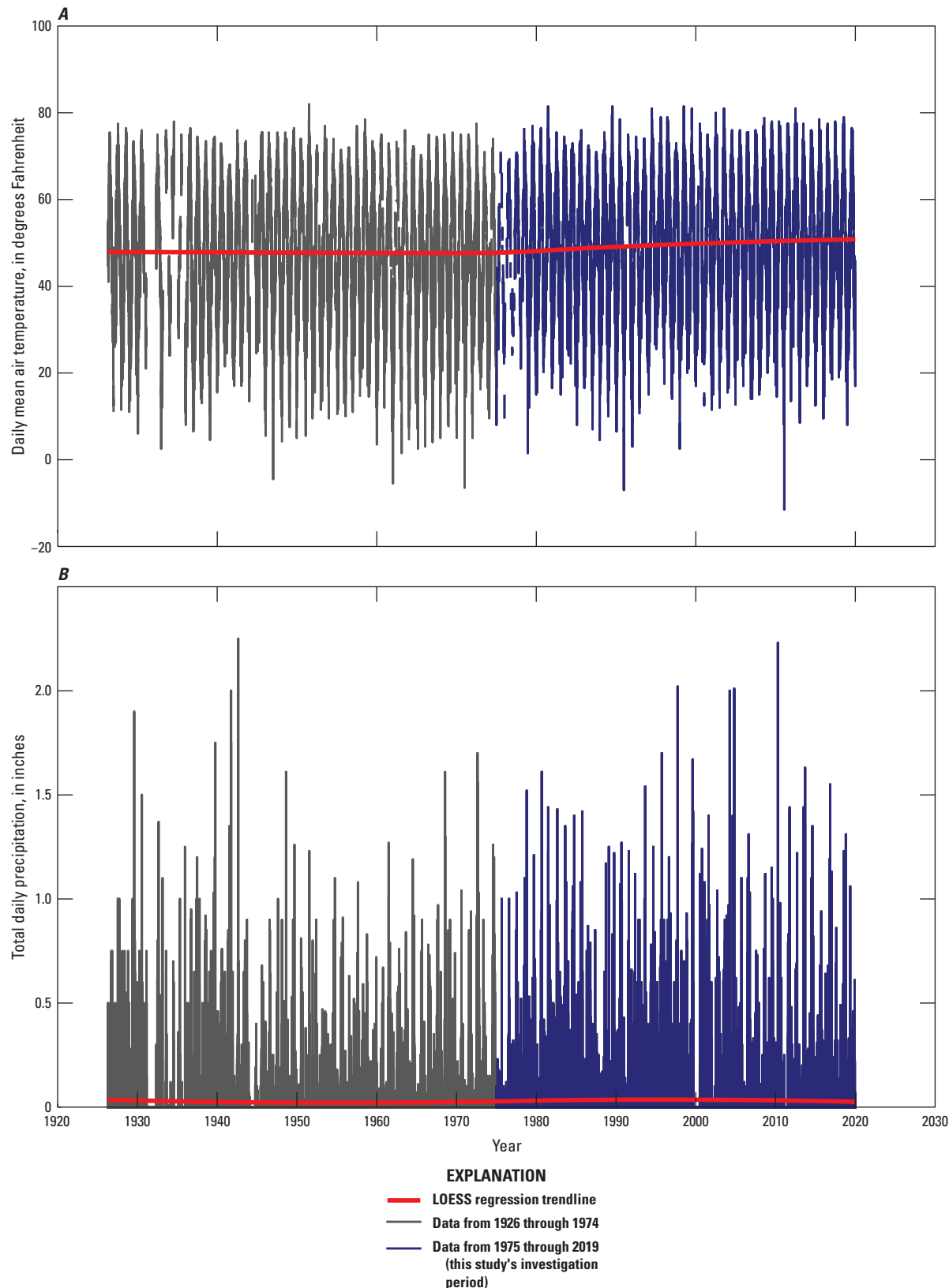
Figure 2.   *A*, Daily mean air temperature and *B*, total daily precipitation from April 19, 1926, through December 31, 2019, at the Augustine 2E weather station in the east subbasin of the San Agustin Basin, west-central New Mexico (New Mexico Climate Center, 2020). Weather station location is shown in figure 1. LOESS, locally estimated scatterplot smoothing.

Surface Water

Surface water features are scarce in the basin because of the rapid evaporation or percolation of runoff and snowmelt, though ephemeral and perennial springs are present in some areas and are prevalent in the Mangas Mountains (Myers and others, 1994). The most prominent nearby surface water features are Alamosa Creek in Monticello Canyon to the southeast, the Tularosa River near the Mangas and Tularosa Mountains to the northwest, and the Gila River with its east fork headwaters to the south of the basin in the northern East Fork Gila River watershed (fig. 1). Alamosa Creek drains towards the Rio Grande in central New Mexico, whereas the Tularosa River and Gila River flow through western New Mexico towards the Colorado River in Arizona; the Tularosa River joins the San Francisco River in western New Mexico before merging with the Gila River in eastern Arizona. Quaternary lacustrine and playa deposits can be found in both the east and west subbasins and are the remnants of Pleistocene paleolakes (fig. 3) (Phillips and others, 1992; Myers and others, 1994). Some researchers believe that these paleolakes were once connected to form a lake that was 34 miles long, 11 miles wide, and 165 ft deep (Myers and others, 1994; Weber, 1994). There is no evidence of any notable local tectonic activity that is younger than the extinct lake, and minimal standing water exists in the basin today (Myers and others, 1994).

Groundwater

The Quaternary basin-fill and alluvial sediments are the principal groundwater aquifers in the basin and store large amounts of accessible groundwater in each of the subbasins (fig. 3). These piedmont, lacustrine, playa, eolian, and alluvial sediments are a mixture of unconsolidated clay, silt, sand, and gravel (Qa, Qpl, Qp, Qoa, Qts, and Qtg in fig. 3). Myers and others (1994) estimated that a total of 53.5 million acre-feet (acre-ft) of freshwater is stored in these sediments, with 34.4 million acre-ft in the east subbasin and 19.1 million acre-ft in the west subbasin. An additional 9 million acre-ft of saline water is thought to be stored in the alluvial fill of the western portion of the west subbasin, where lacustrine paleolake deposits are prevalent (Myers and others, 1994). The Quaternary sediments vary in thickness but are as thick as 4,600 ft in some areas (Myers and others, 1994).

The underlying Tertiary Datil Group, which includes the Spears Formation, is exposed in the highlands and stores lesser amounts of groundwater but is hydraulically conductive where fractured (fig. 3) (Rinehart and others, 2017). These volcanic units vary in composition and include silicic to intermediate volcanic rocks, basaltic to andesitic lava flows, felsic and mafic intrusives, ash-flow tuffs, and pyroclastic rocks.

Recharge to these aquifers is believed to take place primarily in the highlands through precipitation directly falling onto outcrops and permeable soils and runoff infiltration into permeable material in the foothills (Myers and others, 1994).

The playas in the lowlands (fig. 3) sometimes accumulate runoff, but this water is thought to evaporate rather than infiltrate because of the poor drainage of these sediments (Myers and others, 1994). Groundwater conditions in the aquifer system are generally unconfined, and the aquifers are thought to be hydrologically connected to one another (Basabilvazo, 1997).

The small amount of published aquifer property data is presented in tables 1 and 2, which were compiled from Myers and others (1994), Basabilvazo (1997), and New Mexico Office of the State Engineer (2020). These data show that basin-fill and alluvium transmissivity estimates range from 1,949 to 70,600 square feet per day with specific capacities ranging from 5.7 to 90 gallons per minute per foot. The few specific yield and storage coefficients for the basin-fill and alluvium aquifer system average about 15 percent and 0.15, respectively, with the east subbasin having a slightly elevated mean specific yield value (18.4 percent) compared to the west subbasin (13.3 percent). No specific yield, storage coefficient, or transmissivity data are known to be available for the local Datil Group. The interbedded Spears Formation has much smaller transmissivity and specific capacity estimates than the basin fill and alluvium, with values for two wells of 1.6 and 12.24 square feet per day and 0.016 and 0.046 gallons per minute per foot, respectively.

Depth to groundwater in the basin fill and alluvium typically ranges from about 3 to 320 ft below the ground surface (Basabilvazo, 1997). The most recently published groundwater elevation map of the area shows relatively steep hydraulic gradients in the foothills that lead to gently sloping lowland hydraulic gradients (Rinehart and others, 2017). The map depicts groundwater regionally flowing from east to west before discharging into the northern East Fork Gila River watershed, which is consistent with previous researchers (Blodgett and Titus, 1973; Myers and others, 1994; Rinehart and others, 2017). The east and west subbasins are thought to be hydrologically connected via lowlands in the McClure Hills (Rinehart and others, 2017). Groundwater elevation contours also suggest that the northernmost portion of the North graben of the east subbasin may be structurally compartmentalized and disconnected from the rest of the basin (Rinehart and others, 2017). Recent work by the NMB-GMR indicates that there is a negligible hydrologic connection between the basin and Monticello Canyon (Rinehart and others, 2017).

The NMBGMR recently collected water quality data throughout the east subbasin and the eastern portion of the west subbasin; water quality data have not been collected throughout much of the western portion of the west subbasin in the last 40 years (Rinehart and others, 2017; USGS, 2021). Generally, groundwater supplies are fresh with total dissolved solids (TDS) concentrations of less than 1,000 milligrams per liter (mg/L), except in portions of the west subbasin where brackish (1,000–10,000 mg/L) and saline (greater than 10,000 mg/L) water resides in and below playa deposits.

EXPLANATION

- Quaternary alluvium (Qa)
- Quaternary lacustrine and playa deposits (Qpl)
- Quaternary piedmont alluvial deposits (Qp, Qoa)
- Quaternary and Tertiary sedimentary units (QTs, QTg, Tus, Tfl, Tsf)
- Neogene silicic to intermediate volcanic rocks and basaltic to andesitic lava flows (Tmb, Tnr)
- Middle Tertiary volcaniclastic sedimentary units (Tvs)
- Tertiary rhyolites, dacites, andesites, basaltic andesites, pyroclastic rocks, ash-flow tuffs, and intrusive rocks (Tuau, Tual, Turf, Turp, Tlrp, Tla, Tuv, Tlv, Tv, Ti)
- Paleogene sedimentary units (Tps)
- Permian Abo Formation and undivided rocks (P, Pa)
- San Agustin Basin (study area) boundary
- Subbasin boundary
- Dike
- Fault
- ✳ Volcanic vent

Figure 3.   Surface geology of the San Agustin Basin, west-central New Mexico. Lithologic units have been simplified from the "Geologic Map of New Mexico" (New Mexico Bureau of Geology and Mineral Resources, 2003). The abbreviations listed in the explanation correspond to those included in the explanation of the State map; the reader is directed to that resource for detailed lithologic descriptions.

Table 1. Aquifer transmissivity and specific capacity data measured in the San Agustin Basin, west-central New Mexico.

[Data compiled from Myers and others (1994), Basabilvazo (1997), and New Mexico Office of the State Engineer (2020). -, data not available]

Well location identifier	Transmissivity, in square feet per day	Specific capacity, in gallons per minute per foot	Aquifer	Source
Well 7S.19W.23.431	1,949	-	Basin fill and alluvium	Basabilvazo, 1997
NE Plains irrigation wells	2,300–48,000	5.7–90	Basin fill and alluvium	Basabilvazo, 1997
MA no. 1 05S.09W.23. NWSWSW	70,600	-	Basin fill and alluvium	Basabilvazo, 1997; New Mexico Office of the State Engineer, 2020
1S.8W.2.241	20,900	16.95	Basin fill and alluvium	Myers and others, 1994
1N.8W.36.341	46,000	16.8	Basin fill and alluvium	Myers and others, 1994
1S.8W.2.424	48,400	90	Basin fill and alluvium	Myers and others, 1994
1N.8W.35.413	21,700	31.6	Basin fill and alluvium	Myers and others, 1994
1N.8W.35.413	22,700	-	Basin fill and alluvium	Myers and others, 1994
1N.8W.35.242	42,800	-	Basin fill and alluvium	Myers and others, 1994
3S.8W.1.310	2,300	5.7	Basin fill and alluvium	Myers and others, 1994
3S.8W.1.310	2,400	-	Basin fill and alluvium	Myers and others, 1994
Lower well 02S.11W.33.SES-ENWSE	1.6	0.016	Spears Formation	New Mexico Office of the State Engineer, 2020
Upper well 02S.11W.27. NESWSWNW	12.24	0.046	Spears Formation	New Mexico Office of the State Engineer, 2020

Table 2. Basin-fill and alluvium aquifer system specific yields and storage coefficients estimated in the San Agustin Basin, west-central New Mexico.

[Data compiled from Myers and others (1994)]

Subbasin	Zone of subbasin	Specific yield, in percent	Storage coefficient, in dimensionless units
East	Central	17.5	0.175
East	Borders	19.3	0.193
West	West central	12.4	0.124
West	West borders	13.6	0.136
West	East central	13.0	0.130
West	East borders	14.3	0.143

The basin is sparsely populated, with water primarily being used for irrigation, livestock, domestic, and recreational purposes (Rinehart and others, 2017; Magnuson and others, 2019). Groundwater from the basin-fill and alluvium aquifer system is the primary water source for existing water users in the basin (Rinehart and others, 2017). In 2015, the most recent year for which water-use data are published, 278 acre-ft of groundwater were withdrawn for irrigation of 110 acres in the basin, largely in the northern portion of the east subbasin (Magnuson and others, 2019). Irrigation wells in the east subbasin have produced at rates of about 975 gallons per minute (Myers and others, 1994;

Basabilvazo, 1997). Domestic and livestock wells in the area have produced at rates ranging from less than 1 to 20 gallons per minute (Basabilvazo, 1997).

Methods

The analyses presented in this report include evaluation of groundwater elevation and chemistry data to improve the understanding of present-day (1975–2019) groundwater flow patterns and quality. Chemistry analyses used data collected

within the last decade (2010–19), whereas data gaps in groundwater elevation data required using data collected from 1975 through 2019 for the groundwater elevation analyses. Limiting the considered timeframe favors better understanding of recent conditions that are likely most pertinent to future resource management. These analyses do not consider all available data, and their results therefore do not comprehensively represent the historical hydrology in the basin. Lowland temperature and precipitation variations through time in the east subbasin (fig. 2) indicate that the period considered was subject to elevated daily mean air temperatures and total daily precipitation relative to historical values, thus making findings from this study most relevant to present-day conditions.

All sites with data that were used in the groundwater elevation contouring and for the chemistry analyses are presented in figure 4 and listed in table 3. Groundwater elevation data were used to create a groundwater elevation map to estimate groundwater flow patterns in the basin-fill and alluvium aquifer system. The annual variability of groundwater elevation data was also evaluated to gain a sense of the time dependence of groundwater flow patterns. Groundwater chemistry characteristics were investigated by using various plots, principal component analysis (PCA), and Wilcoxon tests to provide further insight into groundwater flow patterns and water quality variability. Emphasis was placed on comparing east and west subbasin groundwater chemistry to better understand geochemical differences between the subbasins. Most analyses were performed by using the R programming language, version 3.5.3 (R Core Team, 2019).

Sources and Descriptions of Data

Groundwater Elevation

Depth to water measurements were collected by the USGS at five wells in March and April 2019. These data were acquired by using steel tapes while following standard USGS protocols for discrete water level measurements (Cunningham and Schalk, 2011). Measured values were combined with historical depth to groundwater data from the USGS National Water Information System (NWIS; USGS, 2021). These data were converted to estimated groundwater elevation by using the digital elevation model of the USGS NWIS (app. 1; USGS, 2021); appendix 1 contains the compiled data. Measurements taken coincidentally with pumping at or near the site were omitted from all analyses (see "Water-level status code description" column of table 1.1 in app. 1). Data with unknown measurement dates were also omitted from all analyses. Median groundwater elevations for 124 wells that are likely completed in the basin-fill and alluvium aquifer system were computed for the time period of 1975–2019 to facilitate groundwater elevation contouring; the earliest measurement considered was taken on November 15, 1975, whereas the latest value was measured on April 10, 2019. The median values that were used to construct the groundwater elevation map are provided in table 4.

Groundwater Chemistry

Groundwater chemistry samples were collected and analyzed by the USGS at 14 sites in 2019, all of which were from the western portion of the west subbasin (fig. 4 and table 3). These data were combined with recent (July 2010 through February 2019) chemistry results provided by the NMBGMR for 30 additional locations dispersed throughout the basin (fig. 4) (Rinehart and others, 2017). Data at the 44 locations were used for all interpretative chemistry analyses unless noted otherwise and are provided for reference in appendix 2. The earliest sample date considered was July 23, 2010, whereas the most recent sample was collected on April 10, 2019. Well depths were available for 27 of the 44 sites (61 percent) and ranged from 65 to 1,000 ft (median = 305 ft). NMBGMR samples were collected and analyzed according to methods in Timmons and others (2013), whereas USGS samples were collected in accordance with the procedures described in the USGS "National Field Manual for the Collection of Water-Quality Data" (USGS, variously dated)—the NMBGMR and USGS protocols are similar, thereby providing high confidence in data quality from both agencies. All samples had an absolute ion mass balance within 10 percent. A compilation of historical USGS NWIS data dating back to December 20, 1933, is provided in appendix 3, although only recent (2010–19) chemistry data were interpreted in this report.

Major ion, trace element, alkalinity, stable isotope, tritium, and carbon-14 data were analyzed for sites sampled by the USGS. Existing windmills or submersible pumps were used to purge borehole water and obtain water quality samples. Carbon-14 was not analyzed for sites with windmills because of the possible introduction of air into the water during pumping. Additionally, trace element chemistry (except for iron and manganese) was not analyzed for windmill sites to avoid elevated, and difficult to quantify, data uncertainties associated with increased exposure of groundwater to the atmosphere and larger pressures imposed on groundwater during pumping. In adherence with USGS sampling protocols, sampling commenced after three borehole volumes were purged and monitored field parameter measurements stabilized; these parameters included dissolved oxygen, specific conductance, pH, and water temperature (USGS, variously dated). Parameter stability was solely used at about half of the sites, as borehole volumes could not be calculated because of incomplete well completion information such as well depth, flow rate, casing diameter at depth, or water level.

Upon reaching field parameter stability, groundwater samples were collected. Samples used for major ion, trace element, alkalinity, and carbon-14 analyses were filtered (0.45 micrometers) at the time of collection. Ultrapure nitric acid was added to samples collected for major ion and trace element analyses until their pH was less than 2 for preservation purposes. Alkalinity analysis was performed in the field by using the incremental equivalence method (USGS, variously dated). Unfiltered samples were collected for tritium and stable isotope analyses.
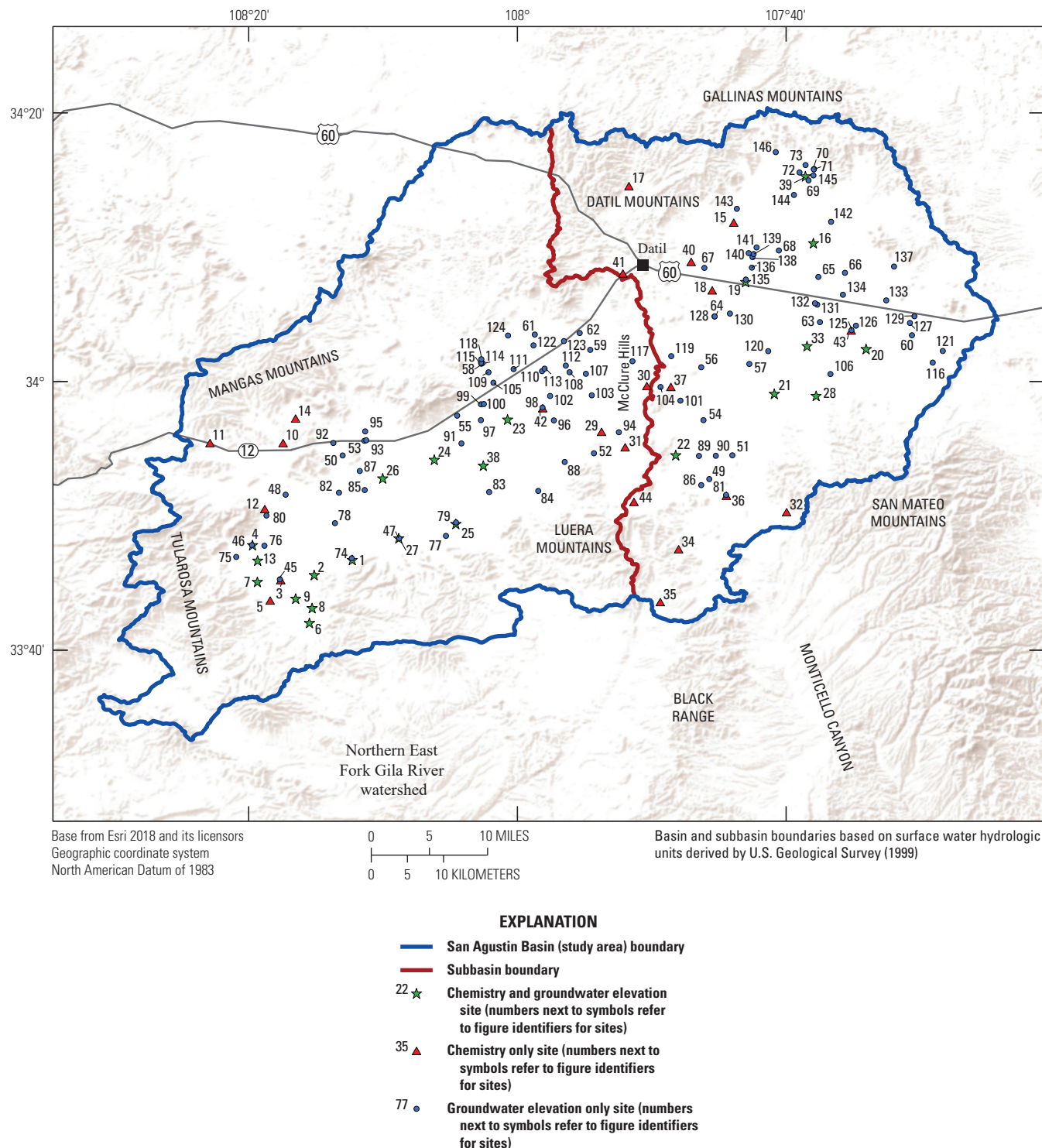
Figure 4. Inventory of sites in the San Agustin Basin, west-central New Mexico, with data that were used in groundwater elevation contouring and for chemistry analyses. Figure identifiers correspond to those used in the tables of this report. Data are from Rinehart and others (2017) and the U.S. Geological Survey (USGS) National Water Information System (USGS, 2021).

Table 3.   Inventory of sites with data that were used in groundwater elevation contouring and for chemistry analyses of groundwater in the San Agustin Basin, west-central New Mexico.

[Analyzed data from Rinehart and others (2017) and the U.S. Geological Survey (USGS) National Water Information System (USGS, 2021). Longitude and latitude are relative to the North American Datum of 1983]

Figure identifier	Site identifier	Site type	Longitude	Latitude	Data collected during this study	Chemistry used	Groundwater elevation contoured
1	334643108121801	Well	−108.2049	33.7786	Depth to water and chemistry	Yes	Yes
2	334536108150701	Well	−108.2521	33.7599	Depth to water and chemistry	Yes	Yes
3	334516108173701	Well	−108.2937	33.7542	Chemistry	Yes	No
4	334747108194401	Well	−108.3286	33.7970	Chemistry	Yes	Yes
5	334344108182401	Well	−108.3068	33.7289	Chemistry	Yes	No
6	334202108152901	Well	−108.2580	33.7005	Depth to water and chemistry	Yes	Yes
7	334503108192601	Well	−108.3226	33.7514	Chemistry	Yes	Yes
8	334307108151501	Well	−108.2547	33.7189	Chemistry	Yes	Yes
9	334348108162801	Well	−108.2751	33.7306	Depth to water and chemistry	Yes	Yes
10	335526108172601	Well	−108.2908	33.9243	Chemistry	Yes	No
11	335528108225301	Well	−108.3814	33.9243	Chemistry	Yes	No
12	335032108184501	Well	−108.3135	33.8424	Chemistry	Yes	No
13	334639108191901	Well	−108.3223	33.7778	Chemistry	Yes	Yes
14	335717108163101	Well	−108.2753	33.9547	Chemistry	Yes	No
15	GT-002	Well	−107.7317	34.1977	None	Yes	No
16	341016107375601	Well	−107.6324	34.1715	None	Yes	Yes
17	341435107514001	Well	−107.8617	34.2430	None	Yes	No
18	340645107451501	Well	−107.7584	34.1137	None	Yes	No
19	340723107425801	Well	−107.7167	34.1231	None	Yes	Yes
20	340225107340001	Well	−107.5670	34.0402	None	Yes	Yes
21	335904107404901	Well	−107.6809	33.9845	None	Yes	Yes
22	335431107481201	Well	−107.8039	33.9087	None	Yes	Yes
23	335709108004201	Well	−108.0123	33.9526	None	Yes	Yes
24	335410108060901	Well	−108.1028	33.9029	None	Yes	Yes
25	334930108043201	Well	−108.0759	33.8232	None	Yes	Yes
26	335243108100201	Well	−108.1667	33.8798	None	Yes	Yes
27	334819108084801	Well	−108.1467	33.8054	None	Yes	Yes
28	335856107374401	Well	−107.6295	33.9823	None	Yes	Yes
29	SA-0119	Well	−107.8957	33.9382	None	Yes	No
30	SA-0123	Well	−107.8395	33.9950	None	Yes	No
31	SA-0124	Well	−107.8664	33.9190	None	Yes	No
32	SA-0183	Well	−107.6661	33.8385	None	Yes	No
33	340238107382301	Well	−107.6403	34.0440	None	Yes	Yes
34	SA-0205	Well	−107.8001	33.7925	None	Yes	No
35	SA-0207	Well	−107.8228	33.7270	None	Yes	No
36	SA-0209	Well	−107.7408	33.8589	None	Yes	No
37	SA-0210	Well	−107.8097	33.9939	None	Yes	No

Table 3.   Inventory of sites with data that were used in groundwater elevation contouring and for chemistry analyses of groundwater in the San Agustin Basin, west-central New Mexico.—Continued

[Analyzed data from Rinehart and others (2017) and the U.S. Geological Survey (USGS) National Water Information System (USGS, 2021). Longitude and latitude are relative to the North American Datum of 1983]

Figure identifier	Site identifier	Site type	Longitude	Latitude	Data collected during this study	Chemistry used	Groundwater elevation contoured
38	335344108023001	Well	−108.0423	33.8956	None	Yes	Yes
39	341517107383401	Well	−107.6427	34.2546	None	Yes	Yes
40	SA-0238	Well	−107.7845	34.1490	None	Yes	No
41	SA-0239	Well	−107.8692	34.1347	None	Yes	No
42	SA-0244	Well	−107.9687	33.9675	None	Yes	No
43	SA-0245	Well	−107.5859	34.0639	None	Yes	No
44	SA-1016	Spring	−107.8555	33.8513	None	Yes	No
45	334516108173902	Well	−108.2948	33.7545	None	No	Yes
46	334751108194901	Well	−108.3294	33.7970	Depth to water	No	Yes
47	334819108084601	Well	−108.1467	33.8053	None	No	Yes
48	335134108171301	Well	−108.2876	33.8595	None	No	Yes
49	335244107454301	Well	−107.7620	33.8789	None	No	Yes
50	335429108125801	Well	−108.2169	33.9082	None	No	Yes
51	335430107435801	Well	−107.7334	33.9084	None	No	Yes
52	335439107541601	Well	−107.9051	33.9109	None	No	Yes
53	335535108112101	Well	−108.1898	33.9264	None	No	Yes
54	335707107460701	Well	−107.7692	33.9520	None	No	Yes
55	335727108042701	Well	−108.0748	33.9576	None	No	Yes
56	340103107461701	Well	−107.7720	34.0176	None	No	Yes
57	340118107424201	Well	−107.7123	34.0217	None	No	Yes
58	340119108023901	Well	−108.0448	34.0220	None	No	Yes
59	340223107543601	Well	−107.9097	34.0392	None	No	Yes
60	340326107303701	Well	−107.5106	34.0573	None	No	Yes
61	340329107584201	Well	−107.9785	34.0582	None	No	Yes
62	340336107552001	Well	−107.9228	34.0601	None	No	Yes
63	340427107373601	Well	−107.6247	34.0736	None	No	Yes
64	340451107452001	Well	−107.7555	34.0808	None	No	Yes
65	340740107373601	Well	−107.6267	34.1297	None	No	Yes
66	340805107353701	Well	−107.5937	34.1348	None	No	Yes
67	340827107460301	Well	−107.7681	34.1409	None	No	Yes
68	340945107403301	Well	−107.6757	34.1625	None	No	Yes
69	341458107381801	Well	−107.6389	34.2495	None	No	Yes
70	341545107384801	Well	−107.6321	34.2637	None	No	Yes
71	341547107375401	Well	−107.6323	34.2631	None	No	Yes
72	341552107384501	Well	−107.6501	34.2593	None	No	Yes
73	341611107381601	Well	−107.6426	34.2685	None	No	Yes
74	334650108121801	Well	−108.2056	33.7806	None	No	Yes
75	334656108205401	Well	−108.3489	33.7823	None	No	Yes
76	334746108184801	Well	−108.3139	33.7962	None	No	Yes
77	334830108051701	Well	−108.0887	33.8084	None	No	Yes

Table 3.   Inventory of sites with data that were used in groundwater elevation contouring and for chemistry analyses of groundwater in the San Agustin Basin, west-central New Mexico.—Continued

[Analyzed data from Rinehart and others (2017) and the U.S. Geological Survey (USGS) National Water Information System (USGS, 2021). Longitude and latitude are relative to the North American Datum of 1983]

Figure identifier	Site identifier	Site type	Longitude	Latitude	Data collected during this study	Chemistry used	Groundwater elevation contoured
78	334927108133301	Well	−108.2264	33.8242	None	No	Yes
79	334930108043202	Well	−108.0762	33.8251	None	No	Yes
80	335001108183901	Well	−108.3114	33.8337	None	No	Yes
81	335133107442601	Well	−107.7412	33.8592	None	No	Yes
82	335143108131501	Well	−108.2214	33.8620	None	No	Yes
83	335146108020401	Well	−108.0351	33.8628	None	No	Yes
84	335151107582501	Well	−107.9742	33.8642	None	No	Yes
85	335155108112001	Well	−108.1895	33.8653	None	No	Yes
86	335217107461701	Well	−107.7720	33.8714	None	No	Yes
87	335320108114201	Well	−108.1956	33.8889	None	No	Yes
88	335400107562701	Well	−107.9414	33.9001	None	No	Yes
89	335427107462701	Well	−107.7748	33.9076	None	No	Yes
90	335428107451201	Well	−107.7539	33.9078	None	No	Yes
91	335523108040801	Well	−108.0695	33.9231	None	No	Yes
92	335525108134002	Well	−108.2284	33.9237	None	No	Yes
93	335537108111301	Well	−108.1876	33.9270	None	No	Yes
94	335613107522501	Well	−107.8742	33.9370	None	No	Yes
95	335617108111801	Well	−108.1889	33.9381	None	No	Yes
96	335706107571501	Well	−107.9548	33.9517	None	No	Yes
97	335707108024101	Well	−108.0453	33.9520	None	No	Yes
98	335803107580601	Well	−107.9689	33.9676	None	No	Yes
99	335818108024101	Well	−108.0453	33.9717	None	No	Yes
100	335819108022801	Well	−108.0417	33.9720	None	No	Yes
101	335834107475001	Well	−107.7978	33.9762	None	No	Yes
102	335855107573201	Well	−107.9595	33.9820	None	No	Yes
103	335858107542601	Well	−107.9078	33.9828	None	No	Yes
104	335935107491901	Well	−107.8225	33.9931	None	No	Yes
105	335954108014501	Well	−108.0298	33.9984	None	No	Yes
106	340033107364001	Well	−107.6117	34.0092	None	No	Yes
107	340034107545201	Well	−107.9151	34.0095	None	No	Yes
108	340041107560501	Well	−107.9353	34.0114	None	No	Yes
109	340041108020701	Well	−108.0359	34.0114	None	No	Yes
110	340046107580801	Well	−107.9695	34.0128	None	No	Yes
111	340055108001501	Well	−108.0048	34.0153	None	No	Yes
112	340111107562401	Well	−107.9400	34.0197	None	No	Yes
113	340121107582401	Well	−107.9663	34.0159	None	No	Yes
114	340122108023401	Well	−108.0434	34.0228	None	No	Yes
115	340123108024001	Well	−108.0451	34.0231	None	No	Yes
116	340124107290301	Well	−107.4848	34.0234	None	No	Yes
117	340130107512401	Well	−107.8573	34.0251	None	No	Yes

Table 3.   Inventory of sites with data that were used in groundwater elevation contouring and for chemistry analyses of groundwater in the San Agustin Basin, west-central New Mexico.—Continued

[Analyzed data from Rinehart and others (2017) and the U.S. Geological Survey (USGS) National Water Information System (USGS, 2021). Longitude and latitude are relative to the North American Datum of 1983]

Figure identifier	Site identifier	Site type	Longitude	Latitude	Data collected during this study	Chemistry used	Groundwater elevation contoured
118	340139108023901	Well	−108.0448	34.0276	None	No	Yes
119	340153107483101	Well	−107.8092	34.0314	None	No	Yes
120	340215107411801	Well	−107.6889	34.0376	None	No	Yes
121	340216107281801	Well	−107.4723	34.0378	None	No	Yes
122	340241107584601	Well	−107.9801	34.0448	None	No	Yes
123	340300107563001	Well	−107.9423	34.0501	None	No	Yes
124	340325108004001	Well	−108.0117	34.0570	None	No	Yes
125	340349107350601	Well	−107.5856	34.0637	None	No	Yes
126	340409107344601	Well	−107.5800	34.0692	None	No	Yes
127	340421107304501	Well	−107.5131	34.0726	None	No	Yes
128	340450107451701	Well	−107.7553	34.0806	None	No	Yes
129	340451107302501	Well	−107.5075	34.0809	None	No	Yes
130	340503107440901	Well	−107.7364	34.0842	None	No	Yes
131	340543107373901	Well	−107.6281	34.0953	None	No	Yes
132	340549107374901	Well	−107.6309	34.0970	None	No	Yes
133	340602107323101	Well	−107.5425	34.1006	None	No	Yes
134	340627107354401	Well	−107.5962	34.1076	None	No	Yes
135	340735107425801	Well	−107.7167	34.1264	None	No	Yes
136	340828107423101	Well	−107.7092	34.1412	None	No	Yes
137	340833107315601	Well	−107.5328	34.1426	None	No	Yes
138	340915107422801	Well	−107.7084	34.1542	None	No	Yes
139	340929107422301	Well	−107.7070	34.1581	None	No	Yes
140	340933107424501	Well	−107.7131	34.1592	None	No	Yes
141	341001107421501	Well	−107.7034	34.1663	None	No	Yes
142	341153107363701	Well	−107.6109	34.1981	None	No	Yes
143	341251107433801	Well	−107.7278	34.2142	None	No	Yes
144	341353107392301	Well	−107.6570	34.2314	None	No	Yes
145	341520107375601	Well	−107.6328	34.2556	None	No	Yes
146	341704107404401	Well	−107.6795	34.2845	None	No	Yes

Major ion and trace element analyses were performed by the USGS National Water Quality Laboratory in Denver, Colorado. Major ions calcium, magnesium, potassium, silica, and sodium, along with trace elements iron and manganese, were analyzed by inductively coupled plasma optical emission spectrophotometry (ICP-OES) (Fishman and Friedman, 1989). Ion-exchange chromatography was used to analyze for bromide, fluoride, chloride, and sulfate (Fishman, 1993). Inductively coupled plasma-mass spectrometry (ICP-MS) was used for the following trace elements: silver, aluminum, arsenic, boron, barium, beryllium, cadmium, cobalt, chromium, copper, lithium, manganese, molybdenum, nickel, lead, antimony, selenium, strontium, thallium, uranium, vanadium, and zinc (Garbarino, 1999; Garbarino and others, 2005). Manganese concentrations acquired from ICP-MS were favored over those obtained from ICP-OES when results from both methods were available. Major ion concentrations are reported in milligrams per liter, whereas trace element concentrations are reported in micrograms per liter (μg/L).

[Analyzed data from the U.S. Geological Survey (USGS) National Water Information System (USGS, 2021). Longitude and latitude are relative to the North American Datum of 1983; median groundwater elevations are relative to the North American Vertical Datum of 1988. NA, not available because of lack of multiple measurements]

Figure identifier	Site identifier	Longitude	Latitude	Number of measurements analyzed	Earliest measurement date analyzed, as month/day/year	Latest measurement date analyzed, as month/day/year	Median annual gradient, in feet per year	Median groundwater elevation, in feet
1	334643108121801	−108.2049	33.7786	1	4/10/2019	4/10/2019	NA	6,748.60
2	334536108150701	−108.2521	33.7599	5	3/10/2015	3/5/2019	0.06	6,751.45
4	334747108194401	−108.3286	33.7970	1	10/5/1977	10/5/1977	NA	6,745.17
6	334202108152901	−108.2580	33.7005	4	2/20/2015	3/7/2019	−0.08	6,721.05
7	334503108192601	−108.3226	33.7514	2	10/20/1977	4/30/2008	−0.02	6,749.28
8	334307108151501	−108.2547	33.7189	1	10/5/1977	10/5/1977	NA	6,739.59
9	334348108162801	−108.2751	33.7306	2	10/5/1977	3/6/2019	−0.02	6,739.96
13	334639108191901	−108.3223	33.7778	1	10/4/1977	10/4/1977	NA	6,736.98
16	341016107375601	−107.6324	34.1715	13	12/14/1977	2/19/2019	−0.09	6,804.40
19	340723107425801	−107.7167	34.1231	18	5/11/1980	2/19/2019	0.05	6,799.15
20	340225107340001	−107.5670	34.0402	19	5/8/1980	2/21/2018	−0.05	6,803.48
21	335904107404901	−107.6809	33.9845	19	2/24/1977	2/22/2018	−0.05	6,797.84
22	335431107481201	−107.8039	33.9087	12	2/24/1977	2/27/2018	−0.13	6,790.89
23	335709108004201	−108.0123	33.9526	12	7/21/1977	2/18/2019	−0.03	6,766.03
24	335410108060901	−108.1028	33.9029	20	9/29/1977	2/25/2019	−0.01	6,759.47
25	334930108043201	−108.0759	33.8232	19	9/23/1977	2/25/2019	−0.01	6,759.52
26	335243108100201	−108.1667	33.8798	16	12/14/1978	2/25/2019	−0.02	6,766.46
27	334819108084801	−108.1467	33.8054	2	9/28/1977	5/1/2008	0.00	6,754.16
28	335856107374401	−107.6295	33.9823	2	5/7/1980	5/10/2008	−0.21	6,861.29
33	340238107382301	−107.6403	34.0440	1	5/8/1979	5/8/1979	NA	6,804.94
38	335344108023001	−108.0423	33.8956	4	2/23/2015	2/25/2019	−0.01	6,758.90
39	341517107383401	−107.6427	34.2546	5	3/25/2015	2/19/2019	−0.41	6,808.93
45	334516108173902	−108.2948	33.7545	12	10/5/1977	2/27/2017	−0.06	6,743.70
46	334751108194901	−108.3294	33.7970	1	3/5/2019	3/5/2019	NA	6,739.38
47	334819108084601	−108.1467	33.8053	11	9/28/1977	2/25/2019	0.00	6,752.87
48	335134108171301	−108.2876	33.8595	12	10/21/1977	2/27/2017	−0.11	6,775.14
49	335244107454301	−107.7620	33.8789	15	5/4/2010	2/21/2019	−0.02	6,795.24
50	335429108125801	−108.2169	33.9082	18	11/29/1978	2/25/2019	−0.14	6,843.94
51	335430107435801	−107.7334	33.9084	9	10/28/1977	2/21/2018	−0.03	6,800.08

Table 4. Median groundwater elevation data used in groundwater elevation contouring of the San Agustin Basin, west-central New Mexico (1975–2019).—Continued

[Analyzed data from the U.S. Geological Survey (USGS) National Water Information System (USGS, 2021). Longitude and latitude are relative to the North American Datum of 1983; median groundwater elevations are relative to the North American Vertical Datum of 1988. NA, not available because of lack of multiple measurements]

Figure identifier	Site identifier	Longitude	Latitude	Number of measurements analyzed	Earliest measurement date analyzed, as month/day/year	Latest measurement date analyzed, as month/day/year	Median annual gradient, in feet per year	Median groundwater elevation, in feet
52	335439107541601	−107.9051	33.9109	27	2/23/1977	2/27/2018	−0.01	6,766.30
53	335535108112101	−108.1898	33.9264	14	7/8/1977	2/25/2019	−0.21	6,872.97
54	335707107460701	−107.7692	33.9520	11	7/14/1978	2/22/2019	−0.14	6,790.65
55	335727108042701	−108.0748	33.9576	8	2/12/2009	2/20/2017	−0.16	6,771.49
56	340103107461701	−107.7720	34.0176	17	8/2/1979	2/22/2019	−0.40	6,799.17
57	340118107424201	−107.7123	34.0217	32	2/24/1977	2/21/2019	−0.12	6,794.16
58	340119108023901	−108.0448	34.0220	14	1/29/1990	2/20/2017	−0.06	7,019.16
59	340223107543601	−107.9097	34.0392	15	12/4/1979	2/20/2018	−0.02	6,767.71
60	340326107303701	−107.5106	34.0573	21	5/9/1980	2/26/2019	0.04	6,798.25
61	340329107584201	−107.9785	34.0582	28	6/25/1980	2/20/2019	0.00	7,009.59
62	340336107552001	−107.9228	34.0601	19	6/30/1980	2/20/2018	0.09	7,022.49
63	340427107373601	−107.6247	34.0736	11	5/2/1980	3/13/2013	−0.05	6,801.98
64	340451107452001	−107.7555	34.0808	7	3/14/2012	2/26/2019	−0.03	6,800.29
65	340740107373601	−107.6267	34.1297	8	5/23/1979	2/19/2019	−0.01	6,803.60
66	340805107353701	−107.5937	34.1348	21	12/14/1977	2/22/2018	−0.03	6,802.42
67	340827107460301	−107.7681	34.1409	6	9/22/2008	3/2/2017	−0.11	6,800.87
68	340945107403301	−107.6757	34.1625	3	3/11/2015	2/23/2017	0.95	6,805.87
69	341458107381801	−107.6389	34.2495	17	12/15/1977	3/13/2013	−0.22	6,802.59
70	341545107384801	−107.6321	34.2637	13	12/15/1977	3/13/2013	−0.20	6,802.14
71	341547107375401	−107.6323	34.2631	14	12/15/1977	3/13/2013	−0.07	6,794.62
72	341552107384501	−107.6501	34.2593	12	12/15/1977	3/13/2013	−0.10	6,797.29
73	341611107381601	−107.6426	34.2685	11	12/15/1977	3/22/2011	−0.46	6,799.79
74	334650108121801	−108.2056	33.7806	1	10/20/1977	10/20/1977	NA	6,756.86
75	334656108205401	−108.3489	33.7823	1	10/20/1977	10/20/1977	NA	6,742.12
76	334746108184801	−108.3139	33.7962	1	10/4/1977	10/4/1977	NA	6,739.93
77	334830108051701	−108.0887	33.8084	1	9/28/1977	9/28/1977	NA	6,755.93
78	334927108133301	−108.2264	33.8242	2	6/13/1979	2/7/1996	0.20	6,738.96
79	334930108043202	−108.0762	33.8251	1	9/23/1977	9/23/1977	NA	6,759.99
80	335001108183901	−108.3114	33.8337	1	10/21/1977	10/21/1977	NA	6,728.42

[Analyzed data from the U.S. Geological Survey (USGS) National Water Information System (USGS, 2021). Longitude and latitude are relative to the North American Datum of 1983; median groundwater elevations are relative to the North American Vertical Datum of 1988. NA, not available because of lack of multiple measurements]

Figure identifier	Site identifier	Longitude	Latitude	Number of measurements analyzed	Earliest measurement date analyzed, as month/day/year	Latest measurement date analyzed, as month/day/year	Median annual gradient, in feet per year	Median groundwater elevation, in feet
81	335133107442601	−107.7412	33.8592	1	2/22/1977	2/22/1977	NA	6,789.04
82	335143108131501	−108.2214	33.8620	1	7/5/1980	7/5/1980	NA	6,759.05
83	335146108020401	−108.0351	33.8628	3	9/28/1977	2/6/1996	−0.31	6,761.26
84	335151107582501	−107.9742	33.8642	9	2/23/1977	2/21/2017	−0.01	6,762.05
85	335155108112001	−108.1895	33.8653	1	7/19/1977	7/19/1977	NA	6,753.89
86	335217107461701	−107.7720	33.8714	1	10/28/1977	10/28/1977	NA	6,795.64
87	335320108114201	−108.1956	33.8889	2	7/19/1977	9/24/1980	1.49	6,750.87
88	335400107562701	−107.9414	33.9001	1	2/23/1977	2/23/1977	NA	6,762.68
89	335427107462701	−107.7748	33.9076	1	5/6/1980	5/6/1980	NA	6,788.77
90	335428107451201	−107.7539	33.9078	2	10/28/1977	2/5/1996	−0.53	6,795.84
91	335523108040801	−108.0695	33.9231	1	9/29/1977	9/29/1977	NA	6,759.24
92	335525108134002	−108.2284	33.9237	1	9/24/1980	9/24/1980	NA	6,974.81
93	335537108111301	−108.1876	33.9270	1	7/8/1977	7/8/1977	NA	6,882.86
94	335613107522501	−107.8742	33.9370	1	10/28/1977	10/28/1977	NA	6,739.04
95	335617108111801	−108.1889	33.9381	4	7/22/1977	4/29/2008	−0.33	6,951.38
96	335706107571501	−107.9548	33.9517	1	9/25/1980	9/25/1980	NA	6,765.19
97	335707108024101	−108.0453	33.9520	1	9/29/1977	9/29/1977	NA	6,765.03
98	335803107580601	−107.9689	33.9676	1	7/21/1977	7/21/1977	NA	6,757.17
99	335818108024101	−108.0453	33.9717	1	7/20/1977	7/20/1977	NA	6,867.17
100	335819108022801	−108.0417	33.9720	2	7/20/1977	2/26/1991	−7.13	6,809.60
101	335834107475001	−107.7978	33.9762	2	2/24/1977	10/28/1977	−0.36	6,794.64
102	335855107573201	−107.9595	33.9820	2	7/21/1977	2/26/1991	0.38	6,764.44
103	335858107542601	−107.9078	33.9828	1	8/29/1979	8/29/1979	NA	6,771.86
104	335935107491901	−107.8225	33.9931	1	1/23/1980	1/23/1980	NA	6,783.27
105	335954108014501	−108.0298	33.9984	1	7/20/1977	7/20/1977	NA	6,966.14
106	340033107364001	−107.6117	34.0092	1	5/6/1980	5/6/1980	NA	6,798.02
107	340034107545201	−107.9151	34.0095	1	8/1/1979	8/1/1979	NA	6,768.90
108	340041107560501	−107.9353	34.0114	1	6/27/1980	6/27/1980	NA	6,767.88
109	340041108020701	−108.0359	34.0114	1	6/30/1980	6/30/1980	NA	6,981.29

Table 4. Median groundwater elevation data used in groundwater elevation contouring of the San Agustin Basin, west-central New Mexico (1975–2019).—Continued

[Analyzed data from the U.S. Geological Survey (USGS) National Water Information System (USGS, 2021). Longitude and latitude are relative to the North American Datum of 1983; median groundwater elevations are relative to the North American Vertical Datum of 1988. NA, not available because of lack of multiple measurements]

Figure identifier	Site identifier	Longitude	Latitude	Number of measurements analyzed	Earliest measurement date analyzed, as month/day/year	Latest measurement date analyzed, as month/day/year	Median annual gradient, in feet per year	Median groundwater elevation, in feet
110	340046107580801	−107.9695	34.0128	2	6/27/1980	2/26/1991	−0.03	6,768.30
111	340055108001501	−108.0048	34.0153	2	6/25/1980	2/25/1991	−0.31	6,819.85
112	340111107562401	−107.9400	34.0197	1	2/9/2009	2/9/2009	NA	6,770.51
113	340121107582401	−107.9663	34.0159	20	2/5/2001	3/3/2017	−0.07	6,770.98
114	340122108023401	−108.0434	34.0228	5	11/29/1978	3/17/1981	−0.05	7,006.86
115	340123108024001	−108.0451	34.0231	1	9/12/1979	9/12/1979	NA	7,012.51
116	340124107290301	−107.4848	34.0234	1	7/14/1978	7/14/1978	NA	6,807.61
117	340130107512401	−107.8573	34.0251	1	7/4/1980	7/4/1980	NA	6,741.90
118	340139108023901	−108.0448	34.0276	1	9/12/1979	9/12/1979	NA	7,010.07
119	340153107483101	−107.8092	34.0314	1	5/24/1979	5/24/1979	NA	6,782.14
120	340215107411801	−107.6889	34.0376	1	5/8/1979	5/8/1979	NA	6,793.26
121	340216107281801	−107.4723	34.0378	1	7/14/1978	7/14/1978	NA	6,809.51
122	340241107584601	−107.9801	34.0448	1	6/25/1980	6/25/1980	NA	7,010.43
123	340300107563001	−107.9423	34.0501	1	6/25/1980	6/25/1980	NA	7,105.81
124	340325108004001	−108.0117	34.0570	1	6/17/1980	6/17/1980	NA	7,007.49
125	340349107350601	−107.5856	34.0637	1	5/10/1979	5/10/1979	NA	6,802.34
126	340409107344601	−107.5800	34.0692	1	5/10/1979	5/10/1979	NA	6,804.65
127	340421107304501	−107.5131	34.0726	1	5/2/1980	5/2/1980	NA	6,822.37
128	340450107451701	−107.7553	34.0806	2	7/4/1980	2/14/1991	0.00	6,801.52
129	340451107302501	−107.5075	34.0809	1	4/25/1979	4/25/1979	NA	6,801.96
130	340503107440901	−107.7364	34.0842	1	7/4/1980	7/4/1980	NA	6,804.55
131	340543107373901	−107.6281	34.0953	1	5/10/1979	5/10/1979	NA	6,801.01
132	340549107374901	−107.6309	34.0970	1	5/9/1979	5/9/1979	NA	6,803.11
133	340602107323101	−107.5425	34.1006	1	5/7/1979	5/7/1979	NA	6,814.90
134	340627107354401	−107.5962	34.1076	1	5/10/1979	5/10/1979	NA	6,801.20
135	340735107425801	−107.7167	34.1264	1	5/1/1980	5/1/1980	NA	6,806.92
136	340828107423101	−107.7092	34.1412	1	5/1/1980	5/1/1980	NA	6,798.93
137	340833107315601	−107.5328	34.1426	1	4/20/1979	4/20/1979	NA	6,898.10
138	340915107422801	−107.7084	34.1542	5	11/15/1978	1/30/1990	−0.32	6,806.07

[Analyzed data from the U.S. Geological Survey (USGS) National Water Information System (USGS, 2021). Longitude and latitude are relative to the North American Datum of 1983; median groundwater elevations are relative to the North American Vertical Datum of 1988. NA, not available because of lack of multiple measurements]

Figure identifier	Site identifier	Longitude	Latitude	Number of measurements analyzed	Earliest measurement date analyzed, as month/day/year	Latest measurement date analyzed, as month/day/year	Median annual gradient, in feet per year	Median groundwater elevation, in feet
139	340929107422301	−107.7070	34.1581	2	11/15/1975	4/30/1980	−0.22	6,802.52
140	340933107424501	−107.7131	34.1592	1	5/1/1980	5/1/1980	NA	6,799.33
141	341001107421501	−107.7034	34.1663	3	7/6/1998	5/9/2008	0.06	6,805.98
142	341153107363701	−107.6109	34.1981	1	12/14/1977	12/14/1977	NA	6,801.84
143	341251107433801	−107.7278	34.2142	1	5/6/1980	5/6/1980	NA	6,802.76
144	341353107392301	−107.6570	34.2314	1	12/15/1977	12/15/1977	NA	6,799.38
145	341520107375601	−107.6328	34.2556	8	12/15/1977	2/11/1991	−0.68	6,816.52
146	341704107404401	−107.6795	34.2845	1	4/19/1979	4/19/1979	NA	6,799.03

Delta hydrogen-2/hydrogen-1(δ^2H) and delta oyxgen-18/oxygen-16 (δ^{18}O) stable isotope ratios were analyzed at the USGS Reston Stable Isotope Laboratory in Reston, Virginia, by using dual-inlet isotope-ratio mass spectrometry (Révész and Coplen, 2008a, b). Stable isotope ratios are reported in per mil relative to Vienna Standard Mean Ocean Water.

Groundwater age tracers were analyzed at two laboratories. Tritium concentrations were analyzed at the University of Miami's Rosenstiel School of Marine and Atmospheric Science Tritium Laboratory in Miami, Florida, by using low-level gas proportional counters (Thatcher and others, 1977) and are reported in picocuries per liter. Carbon-14 analyses were completed by the National Ocean Sciences Accelerator Mass Spectrometry facility at Woods Hole Oceanographic Institution in Woods Hole, Massachusetts. Carbon-14 values are reported as absolute percent modern.

One field blank sample was collected at site 11 during sampling to assess potential bias introduced by the collection, processing, and transportation of the environmental samples. The field blank sample was obtained by running certified inorganic blank water through the tubing and fittings that were used for environmental water sampling. Ideally, the field blank sample analyses would yield negligible concentrations of all constituents and thereby indicate minimal introduced bias. The field blank results indicate very low potential for contamination for nearly all constituents considered in this study (table 4.1 in app. 4), although metals from the windmill and well casing themselves were not accounted for because field blanks could not include this equipment. Vanadium and cobalt were the only two constituents with concentrations that exceeded the laboratory detection limit, thereby indicating potential bias for these two constituents. However, all environmental results for cobalt and vanadium were greater than 10 times the field blank values or were not detected in the sample. This contrast indicates that potential bias introduced from the sampling procedures is likely small relative to measured concentrations and was therefore considered negligible in all interpretations.

A replicate sample was also collected at site 11 at the time of sampling to evaluate the variability and uncertainty of environmental results. Replicate results are provided in appendix 4 (table 4.2). Absolute relative percent differences (ARPDs) were computed between uncensored replicate and environmental values as follows for each constituent:

$$ARPD = 100 \left| \frac{Replicate\ value - Environmental\ value}{(Replicate\ value + Environmental\ value)/2} \right| \quad (1)$$

Resulting ARPDs were all less than 10 percent except for lead (25.8 percent) (table 4.2 in app. 4). The lead concentrations themselves were very small (environmental = 0.0673 µg/L, replicate = 0.0519 µg/L, difference = −0.0154 µg/L), which indicates that the elevated ARPD was the result of high analysis precision (being able to detect very small concentrations) rather than increased data uncertainty. Censored (values less

than the detection limit and [or] reporting level) environmental and replicate results all agreed with one another as well. Tritium was the only censored constituent that differed in the replicate analysis (environmental = 0.29 picocuries per liter [pCi/L]; replicate = R −0.04, where R denotes that the value was less than the tritium reporting level). The uncensored tritium environmental concentration was 0.29 pCi/L, which was slightly less than the tritium detection level of 0.30 pCi/L, although it exceeded the tritium reporting level. Provided the marginal difference between the tritium detection level and the environmental value, the replicate results were essentially equivalent. Overall, the replicate analysis suggests that the environmental results were highly reproducible.

The NMBGMR used different laboratories for analyses of major ions, trace elements, stable isotopes, and carbon-14, which, when combined with slightly different sampling strategies, created reporting and accuracy differences within the overall analyzed dataset. The technologies utilized at those laboratories to analyze constituents were comparable or identical to those used to analyze the USGS data in this study (Timmons and others, 2013; USGS, variously dated). The NMBGMR internally inspects the quality of reported results by analyzing blanks, standards, and replicate samples and checking ion balances as part of their standard protocol (Timmons and others, 2013), although the quality assurance data were not reported with their environmental data. Samples at sites 2 and 7 were collected by both agencies about 4 months apart and showed minor differences. Of the 23 comeasured constituents, 18 yielded ARPDs of less than 10 percent despite the time gap between sample collection (Rinehart and others, 2017; USGS, 2021). Constituents that exceeded this threshold include field temperature (site 7 = 27.4 percent), bromide (site 2 = 29.8 percent, site 7 = 19.4 percent), fluoride (site 7 = 14.4 percent), iron (site 2 = 151.2 percent, site 7 = 19.7 percent), and manganese (site 2 = 98.5 percent, site 7 = 136.6 percent). The most substantial differences were for manganese at both sites and iron at site 2. While it is possible that these differences are a result of sampling and analysis protocols, it is common to see appreciable fluctuations in these two constituents at longstanding steel-cased windmill-powered wells, depending on time of year and flow rate; given that these results were at least twice their analytical detection level, the latter seems most likely. Generally, the collocated samples agreed well with one another, and the minor differences in sampling and analytical protocols between the NMBGMR and USGS are not thought to substantially and systematically bias the analyses performed herein.

Analysis of Groundwater Elevation Data

Interpolation of Groundwater Elevation

To better understand groundwater flow patterns in the San Agustin Basin, a two-dimensional groundwater elevation contour map for the basin-fill and alluvium aquifer system was constructed by using the median groundwater elevations

from 1975 through 2019 presented in table 4. Interpolation between measurement locations was completed by using the kriging geostatistical method (see Fisher, 2013). This approach estimates values at unmeasured locations as a weighted average of measured values. The weights are derived from the spatial correlation of measurements, as indicated by an empirical semivariogram (Fisher, 2013). Kriging assumes stationarity, meaning that the mean value of the data being contoured and the empirical semivariogram are constant throughout the area of interest. A second-order polynomial trend function representative of regional groundwater elevation trend was subtracted from the measured values during semivariogram modeling and kriging to favor stationarity. The removed spatial trend was formulated as follows:

$$
\begin{aligned}
z(s) = &\ \beta_0 + \beta_1 x(s) + \beta_2 y(s) + \\
&\ \beta_3 x(s)^2 + \beta_4 y(s)^2 + \beta_5 x(s)y(s)
\end{aligned}
\tag{2}
$$

where

$z(s)$	is median groundwater elevation at point s, in feet above the North American Vertical Datum of 1988 (NAVD 88);
β_0	is a deterministic unknown trend coefficient, in feet above NAVD 88;
β_i	are deterministic unknown trend coefficients, in dimensionless units ($i = 1$ to 5);
$x(s)$	is the easterly coordinate at point s, in meters; and
$y(s)$	is the northerly coordinate at point s, in meters.

Normally distributed residuals had a mean and median of 0.00 ft and −7.11 ft, respectively, thereby suggesting an acceptable level of spatial stationarity to permit application of kriging. The trend was calculated, removed, and added back to kriged residuals within the R functions that were used for semivariogram development and kriging, as appropriate (functions are listed below). This type of kriging with trend removal is known as universal kriging (Fisher, 2013). The final contoured area was restricted to the basin lowlands, as interpreted from satellite imagery and topographic maps, to avoid elevated universal kriging estimation errors introduced by abrupt groundwater elevation changes in the highlands.

The empirical semivariogram is a graphical representation of how differences in measured values (in terms of semivariance) change as a function of distance between measurement locations (lag distance). A continuous semivariogram model was fit to the curvature of the empirical semivariogram to provide a data-driven method for kriging to estimate spatial correlation at all lag distances. A semivariogram model has four primary characteristics: (1) model type, (2) range, (3) sill, and (4) nugget. The model type defines the overall shape of the semivariogram model and will change depending on how rapidly measured values change as a function of lag distance. Semivariance in semivariograms typically levels off at a certain lag distance, beyond which there is minimal spatial correlation between measured and unmeasured locations. This distance is called the range, and the semivariance value at which the semivariogram levels off is called the sill. The nugget is the semivariance at a lag distance of zero, or the y-intercept of the semivariogram model, and is therefore typically related to measurement error.

The empirical semivariogram in this study was calculated by using the "variogram" function within the "gstat" R package, version 2.0–0 (Pebesma and Graeler, 2019). The maximum lag distance considered in the empirical semivariogram was 15,000 meters (m), or about half the median distance between all observation pairs (29,940 m) and about one-fifth the maximum distance between observation locations (85,923 m). A bin width of 1,000 m was used in the empirical semivariogram calculation because it yielded the most readily identifiable semivariogram curvature (15 bins total). The "fit. variogram" function of the same "gstat" R package was then used to fit a continuous semivariogram model to the empirical semivariogram. The resulting semivariogram model was of spherical type, with a range of 5,791 m, sill of 3,228 square feet, and nugget of 0 square feet (fig. 5). The modeled theoretical semivariogram well represents the general curvature of the empirical semivariogram, as evidenced by their Pearson correlation coefficient of 0.86.

Kriging was then performed by using the "krige" function within the previously mentioned "gstat" R package to estimate groundwater elevations on a uniform raster grid. Interpolation root-mean-square error (RMSE) at measured locations decreased as a function of raster grid cell size. A uniform grid cell size of 35 ft (10.668 m) was selected as a compromise between raster file size and RMSE. Measured values were very well represented by kriged raster estimates, with an RMSE of 0.1638 ft, Pearson correlation coefficient of 1.00, mean residual (measurements minus estimates) of 0.01 ft, and median residual of 0.00 ft. The final kriged contour map is discussed and presented in the "Results and Discussion" section of this report.

Leave-one-out cross validation (LOOCV) was performed to further evaluate the predictive capabilities of the kriging approach. LOOCV provides insight into predictive capability by removing one data point, kriging the remaining data, and computing kriged estimation error at the removed location. This process is repeated for all measurement locations. LOOCV was performed by using the "RunCrossValidation" function within the "ObsNetwork" R package, version 1.0.1.9000 (Fisher, 2013). Mean LOOCV error (measurements minus LOOCV estimations) would ideally be zero and was −1.52 ft in the analysis (fig. 6A), indicating that the kriging approach had a high level of predictive ability with a small bias towards overestimating groundwater elevations. This notion is further emphasized by the very low Pearson correlation coefficient of 0.05 between LOOCV estimations and LOOCV errors, as well as the high Pearson correlation coefficient of 0.88 between measured groundwater elevations and LOOCV estimations (fig. 6B). Nineteen sites had more
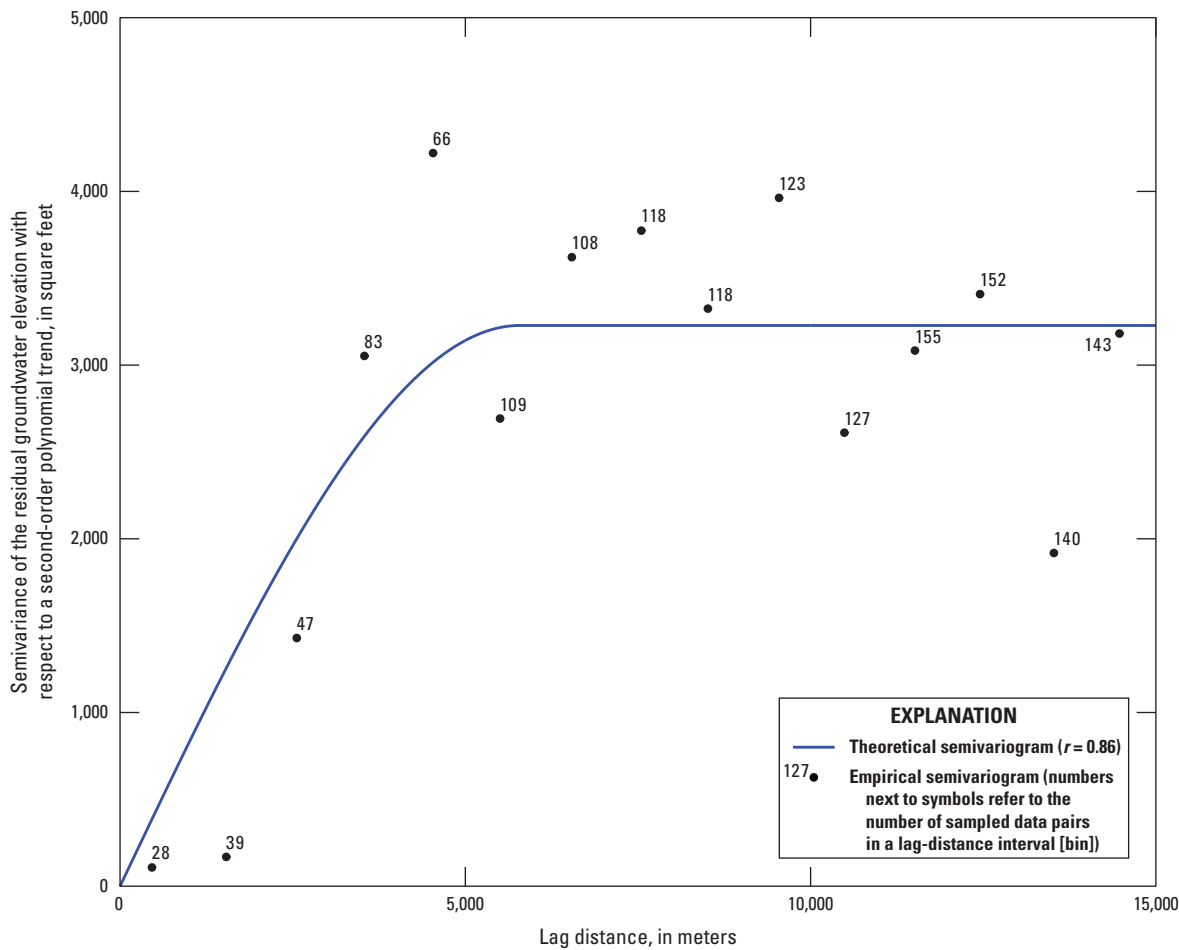
Figure 5. Semivariogram analysis of groundwater elevation residuals after subtraction of trend for median groundwater elevations in the San Agustin Basin, west-central New Mexico (1975–2019). Groundwater elevation data from U.S. Geological Survey (2021); *r*, Pearson correlation coefficient.

than 50 ft of LOOCV error and are labeled in figure 6B. All these sites are in the foothills of the basin (fig. 4), where groundwater elevations show greater variation over short distances than elsewhere in the basin. Fifteen of these sites are in the northern foothills of the west subbasin, whereas four sites are dispersed throughout the foothills of the east subbasin. This pattern of LOOCV errors indicates a greater sensitivity to data density and elevated estimation uncertainty in these areas. Generally, estimation uncertainty increases with distance from measurement locations, which is further discussed in terms of kriging standard error within the "Results and Discussion" section of this report. Overall, the kriged solution performed well and is thought to reasonably estimate the groundwater elevations throughout the area of interest.

Temporal Analysis of Groundwater Elevation

The median annual change in groundwater elevations over time (median annual gradient) was calculated for each site that had multiple measurements from 1975 through 2019 to provide insight into the dynamics of groundwater flow patterns. Unlike the groundwater elevation interpolation,

sites throughout the entire basin and in any aquifer were included in the analysis. The median annual gradient for each site was calculated by using a forward difference derivative approximation, as follows:

$$\frac{dz}{dt}_{median} = median\left[\frac{z(t_2) - z(t_1)}{t_2 - t_1}, \dots \frac{z(t_n) - z(t_{n-1})}{t_n - t_{n-1}}\right]365 \quad (3)$$

where

$\dfrac{dz}{dt}_{median}$ is the median annual gradient for a site, in feet per year;

$z(t_i)$ is groundwater elevation at time i, in feet above NAVD 88 ($i = 1$ to n);

n is the number of groundwater elevation measurements at a site; and

t_i is the date of the ith groundwater elevation measurement, in days ($i = 1$ to n).

Because median annual gradients were calculated for any site that had at least two measurements between 1975 and 2019, the gradients are not necessarily
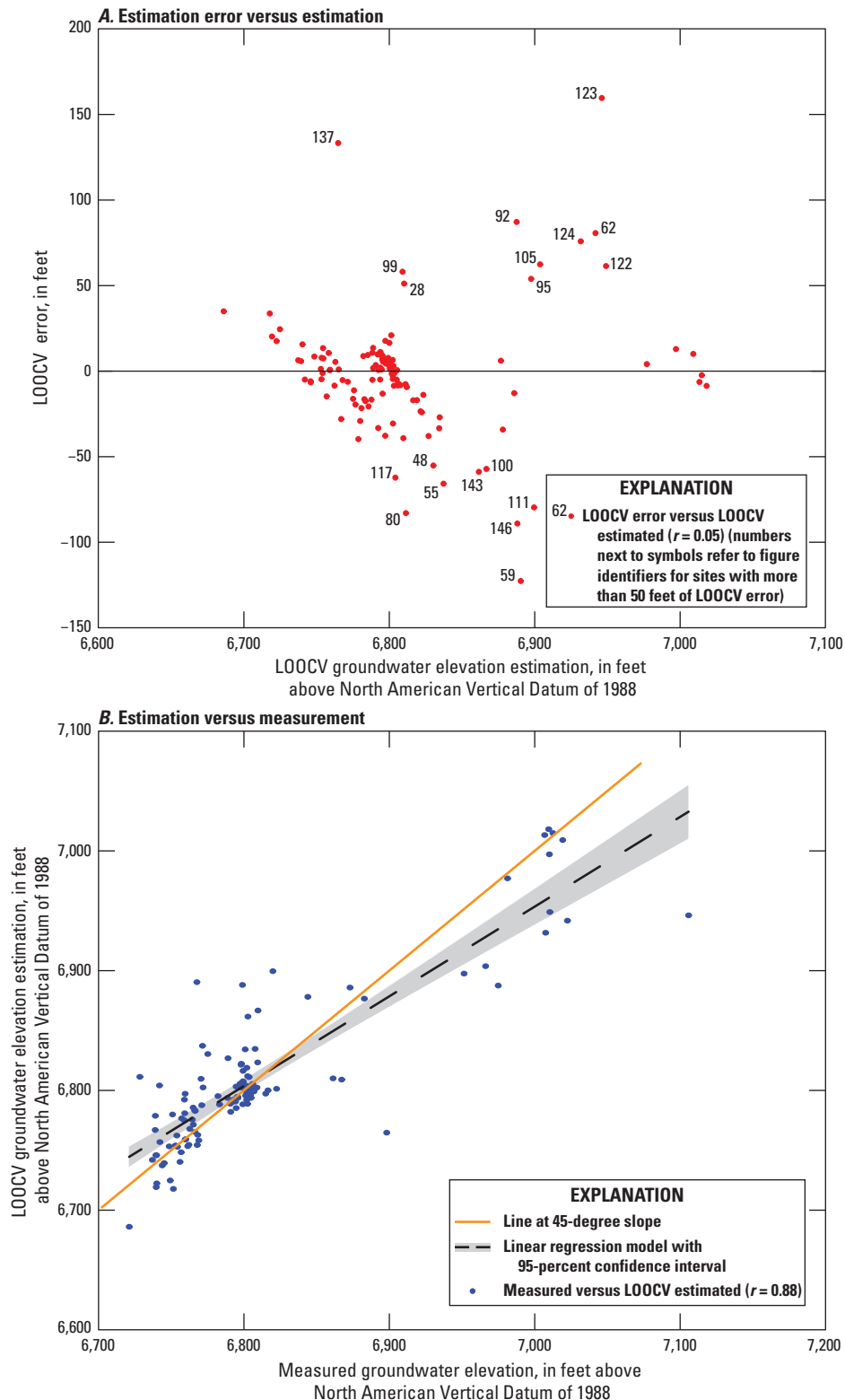
Figure 6.   Leave-one-out cross validation (LOOCV) metrics from the application of kriging to median groundwater elevations in the San Agustin Basin, west-central New Mexico (1975–2019). Metrics include *A*, LOOCV errors versus LOOCV estimations and *B*, LOOCV estimations versus measurements. Groundwater elevation data from U.S. Geological Survey (2021); *r*, Pearson correlation coefficient. Figure identifiers correspond to those used in the tables of this report, and sites are plotted spatially in figure 4.

representative of the entire period of investigation. For example, site 138 had 5 measurements that were collected between November 15, 1978, and January 30, 1990, whereas site 113 had 20 measurements spanning February 5, 2001, through March 3, 2017. The computed median annual gradients for these sites were calculated over different time intervals and do not provide a comprehensive estimate of groundwater elevation change throughout the full period of interest (1975–2019). Seasonality of groundwater elevations through any given year was also not considered. Insufficient repeat measurements restricted the ability to do a more complete analysis, and these potential implicit biases should be considered when interpreting the results. On average, each site had 10 measurements that spanned about 26 years (median = 34 years). Median annual gradients are spatially presented and discussed in the "Results and Discussion" section of this report and are tabulated in table 4 for sites used in the groundwater elevation contouring.

Analysis of Groundwater Chemistry Data

All interpretative chemistry analyses were performed on the 2010–19 groundwater chemistry data, although data were omitted as needed to meet the conditions required for particular analyses. Major ion chemistry (sodium, calcium, magnesium, potassium, carbonate, bicarbonate, sulfate, and chloride) was plotted on a Piper diagram by using The Geochemist's Workbench, version 12 (Bethke and others, 2019). Sites 18 and 42 were excluded from the diagram because of a lack of data for one or more of the major ions. Data were labeled according to the aquifer and subbasin of the corresponding sample location. Major ion, trace element, and TDS concentrations, as well as pH, were compared to the U.S. Environmental Protection Agency (EPA) water quality standards for drinking water. This comparison included maximum contaminant levels (MCLs) and secondary maximum contaminant levels (SMCLs), which are presented in table 5 (EPA, 2020a, b).

Wilcoxon Tests

Probability values (*p*-values) from two-sided Wilcoxon rank sum tests (Wilcoxon tests) were computed to compare the groundwater chemistry of the east and west subbasins. The Wilcoxon test is a nonparametric method to test if the distributions, or percentiles, of two groups of data are similar or not (Helsel and others, 2020). In this case, the data were chemistry values, and the two groups were distinguished by the subbasin (east or west) from which the data were obtained. The nonparametric Wilcoxon test does not assume a shape for the data distribution and is therefore more appropriate for this dataset than are parametric alternatives, while remaining less computationally expensive than permutation tests (Helsel and others, 2020). Wilcoxon tests were performed on uncensored data by using the "wilcox.test" function of the "stats" base R package, version 3.5.3 (R Core Team, 2019), whereas censored data

were processed using the "cendiff" function of the "NADA" package, version 1.6–1.1 (Lee, 2020). The null and alternative hypotheses evaluated by the Wilcoxon tests were as follows:

Null hypothesis = data values are similar in both subbasins;

Alternative hypothesis = data values differ between subbasins.

The two-sided approach used for the Wilcoxon test considers evidence in both directions (values in one dataset are typically larger or smaller than values in the other) when evaluating the likelihood of the null hypothesis being false (Helsel and others, 2020). The *p*-value computed by the Wilcoxon test represents a measure of the likelihood of the null hypothesis being true (Helsel and others, 2020). Smaller *p*-values indicate that it is less likely that the null hypothesis is true and thereby encourage adoption of the alternative hypothesis. A *p*-value threshold of 0.05 is commonly used to reject the null hypothesis and represents a 5 percent chance of incorrectly rejecting the null hypothesis (Helsel and others, 2020). This threshold was adopted for all Wilcoxon-test interpretations in this report to avoid a higher likelihood of incorrectly failing to reject the null hypothesis by selecting a stricter criterion (for example, *p*-value of 0.01) while still being selective. *P*-values were not computed for constituents with fewer than eight data values in a subbasin or for those for which more than one-third of the data were censored.

Boxplots, Dotplots, and Spatial Plots

Boxplots are presented for select constituents and were constructed by using the "geom_boxplot" function of the "ggplot2" R package, version 3.2.1 (Wickham, 2016). Data were aggregated by subbasin, in addition to being presented for the study area as a whole. The five summary statistics presented on these plots are as follows:

(1) Upper whisker = extension from the third quartile to the largest value that is no greater than the third quartile plus 1.5 times the interquartile range (IQR) of the data;

(2) Upper hinge = the third quartile (75th quantile);

(3) Median = the median data value (50th quantile);

(4) Lower hinge = the first quartile (25th quantile); and

(5) Lower whisker = extension from the first quartile (25-percent quantile) to the smallest value that is no less than the first quartile minus 1.5 times the IQR of the data.

Values that fall beyond the upper and lower whiskers are typically plotted individually and are sometimes classified as outliers or outside values (Tukey, 1977). In this case, dotplots were overlaid on the boxplots by using the "geom_dotplot" function in the "ggplot2" R package, version 3.2.1 (Wickham, 2016), and a distinct symbol was used to denote outside values. This approach was taken to favor a more informative presentation of data structure. Dotplot bin width was one-thirtieth (3.33 percent) of each constituent's data range—the default setting for the "geom_dotplot" function (Wickham, 2016).

Table 5.   Select U.S. Environmental Protection Agency water quality standards for drinking water and number of sampled sites in the San Agustin Basin, west-central New Mexico (2010–19), that exceeded contaminant levels.

[Water quality standards for drinking water from U.S. Environmental Protection Agency (2020a, b). Water quality data from Rinehart and others (2017) and U.S. Geological Survey (2021). MCL, maximum contaminant level; SMCL, secondary maximum contaminant level; μg/L, microgram per liter; NA, not available; mg/L, milligram per liter]

Element	Unit	MCL	SMCL	Number of sampled sites that exceeded MCL or SMCL
Aluminum	μg/L	NA	50–200	0
Antimony	μg/L	6	NA	0
Arsenic	μg/L	10	NA	2
Barium	μg/L	2,000	NA	0
Beryllium	μg/L	4	NA	0
Cadmium	μg/L	5	NA	0
Chloride	mg/L	NA	250	0
Chromium	μg/L	100	NA	0
Copper	μg/L	[1]1,300	1,000	0
Fluoride	mg/L	4	2	[2]3
Iron	μg/L	NA	300	0
Lead	μg/L	[1]15	NA	0
Manganese	μg/L	NA	50	0
Nitrate as nitrogen	mg/L	10	NA	1
Nitrite as nitrogen	mg/L	1	NA	0
pH	standard units	NA	6.5–8.5	5
Selenium	μg/L	50	NA	0
Silver	μg/L	NA	100	0
Sulfate	mg/L	NA	250	1
Thallium	μg/L	2	NA	0
Total dissolved solids	mg/L	NA	500	1
Zinc	μg/L	NA	5,000	0

[1]Lead and copper are regulated by a treatment technique that requires systems to control the corrosiveness of their water. If more than 10 percent of tap water samples exceed the action level, water systems must take additional steps. The action level for copper is 1,300 μg/L and for lead is 15 μg/L.

[2]Exceeds SMCL only.

Spatial plots that were made in ArcGIS Pro (version 2.5.0) are also presented for the same select constituents. Data points were sized and colored according to their magnitude and bin thresholds corresponding to the summary statistics described above. The appropriate quartile(s) plus and (or) minus 1.5 times the IQR of the data were included as thresholds in instances where data values extended beyond the upper and (or) lower whiskers—this differed from the boxplot whiskers, which terminated at a data point rather than extending to a calculated value.

Stable Isotopes

Stable isotope ratio interpretation was facilitated by constructing a scatterplot of $\delta^{18}O$ versus δ^2H. Data values were overlaid on the local meteoric water line (LMWL) for the Middle Rio Grande Basin, as estimated by Plummer and others (2012), in addition to the global meteoric water line (GMWL) (Craig, 1961). These data values were colored by subbasin and symbolized by aquifer unit. Spatial plots, like those described above, were also constructed with the stable isotope data, and Wilcoxon tests were performed to compare the east and west subbasin data.

Principal Component Analysis

PCA was used to further compare east and west subbasin groundwater chemistry. PCA is an unsupervised exploratory data analysis technique that is commonly used to better understand and visualize data structure. This technique is accomplished by reprojecting the data as weighted linear combinations of all data variables to ease pattern recognition and identify influential variables (Hastie and others, 2009; James and others, 2013). The linear combinations are called principal components (PCs) and are computed such that they account for a descending amount of dataset variance. Therefore, PC1 accounts for the most variance in the data, followed by PC2, and so on. There are as many PCs as there are analyzed variables, and they have the following mathematical form:

$$PC_i = \lambda_1 V_1 + \lambda_2 V_2 + \ldots + \lambda_{nvar} V_{nvar} \qquad (4)$$

where

PC_i	is principal component score ($i = 1$ to $nvar$);
λ_i	is the weight (also known as loading) derived from PCA, where subscripts denote variable number;
V_i	is the original data value for a given variable, where subscripts denote variable number; and
$nvar$	is total number of variables analyzed.

Loadings are calculated by using eigen decomposition and are related to the correlation between variables and the amount of variance explained by a variable (Hastie and others, 2009; James and others, 2013). In this study, variables were chemical constituents, and the data were a subset of the 2010–19 groundwater chemistry data.

Select chemical constituents and sampled sites were excluded from the PCA to meet the method's requirement of a complete data matrix, meaning no missing or censored values are acceptable. PCA was therefore performed on two dataset variants. The first variant favored more sites (41 total) at the expense of analyzing fewer constituents (17 total), whereas the second variant analyzed more constituents (25 total) but fewer sites (34 total). The results from both analyses were similar; therefore, only the second variant (25 constituents, 34 sites) is presented for simplicity and to permit the evaluation of more constituents. Overall, 51 percent of available chemical constituents were considered at 77 percent of available sites. The considered chemical constituents were arsenic, bicarbonate (filtered), boron, bromide, calcium, chloride, chromium, δ^2H, $\delta^{18}O$, dissolved oxygen, fluoride, hardness, lithium, magnesium, pH (field), potassium, silica, sodium, strontium, sulfate, temperature, TDS (dried), uranium, vanadium, and zinc. The excluded sites were sites 2, 6, 7, 10, 18, 19, 31, 32, 42, and 44. Specific conductance was omitted from the analysis because it was well represented by dried TDS (Pearson correlation coefficient = 0.97). This analysis yielded a nearly even distribution of sites between the east (16 sites, 47 percent) and west (18 sites, 53 percent) subbasins, although data availability limitations resulted in densely spaced sites in the western portion of the west subbasin. West subbasin data and associated interpretations are therefore more biased towards this part of the subbasin.

PCA results can be sensitive to outliers, thereby requiring anomalous data values to be addressed prior to analysis (Hastie and others, 2009). Boxplots were evaluated to identify potential outliers that could skew PCA results. Outlier data were considered to be those that met the "far out" value criterion proposed by Tukey (1977). This criterion flags any data point as a potential outlier when it lies beyond the third or first quartile plus or minus, respectively, three times the interquartile range of the data. This approach is versatile, as it does not require assumptions about the distribution of the data, and is typically considered to be a conservative outlier classification scheme (Iglewicz and Hoaglin, 1993). Overall, just 1.6 percent (14 of 850) of data values for a total of nine constituents met this criterion. Five constituents (arsenic, boron, chloride, sulfate, uranium) had just one anomalous data value, three constituents (bromide, lithium, strontium) had two values, and one constituent (zinc) had three values. All identified outliers were anomalously high, rather than low, relative to the rest of the data. The influence of outliers on PCA was reduced by lowering the values of outlier data to the corresponding "far out" value criteria, thus making the outlier data less extreme but still maintaining a degree of their abnormality. This approach is called winsorizing and was favored over removal of the outliers and their corresponding site or constituent (Ghosh and Vogt, 2012).

PCA was implemented by using the "prcomp" function of the "stats" base R package, version 3.5.3 (R Core Team, 2019). Data were shifted to be zero centered and scaled to have a unit variance, as advised in most cases, especially when constituent units differ (Hastie and others, 2009; James and others, 2013). Biplots were produced by using the "ggbiplot" function within the "ggbiplot" R package, version 0.55 (Vu, 2011). Biplot data were colored by east and west subbasin to facilitate comparison. Additionally, Wilcoxon tests, as described above, were performed on all PC scores to further compare the chemistry variability between the subbasins.

Clustering algorithms are often applied to PCA results to identify groups of similar data within the reprojected PC domain. K-means and hierarchical clustering techniques (Hastie and others, 2009; James and others, 2013) were performed on the PCA results, but a lack of strong cluster structure in the data and seemingly ambiguous cluster patterns discouraged interpretation and presentation of the clustering results. Cluster structure was evaluated in terms of the mean silhouette widths computed for cluster solutions of 1–10 clusters by using the "silhouette" function of the "cluster" base R package, version 2.0.7–1 (Maechler and others, 2019). The mean silhouette width metric attempts to classify the likeness, or similarity, of data that are assigned to the same clusters and ranges from −1 to 1 (Everitt and others, 2011). Cluster solutions with a mean silhouette width of about 0.5 or greater are thought to be reasonable solutions, whereas those of about 0.2 or less represent a lack of substantial cluster structure (Everitt and others, 2011). Maximum mean silhouette width calculated in this study was 0.34, which was between the aforementioned criteria. Further inspection of clustering results revealed minimal aquifer or spatial dependence of clustering results, which further suggested a lack of meaningful cluster structure.

Groundwater Age

Qualitative groundwater age, or residence time, was evaluated by using the 2010–19 tritium data. Tritium is a radioactive isotope of hydrogen with a half-life of 12.32 years (Lucas and Unterweger, 2000). Widespread atomic bomb testing in the 1950s and 1960s substantially increased atmospheric tritium concentrations, which have been declining following the suspension of aboveground atomic testing (Motzer, 2008). This anthropogenic flux of atmospheric tritium elevated the tritium concentrations in groundwater that was recharged after about 1953, relative to that which recharged prior to 1953. As a result, groundwater tritium concentrations can qualitatively indicate groundwater age. The classification system developed by Lindsey and others (2019) was used to determine premodern (before 1953) and modern (1953 and after) age thresholds for the tritium measurements, where values between these two thresholds were classified as being mixed. Tritium estimates in precipitation for threshold computations were obtained from a quadrangle map (lat 33° to 35° N., long −105° to −110° W.) of Michel and others (2018). Following Lindsey and others (2019), a premodern threshold of 0.61 pCi/L was computed by using the average estimated precipitation tritium concentration from 2008 through 2012 (Michel and others, 2018). Modern thresholds were calculated for 2010 (7.16 pCi/L) and again for 2019 (4.32 pCi/L) to give a range of thresholds to account for the short half-life of tritium.

Groundwater ages were also estimated by using carbon-14, which is a naturally occurring radioactive isotope of carbon with a half-life of about 5,730 years (Plummer and others, 2012). The long half-life of carbon-14 makes it ideal for estimating the age of groundwater that recharged about 100 years ago to groundwater that recharged more than 20,000 years ago (Nishikawa and others, 2004). Per standard practice, carbon-14 data were reported as absolute percent modern, which had been normalized to a common carbon-13 value of −25 per mil by the reporting laboratory. To facilitate interpretation, these values were denormalized to units of percent modern carbon by using the approach of Plummer and others (2012) as follows:

$$a_D = a_N \left[(1 + \delta^{13}C/1{,}000)/0.975 \right]^2 \exp\left[-(t - 1{,}950)/8{,}267 \right] \qquad (5)$$

where

a_D is the denormalized carbon-14 of the sample at the time of sample collection, in percent modern carbon;

a_N is the reported normalized carbon-14, in absolute percent modern;

$\delta^{13}C$ is the delta carbon-13/carbon-12 of the dissolved inorganic carbon, in per mil;

t is the calendar year of sample collection, in YYYY format; and

8,267   is $1/\lambda$, where λ is the carbon-14 decay constant, or $(ln\ 2)/(5{,}730)$ in this study, where 5,730 is the modern carbon-14 half-life in years.

The denormalized carbon-14 data in percent modern carbon were derived relative to the specific activity of National Bureau of Standards oxalic acid, where 13.56 disintegrations per minute per gram of carbon in the year 1950 equals 100 percent modern carbon (pmC) (Nishikawa and others, 2004). As for tritium, atomic testing in the 1950s and 1960s increased atmospheric carbon-14 levels, sometimes yielding percent modern carbon values exceeding 100 pmC for waters recharged after about 1950 (Nishikawa and others, 2004). Generally, larger carbon-14 values indicate younger waters, whereas smaller carbon-14 values represent older waters. Carbon-14 values were spatially plotted to permit qualitative interpretation of their relative concentrations. The measured percent modern carbon concentrations that were qualitatively interpreted were not corrected for subsurface sources of carbon-14 that can commonly make groundwater seem older than it truly is (Nishikawa and others, 2004).

Corrected carbon-14 ages that considered radioactive decay and subsurface chemical reaction with carbonate sources were calculated to provide quantitative groundwater age estimates. Sites that had carbon-14 data but lacked dissolved inorganic carbon data, such as bicarbonate and carbonate, were excluded from correction analysis because of the inability to make reasonable corrections. Corrected carbon-14 groundwater ages in general are inherently uncertain because of the difficulty in comprehensively accounting for subsurface chemical reactions and mixing that may affect computed ages. This uncertainty should be kept in mind when interpreting results from this type of analysis and an estimated age range is reported herein. Model 11 "Revised F&G solid ex" (revised Fontes and Garnier solid exchange; Han and Plummer, 2013) in NetpathXL was used to model corrected groundwater ages on the basis of total dissolved inorganic carbon (sum of inorganic carbon species carbonic acid, bicarbonate, and carbonate), carbon-13, and carbon-14 data (Parkhurst and Charlton, 2008). The model assumes that the carbon inputs to the system are from soil gas and dissolution of carbonate species and estimates groundwater age based on the carbonate dissolution and change in carbon isotopic value (Han and Plummer, 2013). The presence of bicarbonate and calcium, along with relatively low delta carbon-13/carbon-12 values, in sampled groundwater implied groundwater interaction with a carbonate source and thereby suggested that the selected model was appropriate for the study area. Carbon-14 values of 0 pmC for solid carbonate and 100 pmC for soil gas were assumed, along with carbon-13 values of −1.85 per mil for solid carbonate (Muller and Mayo, 1986) and −21 and −16 per mil for soil gas (Huth and others, 2019). The two soil gas values were assumed to be reasonable bounding representations of anticipated soil conditions on the basis of typical values and were both modeled to provide a range for the corrected carbon-14 ages at each site. These corrected age calculations made no attempt to account for younger waters mixing with older waters. Samples were then plotted using the method from Han and Plummer (2016) and the aforementioned assumed values to further understand the reaction and mixing

processes potentially influencing the carbon-14 age results. This plotting procedure was used to qualify age estimates on the basis of their expected reliability. The details of this plotting procedure are discussed in the "Results and Discussion" section of this report.

Results and Discussion

Groundwater Elevation

Results from the groundwater elevation analyses can be used to interpret prominent groundwater flow patterns in the San Agustin Basin, along with the temporal dynamics of those patterns over the 1975 through 2019 period. Kriging estimations of median groundwater elevation within the basin-fill and alluvium aquifer system are shown in figure 7. Groundwater elevations were highest and had the steepest gradients near the foothills of the Mangas and Datil Mountains. Gradients were lowest along the east-west central axis of the basin. East subbasin groundwater elevations were generally higher than those of the west subbasin.

Interpreted groundwater flow patterns are illustrated in figure 7. These patterns were derived by using the hydrologic principle that groundwater flows in directions that are perpendicular to groundwater elevation contours and from high to low values of hydraulic head (Ingebritsen and others, 2006). These results indicate that groundwater flows from the highlands towards the east-west central axis of the basin, where it then generally moves from east to west. There were localized areas of relatively low groundwater elevations in the eastern portion of the east subbasin, but nearby historical median groundwater elevation data near the watershed boundary were larger than the interpolated elevations (fig. 7). These lower elevations are therefore not an implication of eastward groundwater movement but are instead localized map features that are driven by data scarcity. The lowest groundwater elevations were in the southwestern portion of the west subbasin, suggesting underflow through the local highlands into the northern East Fork Gila River watershed. Data from site 6 informed the lowest estimated groundwater elevations in this area, with a median groundwater elevation of 6,721.05 ft, which was about 19 ft less than the nearest observed median values at sites 8 and 9 (table 4, fig. 4). Therefore, additional data are required to more confidently evaluate the groundwater connectivity of the basin with the northern East Fork Gila River watershed. Historical median groundwater elevations observed outside of the contoured area in the northern East Fork Gila River watershed (6,592 and 6,545 ft) were more than 125 ft lower than that of site 6 (figs. 4 and 7), thereby further supporting underflow from the basin into the northern East Fork Gila River watershed. Overall, kriged groundwater elevations indicated prevalent regional east to west groundwater flow with possible underflow leaving the basin towards the northern East Fork Gila River watershed.

Scarcity of groundwater elevation data resulted in zones of greater estimation uncertainty, as indicated by the standard error from the application of kriging in figure 8. Areas with the greatest standard errors were along the perimeter of the contoured region in the east subbasin and were excluded from the groundwater elevation map because of their high uncertainty (figs. 7 and 8). Remaining areas of elevated standard errors are less certain than those of smaller standard errors, which should be considered when making localized interpretations.

Estimated groundwater elevation gradients were gentle (about 2 feet per mile) near the McClure Hills (fig. 7), thereby suggesting that groundwater slowly flows from the east subbasin into the west subbasin. The overall difference in groundwater elevations between the subbasins supports groundwater flow from east to west (fig. 7), though elevated standard errors near the McClure Hills highlight the uncertainty of the hydrologic connectivity between the two subbasins (fig. 8). Previous researchers who considered different time periods of groundwater elevation data reported similar groundwater flow patterns, thereby suggesting that subbasin connectivity is common through time (Blodgett and Titus, 1973; Myers and others, 1994; Rinehart and others, 2017).

Median annual gradients (groundwater elevation change over time) for 1975 through 2019 are presented in figure 9. Unlike the kriging analysis, the temporal analysis considered all wells with repeat measurements, regardless of aquifer type, throughout the entire study area (98 wells). Because median annual gradients were calculated for any site that had at least two measurements from 1975 through 2019, the gradients are not necessarily representative of the entire period of investigation but serve as reasonable estimates. The region considered for the groundwater elevation map is outlined in figure 9 for context. Generally, temporal gradients indicate that most groundwater elevations in the lowlands changed little (−0.2 to 0.2 foot per year [ft/yr]), thereby also suggesting that lowland groundwater flow patterns have likely been more or less stable over time under current climate and development conditions. This finding supports the use of median data values in the kriging analysis as a reasonable representation of lowland groundwater elevations within the basin-fill and alluvium aquifer system; 71 percent of the 63 contoured sites with repeat measurements had annual gradients between −0.2 and 0.2 ft/yr. A group of irrigation wells in the northeast basin was a notable exception to the stability of lowland groundwater elevations over time; this deviation was likely due to variable irrigation pumping throughout the period of interest. Groundwater elevations were more time sensitive in the highlands, where precipitation is more prevalent and relatively shallow depths to groundwater are more common (Phillips and others, 1992; Myers and others, 1994; Rinehart and others, 2017). This contrast with the lowlands is evidence that most groundwater recharge takes place in the highlands, with minimal recharge in the lowlands, and is consistent with the groundwater flow patterns depicted in figure 7. Median change for all sites was −0.05 ft/yr, which indicates that groundwater elevations may have slightly declined on average between 1975 and 2019. Overall, 86 of the 98 sites (88 percent) had median annual gradients between −0.5 and 0.5 ft/yr, and 51 of those sites (52 percent) had values between −0.1 and 0.1 ft/yr (fig. 9).
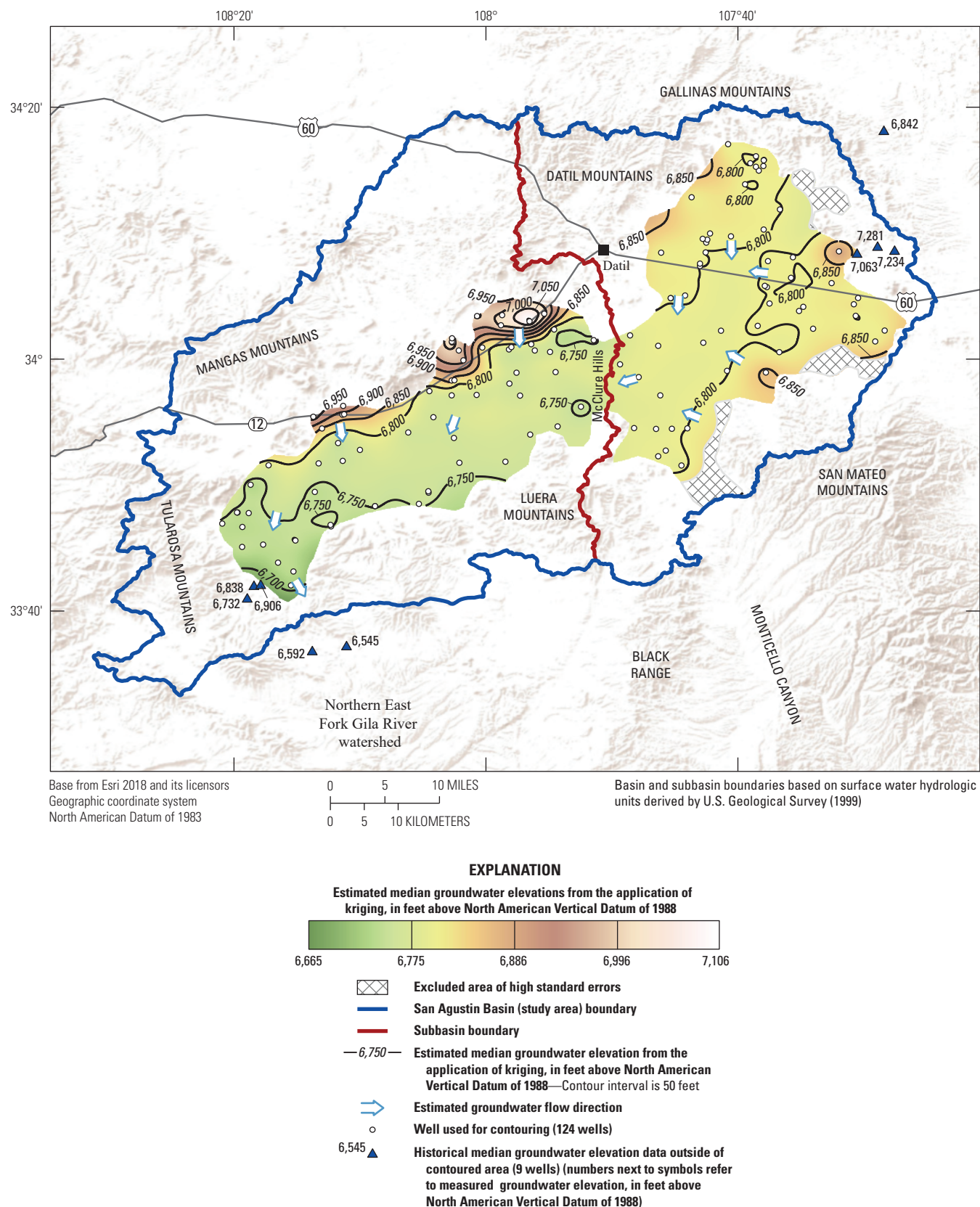
Figure 7.   Estimated median groundwater elevations and groundwater flow patterns in the basin-fill and alluvium aquifer system in the lowlands of the San Agustin Basin, west-central New Mexico (1975–2019). Historical groundwater elevation data from the U.S. Geological Survey (USGS) National Water Information System (USGS, 2021) are also provided to aid interpretations.
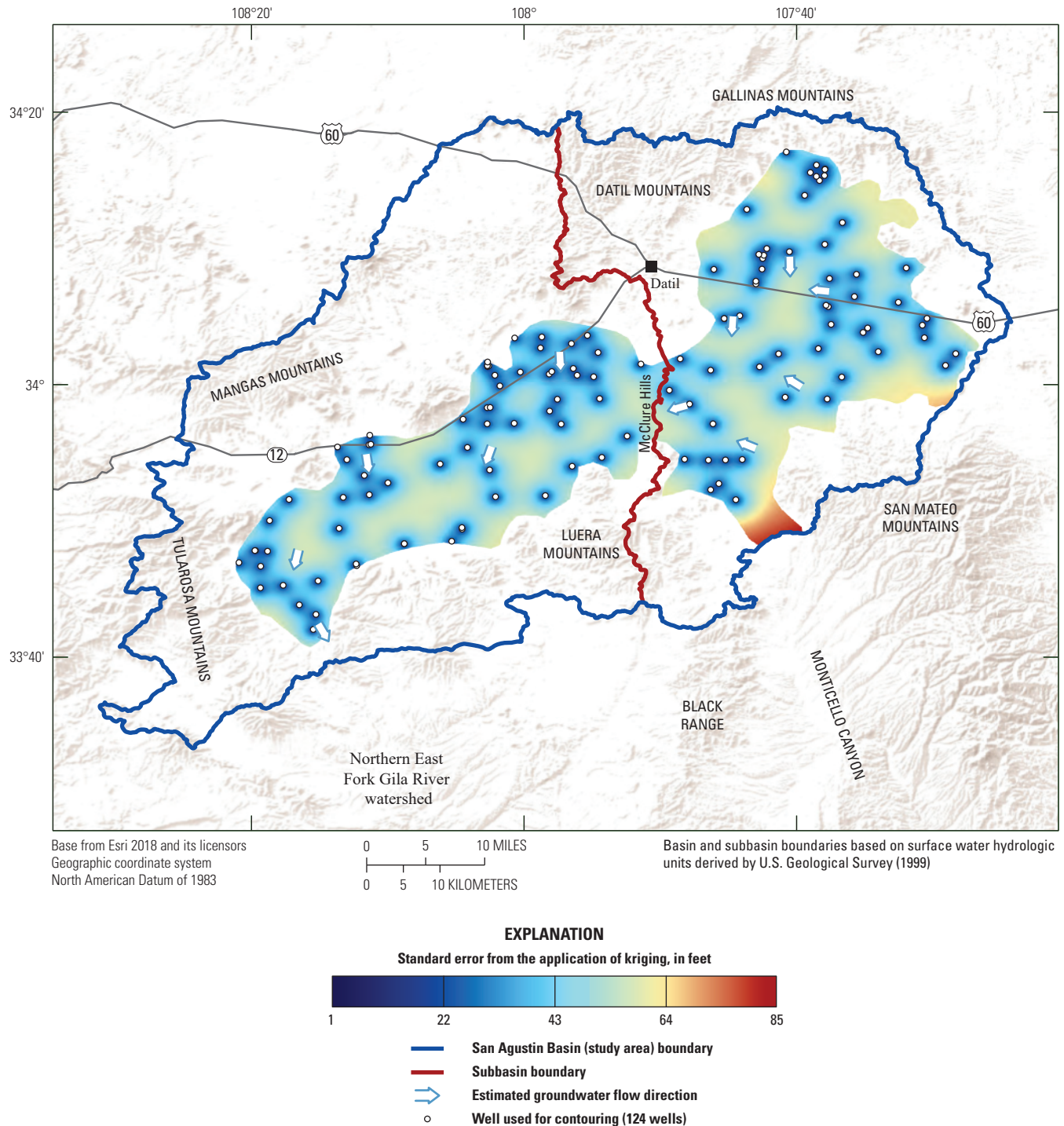
Figure 8. Standard error of groundwater elevation estimations in the lowlands of the San Agustin Basin, west-central New Mexico (1975–2019), from the application of kriging.
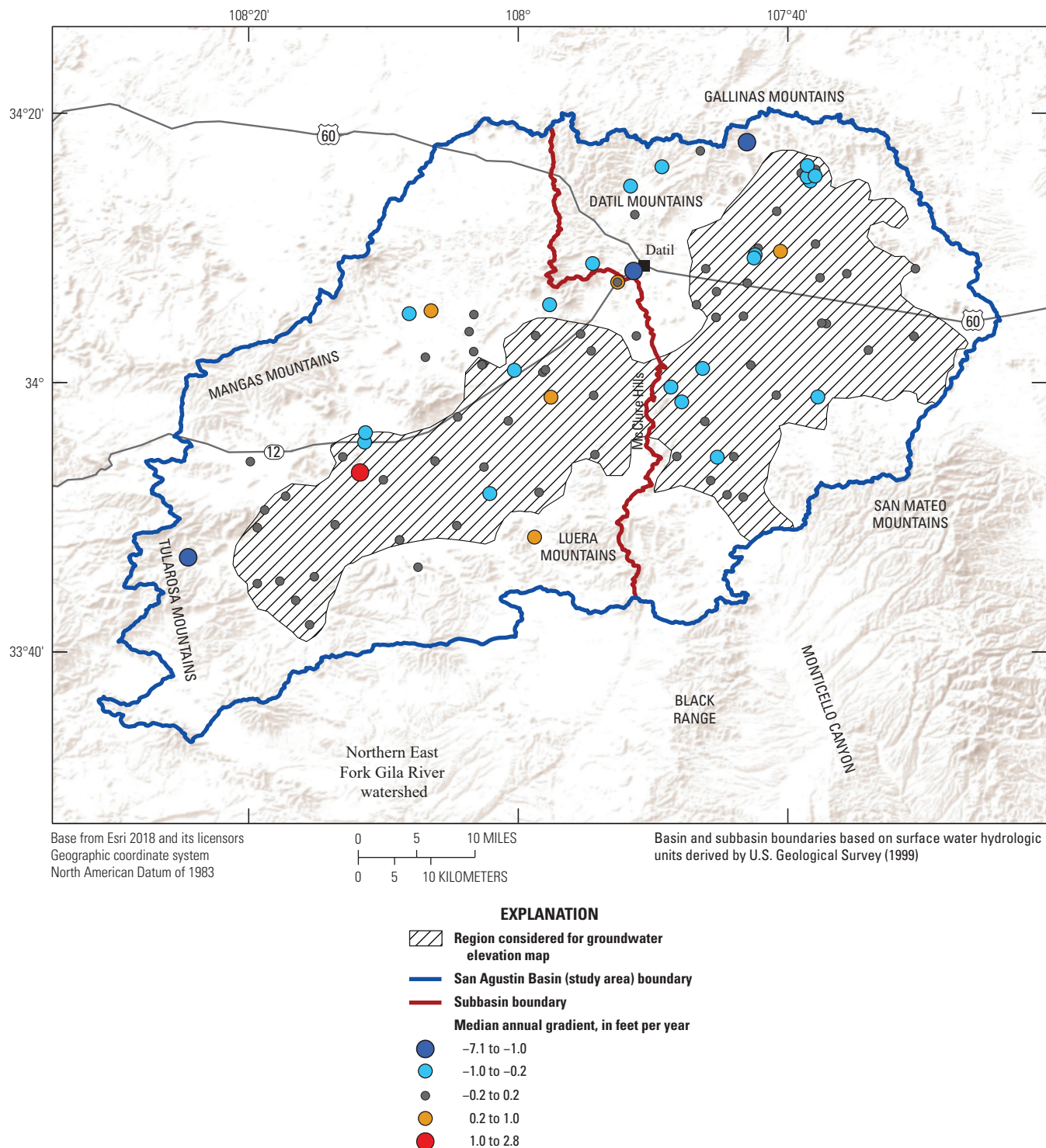
Figure 9.   Median annual gradients (groundwater elevation change over time) for all wells with repeat measurements from 1975 through 2019, regardless of aquifer type, throughout the San Agustin Basin, west-central New Mexico (98 wells). Because median annual gradients were calculated for any site that had at least two measurements from 1975 through 2019, the gradients are not necessarily representative of the entire period of investigation but serve as reasonable estimates.

Groundwater Chemistry

Groundwater chemistry results can further illustrate the dynamics of groundwater flow in the San Agustin Basin, and general water quality knowledge is helpful for residents, resource managers, and other stakeholders. The major ion chemistry of basin groundwater is presented on a Piper diagram in figure 10. Waters were mainly bicarbonate-carbonate type with a broad distribution of cation chemistry across calcium, sodium, and potassium. Three sites (1, 2, and 6) in the west subbasin had notably elevated chloride concentrations, and one site (31) in the west subbasin had a larger sulfate concentration relative to most sites (labeled in fig. 10). Major ion chemistry showed minimal dependence on aquifer type, suggesting that the aquifers are generally well connected. Major ion chemistry was also similar in both the east and west subbasins.

Subbasin chemistry results for 2010 through 2019 were quantitatively compared to one another by using Wilcoxon tests, where p-values less than 0.05 were assumed to indicate statistically distinct chemistry between subbasins. The Wilcoxon test results for all analyzed constituents are presented in figure 11 and table 6. Of the constituents considered, only potassium (p-value = 0.04) and temperature (p-value = 0.04) yielded statistically significant p-values. Thus, with these two slight exceptions, the data did not demonstrate a statistically significant difference between subbasins. Spatial plots, dotplots, and boxplots of groundwater potassium concentrations and temperatures are shown in figures 12 and 13, respectively. Colors and sizes of data points in the spatial plots were selected on the basis of quartiles for each constituent (see "Methods" section). Potassium concentrations were greater in the west subbasin (median = 2.13 mg/L) compared to the east subbasin (median = 1.60 mg/L). Potassium concentrations were highest in the southwestern portion of the west subbasin; the process resulting in these larger concentrations was not readily apparent but could be further explored in the future. Temperatures varied more and were larger in the east subbasin (median = 17.50 degrees Celsius) relative to the west subbasin (median = 16.00 degrees Celsius). Sampling conditions, such as air temperature and flow rate, can affect measured groundwater temperature. However, median well depths of sampled sites in the east and west subbasins were 469 ft and 210 ft, respectively. Therefore, the subbasin temperature contrast is consistent with a relation to well depth, since subsurface temperatures typically increase linearly with depth (Ingebritsen and others, 2006). A Wilcoxon test comparing well depths in the subbasins yielded a p-value of 0.002, which was substantially less than the assumed significance level of 0.05 and offered further support that the temperature differential is a result of well depth variation.

Groundwater quality was generally good throughout the basin in comparison with EPA drinking water standards. TDS concentrations had a median of 211 mg/L and ranged from 154 to 572 mg/L (fig. 14). Site 31 near the McClure

Hills (fig. 14) was the only sampled site in excess of the TDS SMCL of 500 mg/L (table 5). TDS concentrations were greater than average in groundwater from some sites within the southwestern portion of the west subbasin (fig. 14). A prominent gap in recent TDS data exists for the lowest elevations of the west subbasin (between sites 13 and 26) because the lack of wells with existing groundwater pumps does not allow practical sampling. Historical data and anecdotal accounts indicated poor water quality within the lacustrine and playa deposits in this area, with TDS, as estimated from specific conductance data, exceeding 25,000 mg/L (site identifier 334927108133301 in table 3.1 in app. 3). A systematic lateral trend in TDS was not observed despite the east to west regional groundwater flow pattern indicated in the groundwater elevation map (fig. 7). Generally, TDS would be expected to increase downgradient because of rock/water interactions. The lack of this pattern may be the result of mixing with local recharge and variable sediment reactivity. Depending on the local geology where recharge occurs, that groundwater could have either larger TDS, contributing to the typical pattern of larger TDS downgradient, or smaller TDS, contributing to the lack of a clear pattern. It is also possible that localized flow paths may pass through low-permeability playa deposits that are continuing to release high TDS groundwater over time, whereas other flow paths travel around these locations. Faulting and the complex multigraben structure of the basin also likely lead to variable groundwater residence times and regional flow rates, further obscuring the expected TDS pattern.

The median groundwater pH value was 7.90, which is slightly basic but still within the EPA SMCL range of 6.5–8.5 for pH (table 5). Measured pH values ranged from 6.4 to 9.0. Two sites (19 and 20) had pH values that were less than the SMCL, whereas three sites (32, 37, and 44) had values in excess of the SMCL. Groundwater pH in the east subbasin spatially varied more than that of the west subbasin (fig. 15), with variances of 0.52 and 0.07, respectively. Measured pH values were predominantly more basic along the subbasin divide near the McClure Hills and Luera Mountains.

While most sites complied with EPA drinking water standards for TDS and pH, some sites exceeded EPA levels for other constituents (table 5). Two sites (27 and 41) exceeded the EPA MCL for arsenic of 10 µg/L. Three sites (2, 21, and 27) exceeded the SMCL of 2 mg/L for fluoride. One site (38) slightly exceeded the nitrate MCL of 10 mg/L. In addition to exceeding the TDS SMCL, one site (31) had a sulfate concentration of 275 mg/L (table 3.1 in app. 3), which slightly exceeded the sulfate SMCL of 250 mg/L. Overall, exceedances of EPA drinking water standards were rare and not extreme, thereby suggesting that water quality in the sampled wells is generally favorable for consumption.

The composition of stable isotopes in groundwater can help identify recharge elevation and season, evaporative signals, and geothermal contributions to further inform the understanding of groundwater dynamics (Faure, 1986; Kendall and others, 1995). A scatterplot of $\delta^{18}O$ and $\delta^{2}H$ groundwater
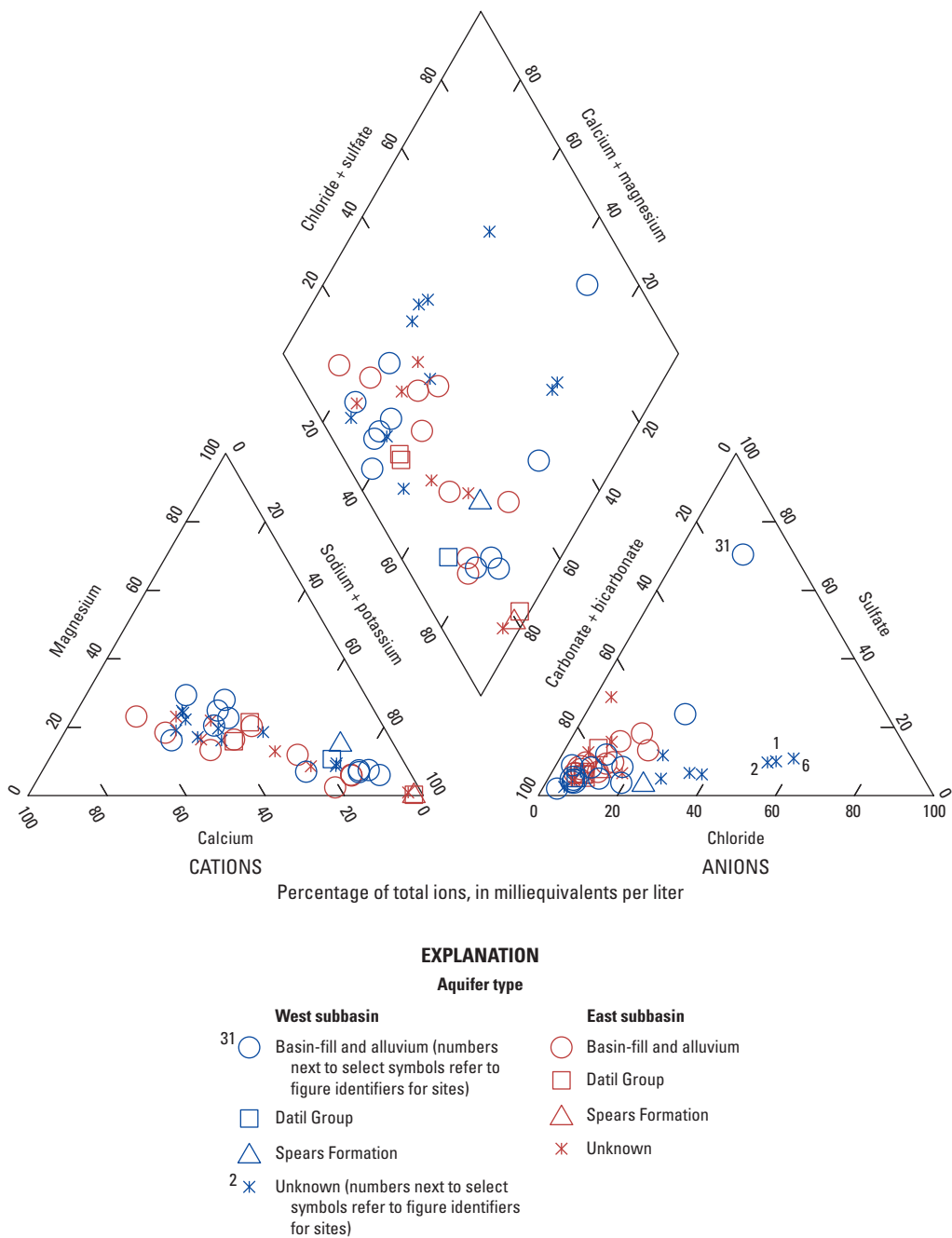
Figure 10. Piper diagram showing the major ion proportion of groundwater samples collected in the San Agustin Basin, west-central New Mexico (2010–19). Figure identifiers correspond to those used in the tables of this report, and sites are plotted spatially in figure 4.

stable isotope ratios, along with the LMWL and GMWL, is presented in figure 16. δ²H values ranged from −88.80 to −61.39 per mil, and δ¹⁸O values ranged from −12.25 to −7.69 per mil. Most samples plotted along the LMWL for the Middle Rio Grande Basin (Plummer and others, 2012) and approximately paralleled the GMWL (Craig, 1961) with a right shift. Site 27 plotted notably to the left of both meteoric water lines, whereas sites 23 and 38 plotted notably to the

right. The latter samples may be associated with evaporation prior to infiltration, a minor geothermal component, or mixing with evaporated or geothermal waters. Stable isotope values showed no clear dependence on aquifer type or subbasin (figs. 11 and 16). Furthermore, no correlation was found with land-surface elevation for the sampled wells (δ²H Pearson correlation coefficient = 0.02; δ¹⁸O Pearson correlation coefficient = −0.05), which is expected because of
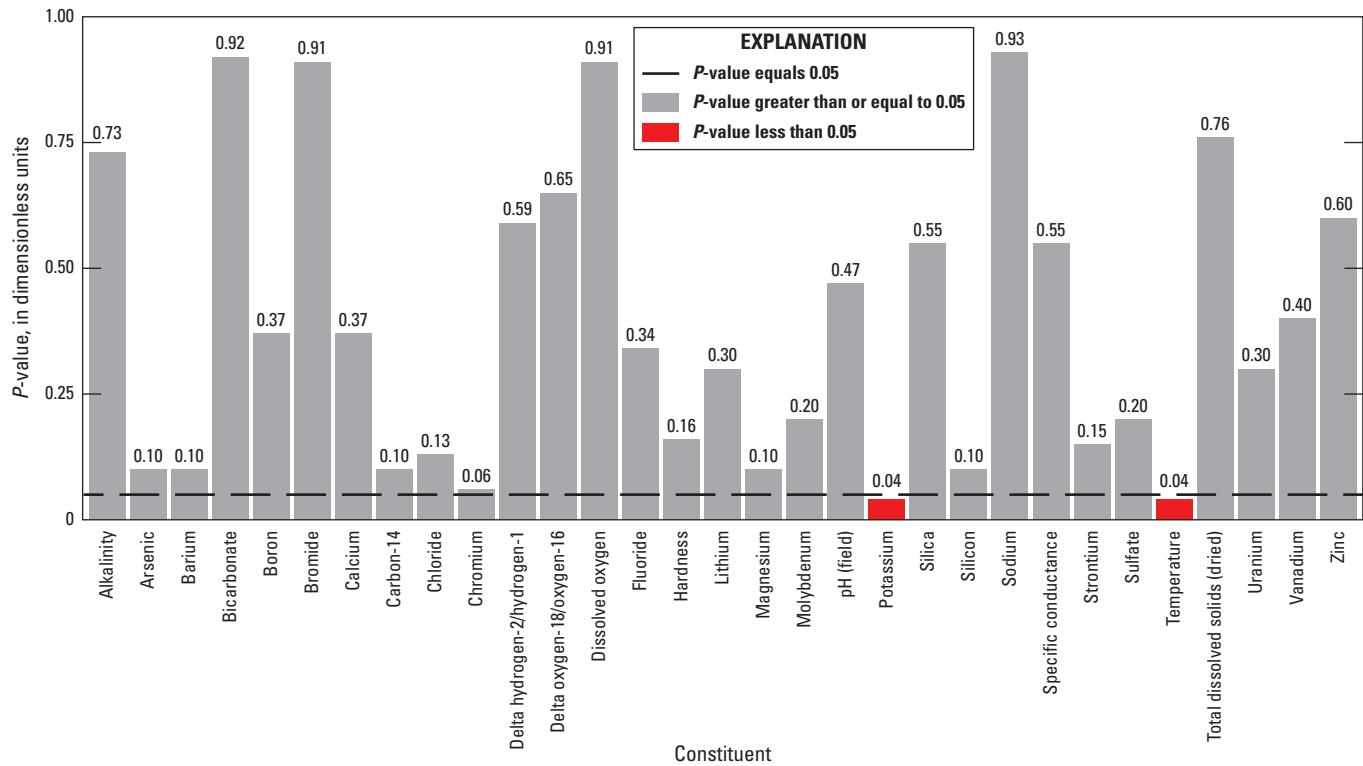
Figure 11. Wilcoxon probability values (*p*-values) that resulted from comparing the east and west subbasins in the San Agustin Basin, west-central New Mexico (2010–19), for analyzed constituents.

the lack of widespread recharge across the basin. Wilcoxon tests comparing east and west subbasin groundwater isotopes yielded *p*-values of about 0.6 for both isotopes (fig. 11). Despite minimal quantitative distinction between east and west subbasin stable isotope values, the most isotopically depleted (most negative) values were more common in the eastern portion of the basin (figs. 17 and 18). This pattern may be influenced by recharge at higher elevations and (or) colder temperatures.

Principal Component Analysis

PCA was performed on select constituents to further compare east and west subbasin groundwater chemistry. A biplot displaying reprojected PC values (scores) and corresponding variable loading vectors for PC1 and PC2 is presented in figure 19. The length and orientation of loading vectors correspond to variable influence on the associated PCs. Loading vector arrowheads point in the direction of high original data values, whereas low values plot directly 180 degrees from arrowheads. The first two PCs accounted for 52.2 percent of total dataset variance and had loading vectors that were generally similar in length. Much of the data grouped towards the top of the biplot opposite from most loading-vector arrowheads, indicating that low values of constituents were common with dataset variance largely being the result of less

common elevated values. No systematic point separation by subbasin was evident in the biplot. This overlap of sites from both subbasins within the PC domain is further evidence that groundwater chemistry is largely similar in the two subbasins.

Wilcoxon tests were performed on the PC scores from each subbasin to quantitatively compare subbasin chemistry in the reprojected PC domain; a *p*-value significance level of 0.05 was again assumed to indicate distinct PC scores for the subbasins. Resulting *p*-values are presented in figure 20. *P*-values for all PCs, except for PC6 (*p*-value = 0.003) and PC9 (*p*-value = 0.01), were greater than the significance level. A biplot of PC6 and PC9 is presented in figure 21, which shows a clear separation between points from each subbasin. Examination of the PCA loadings in this plot indicated larger pH, enriched stable isotopes, and larger chloride concentrations in the west subbasin and larger temperatures and sulfate concentrations in the east subbasin. On the basis of PCA, these constituents therefore represent the main groundwater chemistry differences between the subbasins, although Wilcoxon tests indicated that temperature (*p*-value = 0.04) was the only statistically significant of these constituents between the subbasins, as previously discussed. Furthermore, PCs 6 and 9 combined accounted for only 7.6 percent of total dataset variance, thereby indicating that these differences between the subbasins are minor. Overall, the PCA results indicate that groundwater chemistry is similar in each subbasin. Given the connectivity

Table 6.   Wilcoxon probability values (p-values) that resulted from comparing the east and west subbasins in the San Agustin Basin, west-central New Mexico (2010–19), for constituents measured in groundwater samples.

Constituent	P-value, in dimensionless units	Total number of measurements	Number of measurements in east subbasin	Number of measurements in west subbasin	Number of censored measurements
Alkalinity	0.73	27	8	19	0
Arsenic	0.10	38	19	19	2
Barium	0.10	38	19	19	8
Bicarbonate	0.92	42	19	23	0
Boron	0.37	38	19	19	0
Bromide	0.91	42	19	23	0
Calcium	0.37	42	19	23	0
Carbon-14	0.10	29	14	15	0
Chloride	0.13	42	19	23	0
Chromium	0.06	38	19	19	1
Delta hydrogen-2/hydrogen-1	0.59	44	20	24	0
Delta oxygen-18/oxygen-16	0.65	44	20	24	0
Dissolved oxygen	0.91	44	20	24	0
Fluoride	0.34	42	19	23	0
Hardness	0.16	42	19	23	0
Lithium	0.30	38	19	19	0
Magnesium	0.10	42	19	23	1
Molybdenum	0.20	38	19	19	12
pH, field	0.47	44	20	24	0
Potassium	0.04	42	19	23	0
Silica	0.55	42	19	23	0
Silicon	0.10	28	19	9	0
Sodium	0.93	42	19	23	0
Specific conductance	0.55	44	20	24	0
Strontium	0.15	38	19	19	0
Sulfate	0.20	42	19	23	0
Temperature	0.04	44	20	24	0
Total dissolved solids, dried	0.76	42	19	23	0
Uranium	0.30	38	19	19	3
Vanadium	0.40	38	19	19	1
Zinc	0.60	38	19	19	1

suggested by groundwater elevation analysis, these chemistry results suggest that the aquifer sediments are relatively unreactive, that mixing is prevalent, and that groundwater recharge conditions to both subbasins are likely similar.

Groundwater Age

Tritium is a useful tracer for determining if groundwater was recharged approximately before or after the year 1953. Following the approach of Lindsey and others (2019), tritium concentrations less than or equal to 0.61 pCi/L were classified as indicating premodern groundwater (before 1953), those greater than 4.32 pCi/L (2019 threshold) and 6.41 pCi/L (2010 threshold) were classified as indicating modern (1953 and after) recharge, and those in between were classified as indicating a mixture of premodern and modern recharge. Measured tritium concentrations ranged from less than the reporting level to 4.31 pCi/L (table 7). Eight of forty-four total sites (18.2 percent) exceeded the 0.61 pCi/L threshold for premodern waters; these eight sites were less than the thresholds set for modern waters, indicating that they are likely a mixture of old and modern waters. These low concentrations indicated
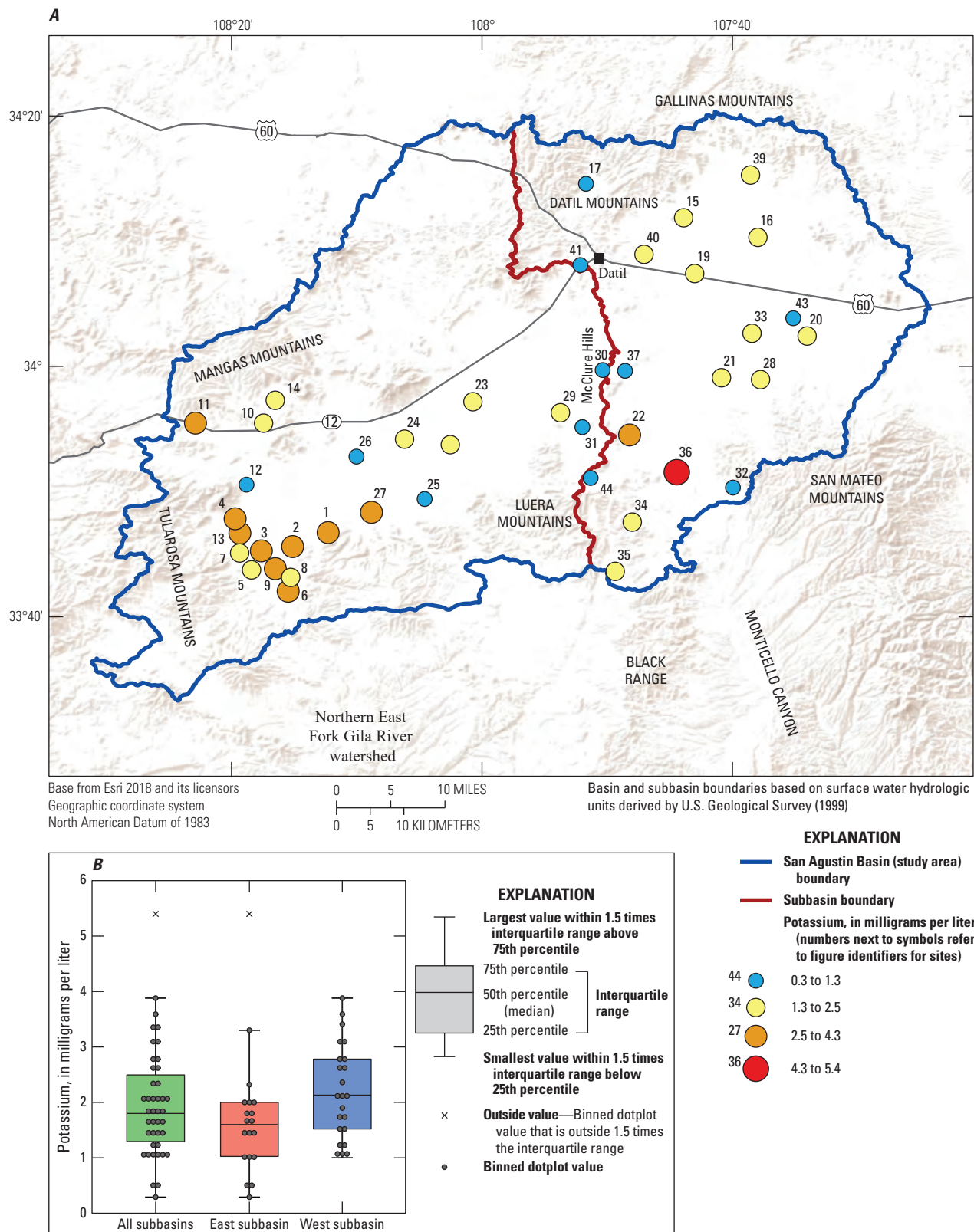
Figure 12. *A*, Spatial plot and *B*, dotplot and boxplot of groundwater potassium concentrations measured in samples collected in the San Agustin Basin, west-central New Mexico (2010–19). Bin thresholds for spatially plotted data points were based on data quartiles (see "Methods" section for more details). Figure identifiers correspond to those used in the tables of this report.
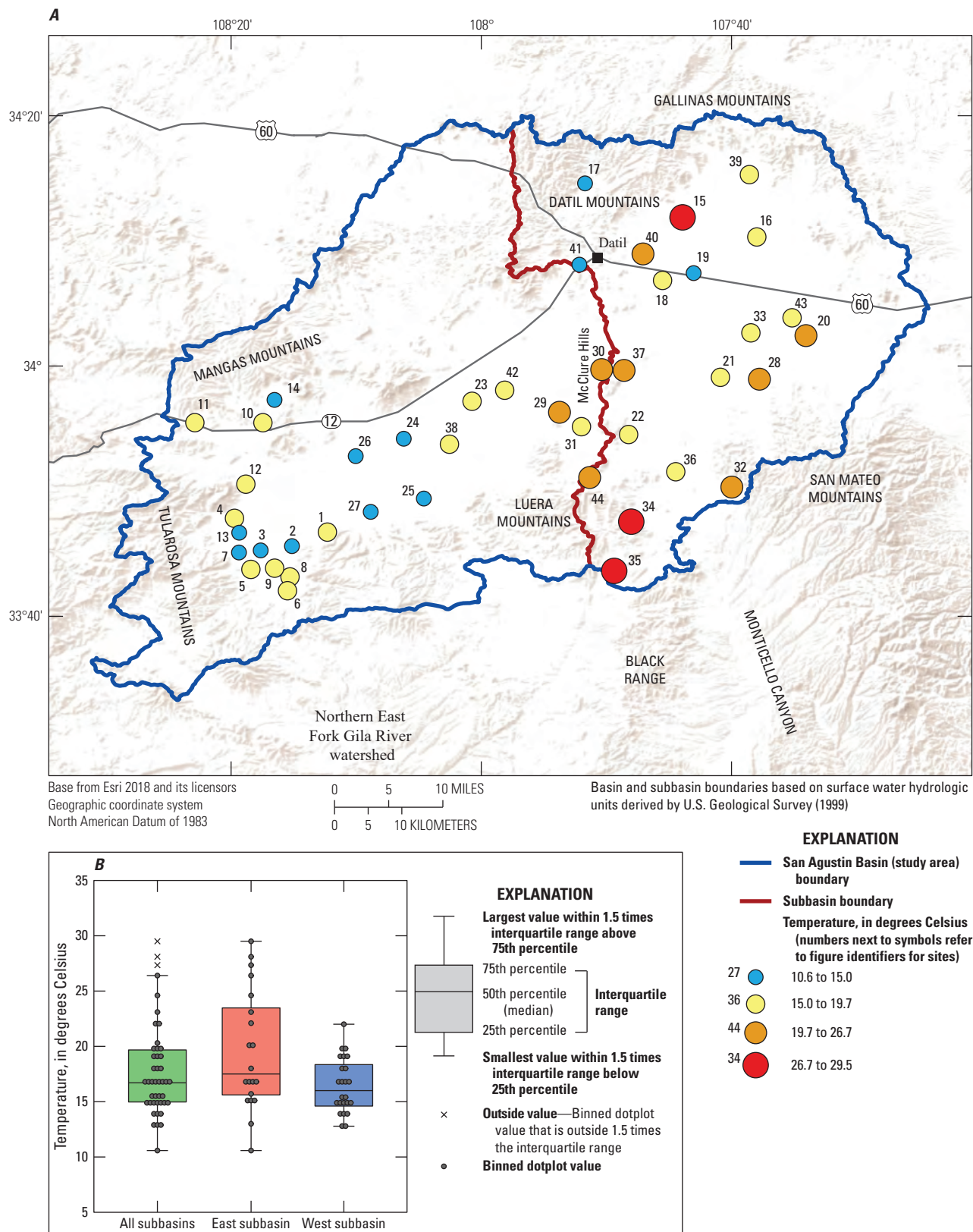
Figure 13. *A*, Spatial plot and *B*, dotplot and boxplot of groundwater temperatures measured in samples collected in the San Agustin Basin, west-central New Mexico (2010–19). Bin thresholds for spatially plotted data points were based on data quartiles (see "Methods" section for more details). Figure identifiers correspond to those used in the tables of this report.
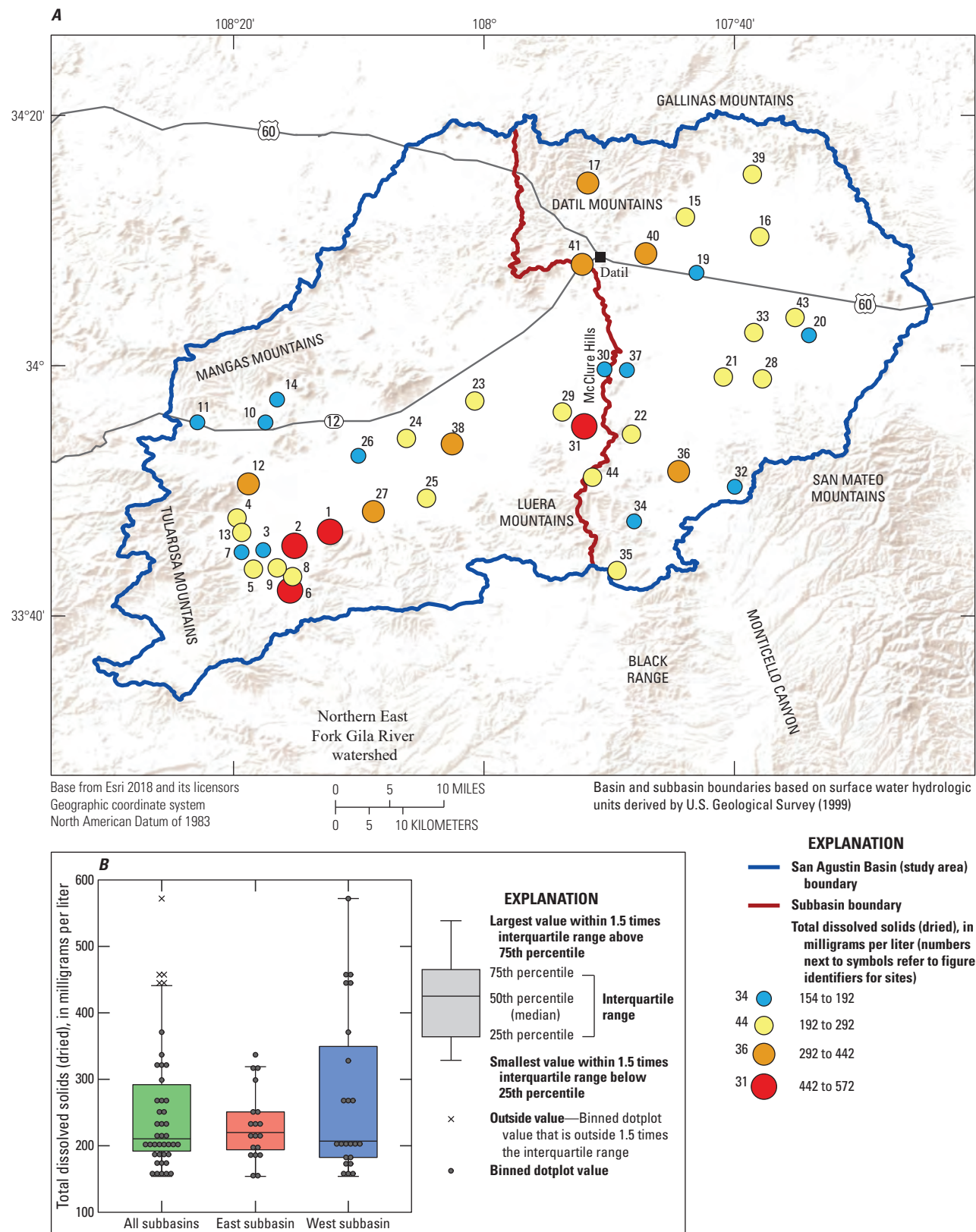
Figure 14. *A*, Spatial plot and *B*, dotplot and boxplot of groundwater total dissolved solids (dried) concentrations measured in samples collected in the San Agustin Basin, west-central New Mexico (2010–19). Bin thresholds for spatially plotted data points were based on data quartiles (see "Methods" section for more details). Figure identifiers correspond to those used in the tables of this report.
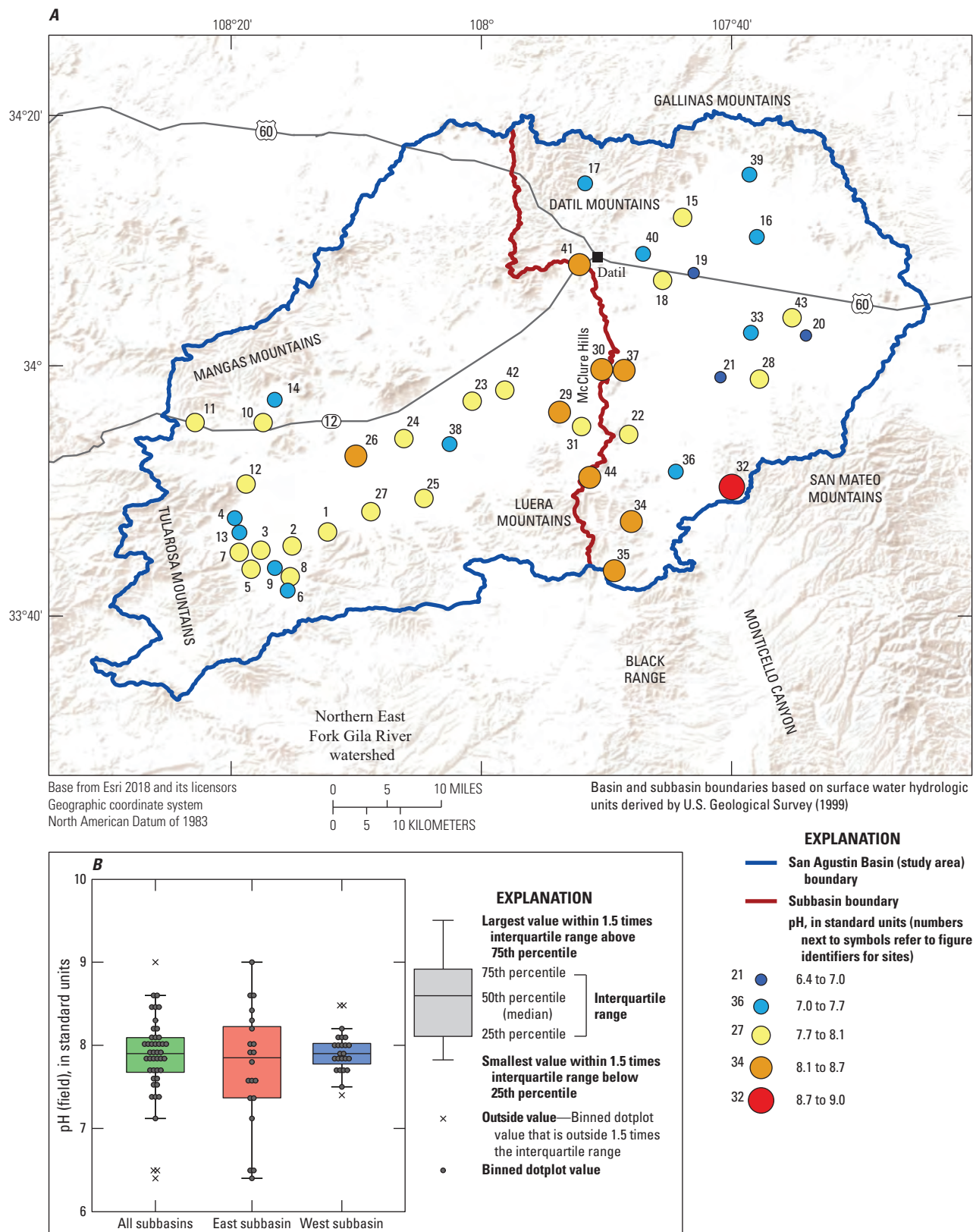
Figure 15. *A*, Spatial plot and *B*, dotplot and boxplot of groundwater pH values measured in samples collected in the San Agustin Basin, west-central New Mexico (2010–19). Bin thresholds for spatially plotted data points were based on data quartiles (see "Methods" section for more details). Figure identifiers correspond to those used in the tables of this report.
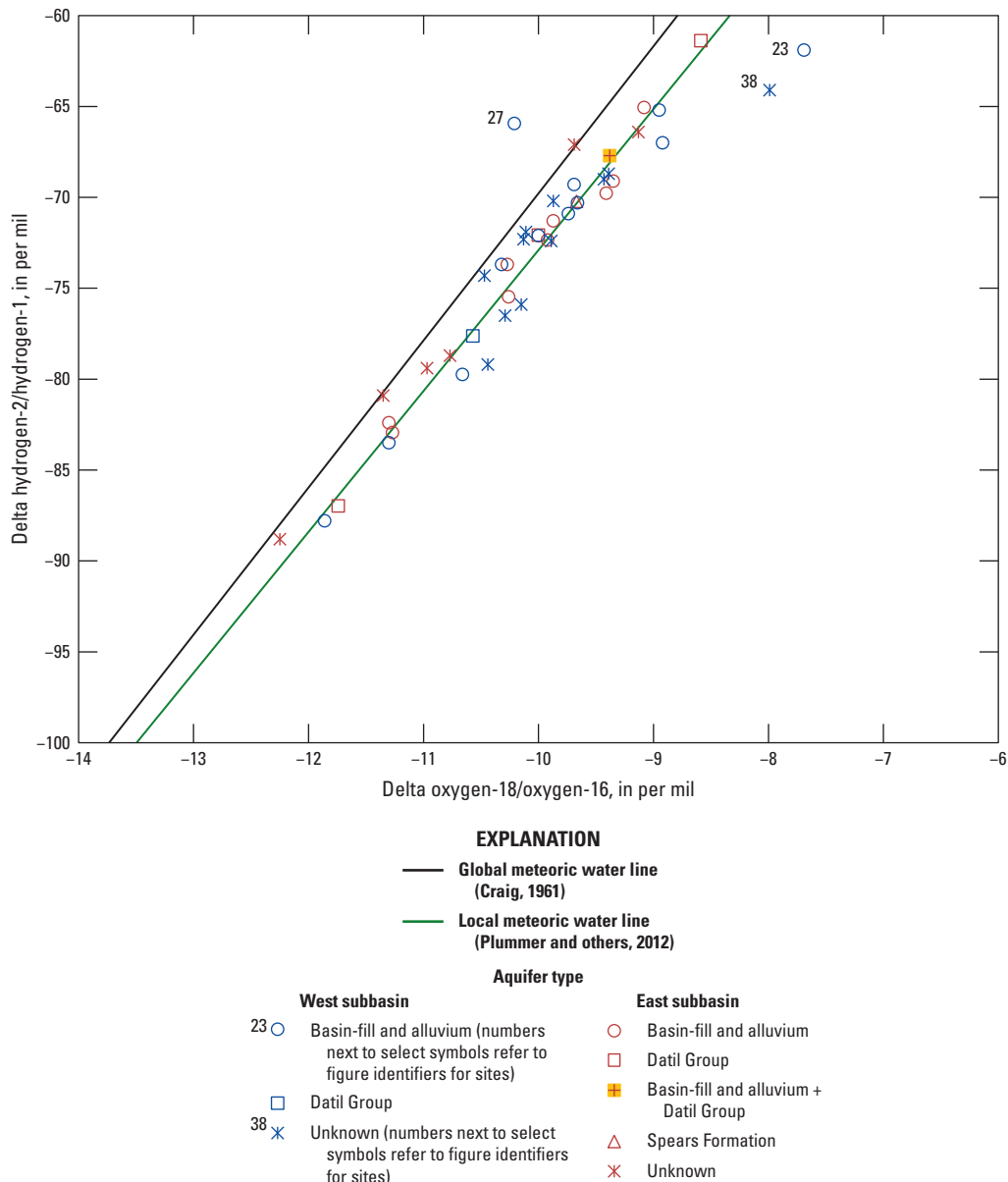
Figure 16. Scatterplot of measured groundwater stable isotope ratios (delta oxygen-18/oxygen-16 and delta hydrogen-2/hydrogen-1) in samples collected in the San Agustin Basin, west-central New Mexico (2010–19), overlaid on the global and local meteoric water lines from Craig (1961) and Plummer and others (2012), respectively. Figure identifiers correspond to those used in the tables of this report, and sites are plotted spatially in figure 4.

that there was minimal presence of modern (1953 and after) groundwater in the sampled basin aquifer system, which suggests that current recharge rates are very low. Sites classified as being of mixed age were mainly located in the highlands, within arroyos, and (or) near the outlet of prominent arroyos within both subbasins (fig. 22). This pattern implies that most recharge likely occurs at higher elevations through mountain-block recharge and as focused recharge within arroyos, which is consistent with the findings of previous studies (Myers and others, 1994).

Denormalized carbon-14 concentrations in percent modern carbon and corrected carbon-14 groundwater ages can add additional insight into groundwater flow patterns and recharge characteristics. Generally, larger carbon-14 concentrations indicate younger waters, whereas smaller carbon-14 concentrations indicate older waters, thereby permitting qualitative interpretation of relative values. Carbon-14 values near 100 pmC represent young (hundreds of years) waters, and values closer to 0 pmC represent old (tens of thousands of years) waters (Nishikawa and others, 2004). The spatial
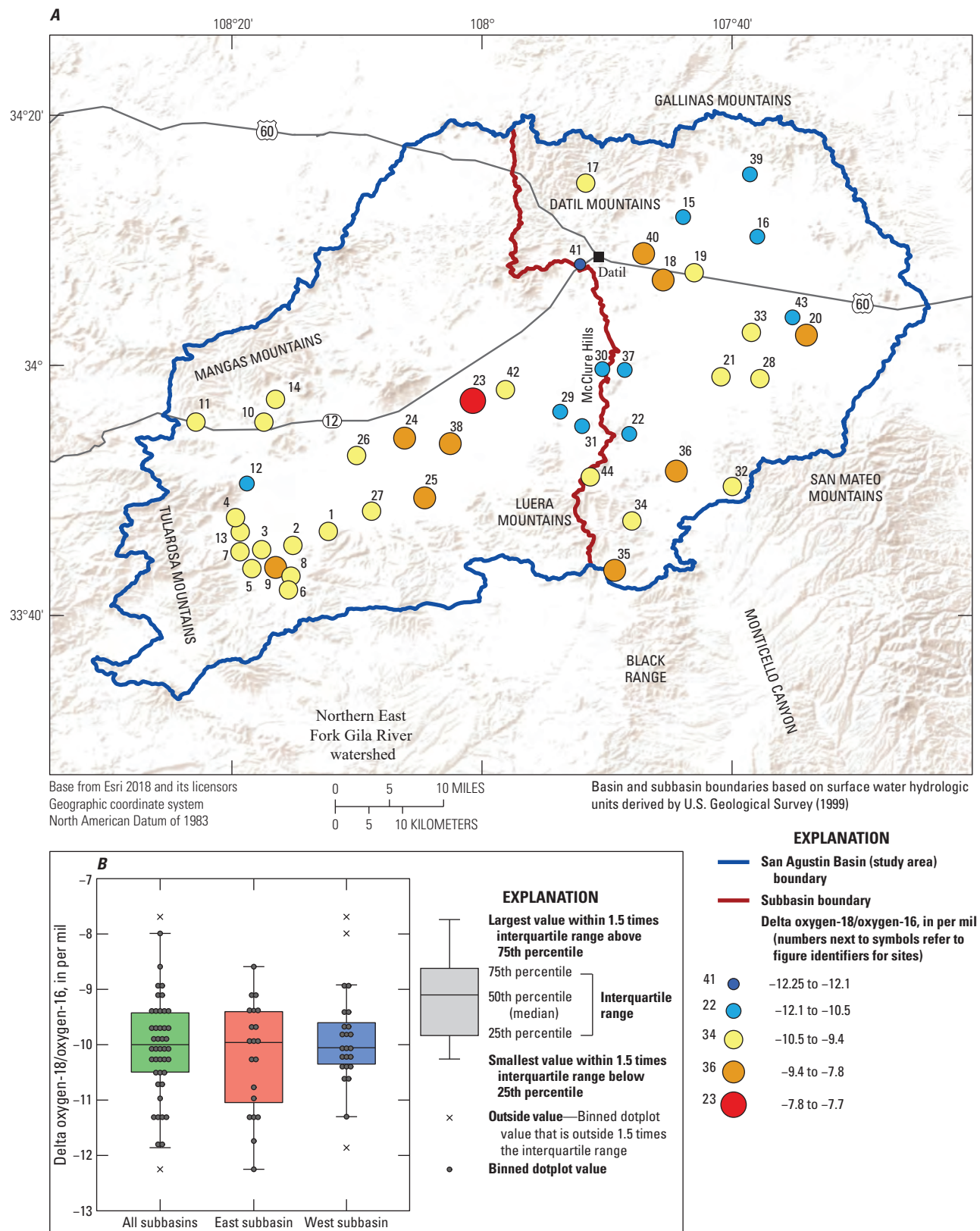
**Figure 17.** *A*, Spatial plot and *B*, dotplot and boxplot of groundwater oxygen stable isotope ratio (delta oxygen-18/oxygen-16) in samples collected in the San Agustin Basin, west-central New Mexico (2010–19). Bin thresholds for spatially plotted data points were based on data quartiles (see "Methods" section for more details). Figure identifiers correspond to those used in the tables of this report.
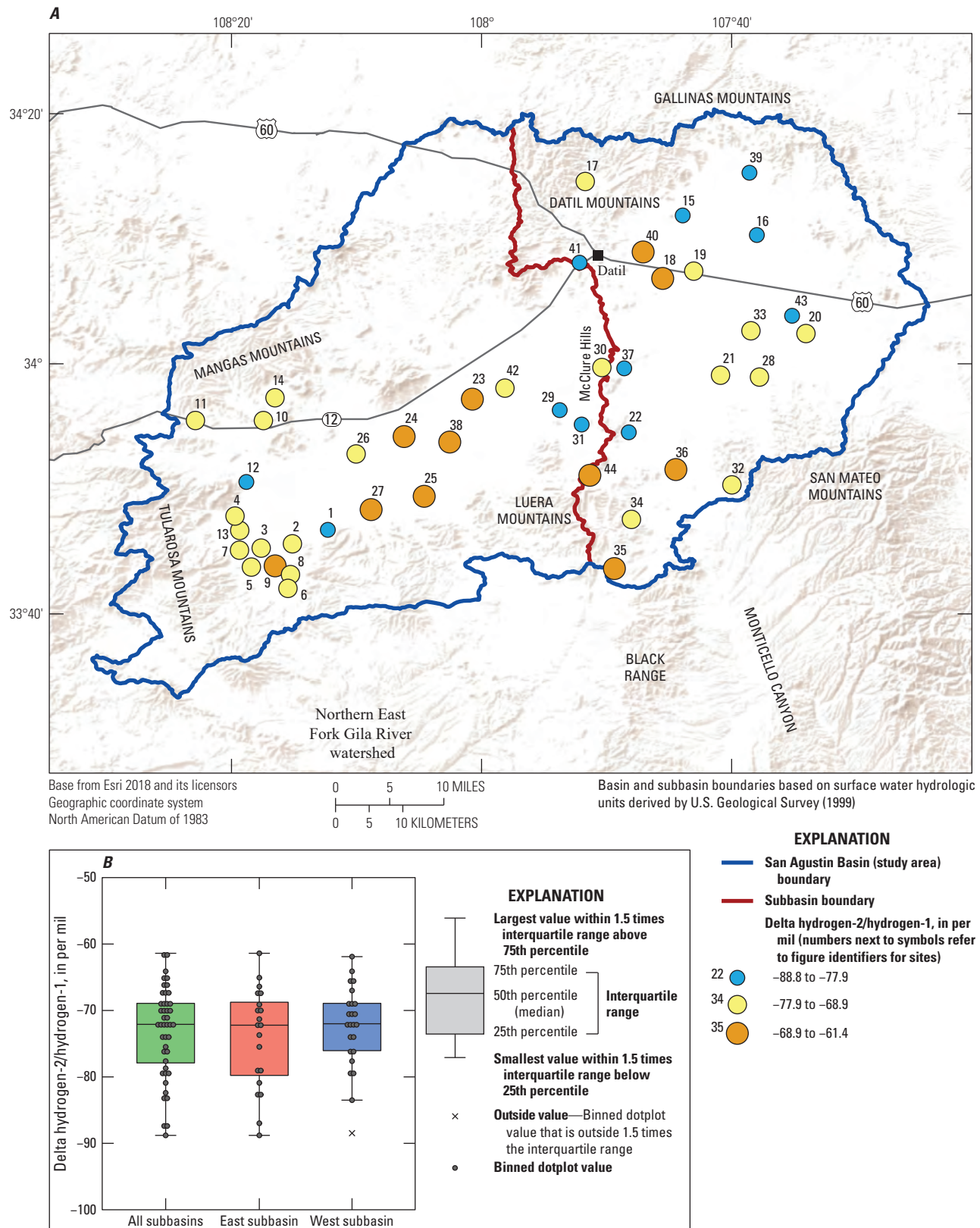
Figure 18. *A*, Spatial plot and *B*, dotplot and boxplot of groundwater hydrogen stable isotope ratio (delta hydrogen-2/hydrogen-1) in samples collected in the San Agustin Basin, west-central New Mexico (2010–19). Bin thresholds for spatially plotted data points were based on data quartiles (see "Methods" section for more details). Figure identifiers correspond to those used in the tables of this report.
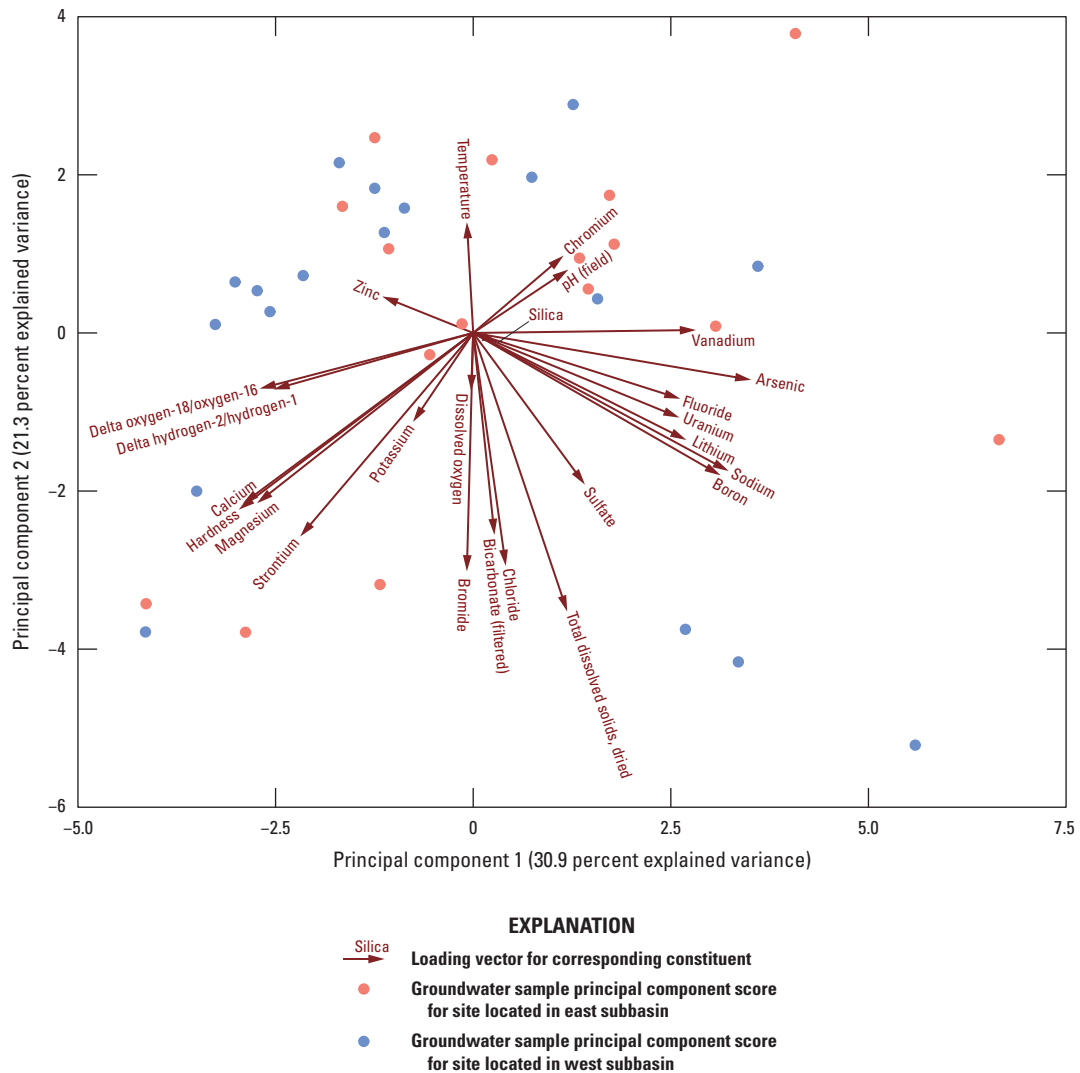
Figure 19. Principal component analysis biplot for principal component 1 and principal component 2 for constituents measured in groundwater samples collected in the San Agustin Basin, west-central New Mexico (2010–19).

distribution of carbon-14 values was similar to that for tritium concentrations (fig. 22), with the highest carbon-14 measurements (59.1–95.0 pmC, younger waters) corresponding to sites in highlands and near or within arroyos (fig. 23 and table 7). Smaller carbon-14 values (9.6–25.5 pmC, older waters) were more common in the east subbasin, though low values, notably near the McClure Hills, were measured in both subbasins. Carbon-14 values may be expected to decrease from east to west in accordance with evidenced regional groundwater flow patterns (fig. 7), but that pattern is not prominent in figure 23. The lowest measured carbon-14 values were near or within the grabens of the east subbasin (fig. 1). This pattern suggests that these grabens have prolonged groundwater residence times and may strongly influence groundwater flow rates in the basin. The lack of a clear regional trend is also likely influenced by heterogeneity in subsurface permeability that creates spatially inconsistent groundwater flow rates and mixing with

local recharge of variable age. Sites 22, 31, and 37 formed a group of low carbon-14 values. This group is bisected by the subbasin divide of the McClure Hills, thereby indicating that the subbasins are likely hydrologically connected through the McClure Hills. Other low carbon-14 values at sites 12 and 26 were located near the lowest elevations of the basin in the west subbasin. Larger measured carbon-14 concentrations near the potential basin discharge area support the role of groundwater mixing and recharge in the observed spatial distribution of carbon-14 values.

Corrected carbon-14 groundwater ages are presented in table 7 and further support the groundwater dynamics identified in the tritium and carbon-14 concentration interpretations. Corrected groundwater ages are inherently uncertain because of the difficulty in comprehensively accounting for subsurface carbon exchange and mixing. However, graphing carbon species data by using the method from Han and Plummer (2016)
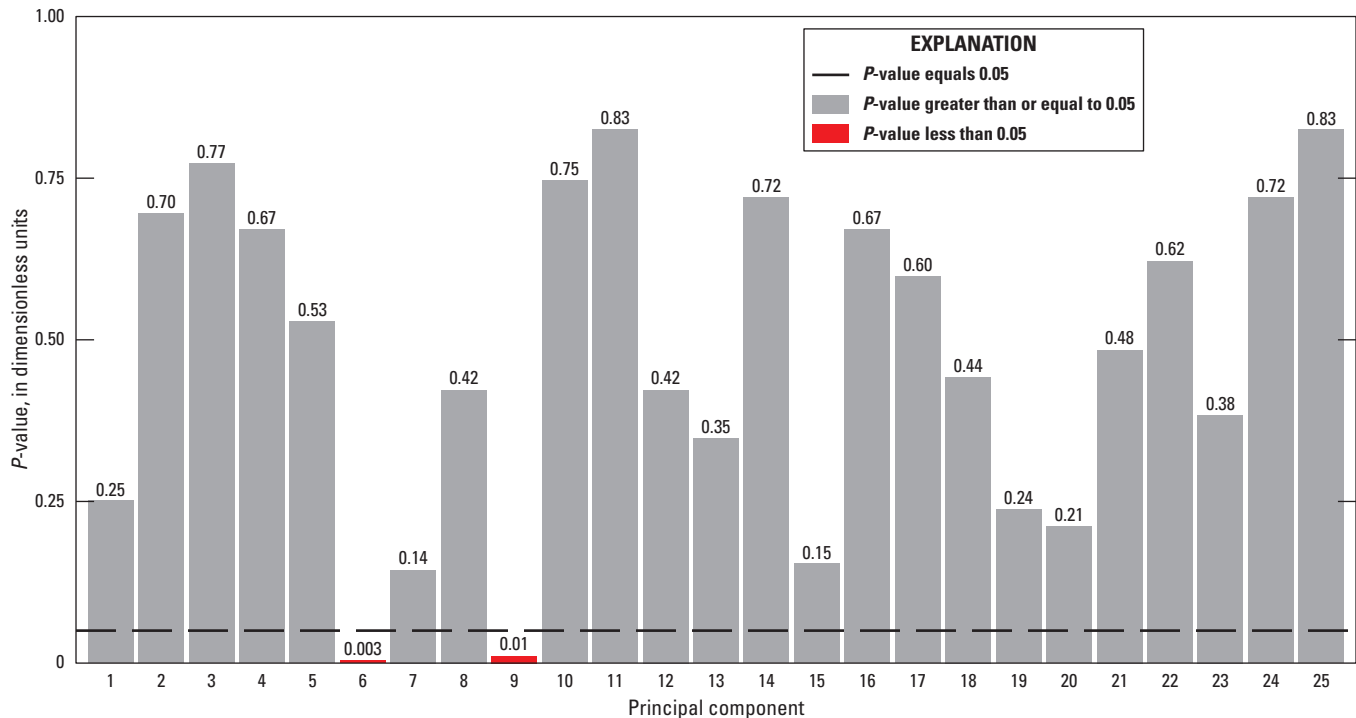
Figure 20. Wilcoxon probability values (*p*-values) that resulted from comparing the east and west subbasins for all principal component scores for constituents measured in groundwater samples collected in the San Agustin Basin, west-central New Mexico (2010–19).

can help elucidate potential processes influencing carbon water chemistry and age uncertainties (fig. 24). The solid black and dashed black lines on this plot represent the "zero age" lines, which are determined from representative carbon-14 and carbon-13 estimates of soil gas and solid carbonate. The solid black lines represent −21 per mil carbon-13 for soil gas, whereas the dashed black lines represent −16 per mil. The areas enclosed by the "zero age" lines are referred to as the "zero age" areas. Samples plotting in these areas do not have a calculated radiocarbon age and may be explained by geochemical reaction with no radiocarbon decay and could therefore be young waters. Samples plotting above these areas are potentially a mixture of young and old waters. Samples plotting below these areas are more likely to have undergone radiocarbon decay and are thereby considered to be associated with reliable age estimates. Several samples plotted within and above the "zero age" areas and have estimated ages listed as "NA" in table 7 to reflect the poor reliability of their age estimates. Samples from several sites, in both the east and west subbasins, plotted below the "zero age" areas when using the −21 per mil carbon-13 for soil gas. These sites included 15, 16, 19, 39, and 43 in the east subbasin and sites 5, 11, 12, 24, and 26 in the west subbasin (fig. 24 and table 7). Site 41 (east subbasin) is the only additional site below the "zero age" area when using the −16 per mil carbon-13 for soil gas. Sites 8 and 14 plot below the "zero age" areas but are to the upper left of the Tamers' X and Y crossings (also known as the Tamers' points; eqs. 22 and 23, respectively, from Han

and Plummer, 2016), which indicates that these samples have likely undergone isotopic exchange primarily with soil gas. The methods needed to estimate corrected ages for these two samples require additional simplifying assumptions and yield highly uncertain results without local carbon-13 soil gas concentration measurements; estimated corrected ages were therefore not computed for these samples ("NC" in table 7). Corrected age estimates ranged from 232 to 13,916 years before present with a median of 5,409 years old. These results indicate that a wide range of groundwater ages is present in the basin with waters commonly being thousands of years old, thereby suggesting that regional groundwater movement is generally slow. Eight of the eighteen sites (44 percent) for which corrected age estimates could not be obtained were classified as mixed in the tritium analysis (table 7) or consistently plotted in the "zero age" areas, thereby suggesting that a component of relatively young groundwater is present in the basin and that it often mixes with older waters.

Synthesis and Implications for Present-Day (1975–2019) Groundwater Flow

Groundwater elevation and geochemical results from this study can be used to update the present-day conceptual model of groundwater flow in the San Agustin Basin. A lack of evidenced chemistry dependence on aquifer type suggests that the regional aquifers are generally well connected.
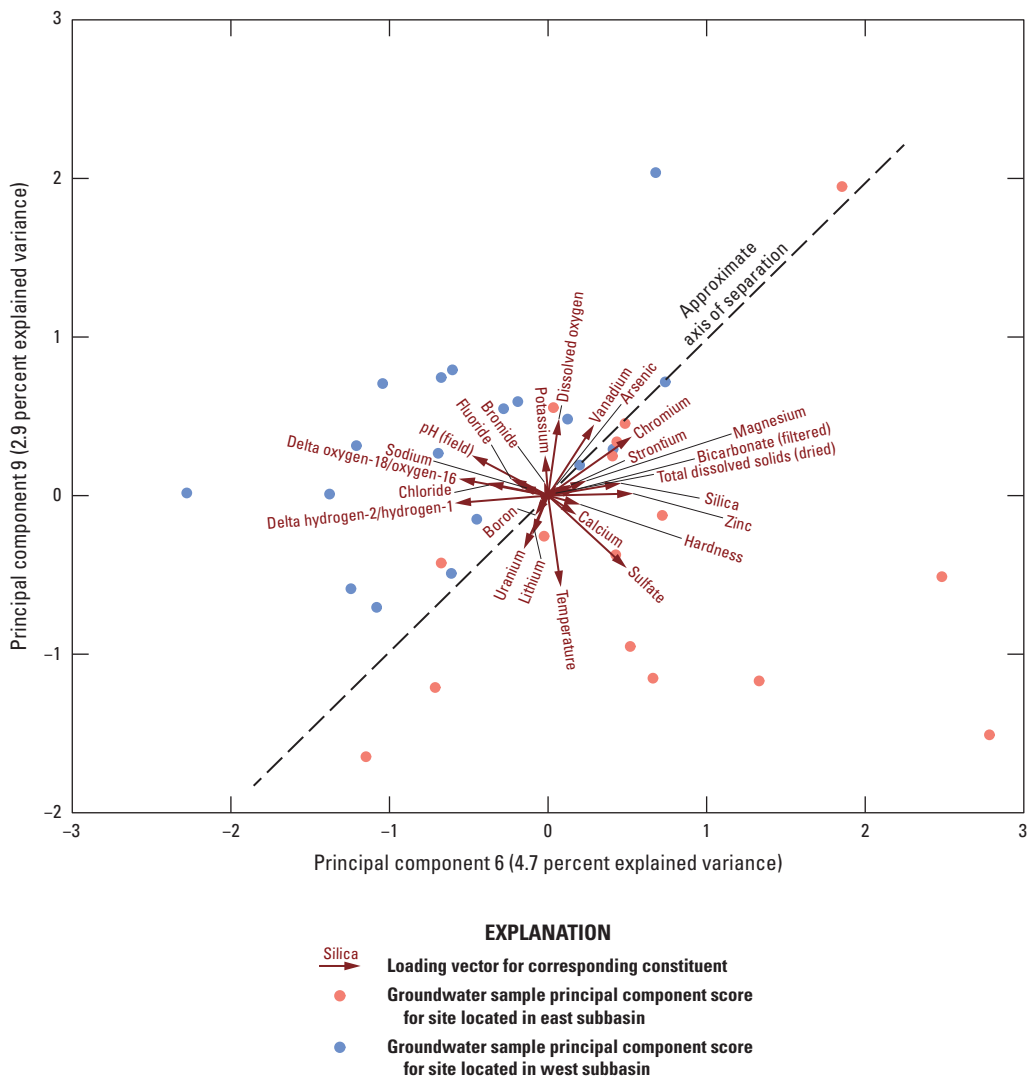
Figure 21.   Principal component analysis biplot for principal component 6 and principal component 9 for constituents measured in groundwater samples collected in the San Agustin Basin, west-central New Mexico (2010–19).

Groundwater elevations indicate that groundwater tends to move from the highlands to the lowlands, with a prominent east to west regional trend. Gradual groundwater elevation gradients near the east and west subbasin divide suggest that any groundwater moving from the east subbasin to the west subbasin moves at slow rates, which is further supported by groundwater age estimates near the subbasin divide. Despite evidenced subbasin connectivity and regional east to west estimated groundwater flow patterns, a systematic east to west groundwater evolution in water chemistry was not observed, and groundwater chemistry in the subbasins was generally similar. These findings suggest that groundwater mixing is regionally prevalent, sediment reactivity is low and variable, and (or) recharge conditions are comparable in both subbasins. Additional geochemical analyses may be able to further evaluate the degree of subbasin connectivity through advanced geochemical modeling techniques in the future.

Groundwater elevations were lowest in the southwestern portion of the west subbasin, where estimated groundwater flow directions suggest underflow through the local highlands into the northern East Fork Gila River watershed, which is further supported by historical groundwater elevation data from the northern East Fork Gila River watershed. Low groundwater elevations upgradient from this potential regional discharge area suggest that groundwater movement towards the northern East Fork Gila River watershed is likely at slow rates. Relatively young groundwater age estimates in this portion of the basin suggest that groundwater mixes with local recharge in this area.

The wide range of estimated groundwater ages in the basin supports regionally prevalent groundwater mixing and generally slow regional groundwater movement. A component of relatively young groundwater is present in the basin, and these younger waters commonly mix with older waters,
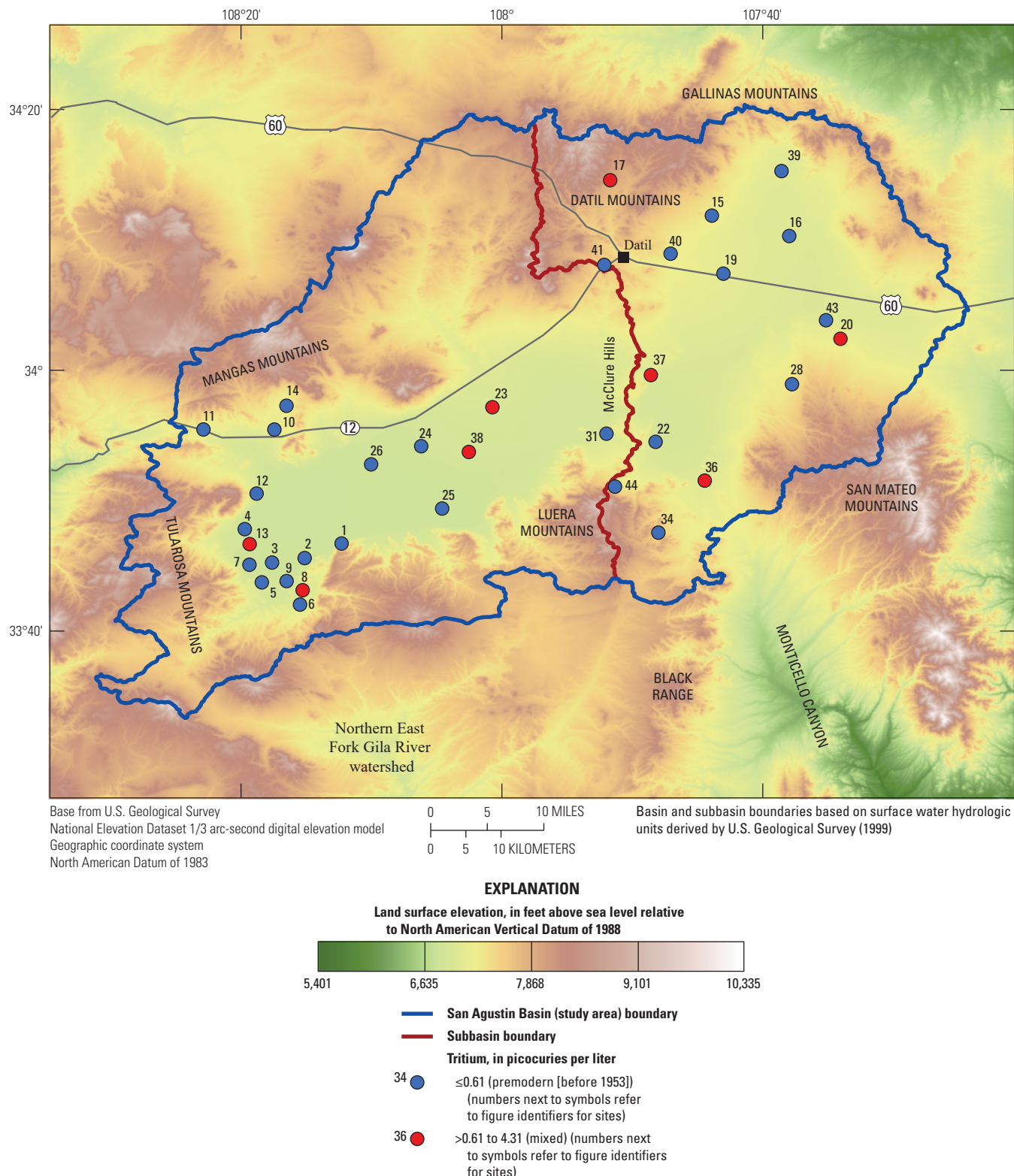
Figure 22.　Spatial plot of categorized groundwater tritium concentrations in samples collected in the San Agustin Basin, west-central New Mexico (2010–19). Figure identifiers correspond to those used in the tables of this report.
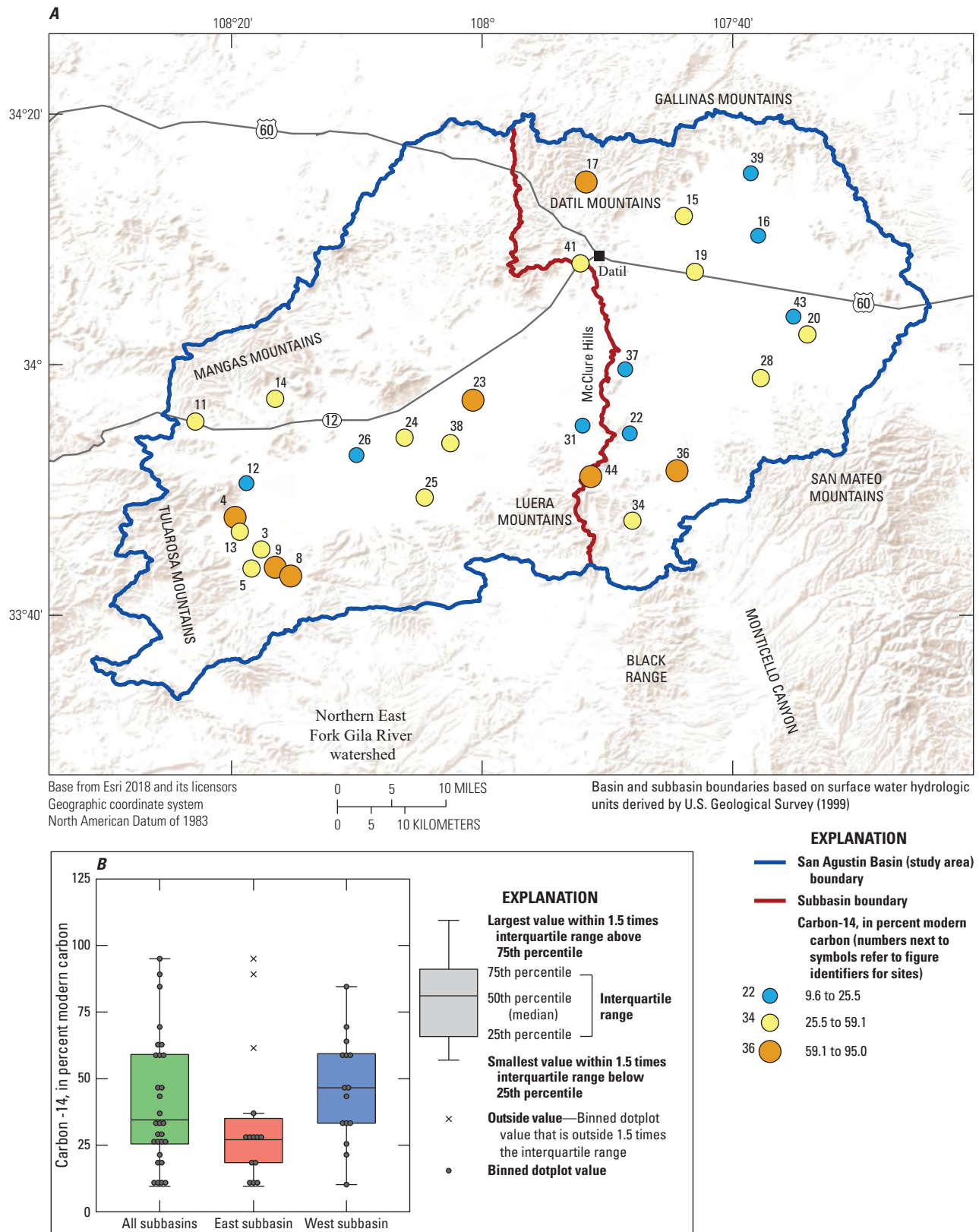
Figure 23.   *A*, Spatial plot and *B*, dotplot and boxplot of groundwater denormalized carbon-14 values in samples collected in the San Agustin Basin, west-central New Mexico (2010–19). Bin thresholds for spatially plotted data points were based on data quartiles (see "Methods" section for more details). Figure identifiers correspond to those used in the tables of this report.

Table 7. Quantitative and qualitative groundwater age estimates from carbon isotope and tritium analyses of samples collected in the San Agustin Basin, west-central New Mexico (2010–19).

[Analyzed data from Rinehart and others (2017) and the U.S. Geological Survey (USGS) National Water Information System (USGS, 2021). R, reported tritium value is less than the reporting level; NA, not available (does not have a corrected age); NC, not computed because of lack of input data]

Figure identifier	Subbasin	Tritium classification	Tritium, in picocuries per liter	Normalized carbon-14, in absolute percent modern	Denormalized carbon-14, in percent modern carbon	Carbon-14 counting error, in percent modern carbon	Delta carbon-13/carbon-12, in per mil	Minimum corrected age,[1] in years before present	Maximum corrected age,[2] in years before present
3	West	Premodern	R −0.21	42.22	43.37	0.13	−7.67	NA	NA
4	West	Premodern	R 0.13	58.10	59.66	0.14	−7.9	NA	NA
5	West	Premodern	R 0.04	33.88	34.56	0.12	−11.16	2,301	4,827
8	West	Mixed	1.74	62.90	63.97	0.23	−12.6	NC	NC
9	West	Premodern	R −0.04	81.85	84.52	0.18	−5.1	NA	NA
11	West	Premodern	0.29	45.60	46.55	0.12	−10.8	NA	2,020
12	West	Premodern	R −0.16	24.85	25.49	0.12	−8.38	1,636	4,155
13	West	Mixed	0.89	57.46	59.06	0.13	−7.36	NA	NA
14	West	Premodern	0.25	56.93	57.93	0.15	−12.39	NC	NC
15	East	Premodern	R 0.13	26.60	27.18	NA	−10.3	3,342	6,014
16	East	Premodern	0.16	12.00	12.26	NA	−10.5	10,193	12,663
17	East	Mixed	1.32	93.00	95.00	NA	−10.5	NA	NA
19	East	Premodern	R 0.13	26.40	26.97	NA	−10.5	3,526	5,990
20	East	Mixed	1.51	28.34	29.04	NA	−9.4	NC	NC
22	East	Premodern	0.23	17.94	18.46	NA	−7.4	NC	NC
23	West	Mixed	1.38	67.60	69.39	NA	−8.1	NA	NA
24	West	Premodern	R 0.13	31.30	31.99	NA	−10.2	1,991	4,455
25	West	Premodern	R 0.03	33.50	34.51	NA	−6.3	NA	NA
26	West	Premodern	0.19	10.00	10.22	NA	−10.2	11,459	13,916
28	East	Premodern	R 0.06	28.58	29.25	NA	−10	NC	NC
31	West	Premodern	R 0.12	20.99	21.41	NA	−11.7	NC	NC
34	East	Premodern	R −0.16	26.30	26.85	NA	−11.2	NC	NC
36	East	Mixed	4.31	60.25	61.49	NA	−11.4	NC	NC
37	East	Mixed	0.68	9.37	9.58	NA	−10.7	NC	NC
38	West	Mixed	1.00	45.40	46.63	NA	−7.8	NA	NA
39	East	Premodern	0.19	18.10	18.47	NA	−11.1	7,367	9,832
41	East	Premodern	R 0.06	36.00	36.98	NA	−7.7	NA	232
43	East	Premodern	R 0.13	11.50	11.75	NA	−10.2	10,263	12,753
44	East	Premodern	R 0.13	88.08	89.17	NA	−15.4	NC	NC

[1]Delta carbon-13/carbon-12 soil gas = −22 per mil.

[2]Delta carbon-13/carbon-12 soil gas = −12 per mil.
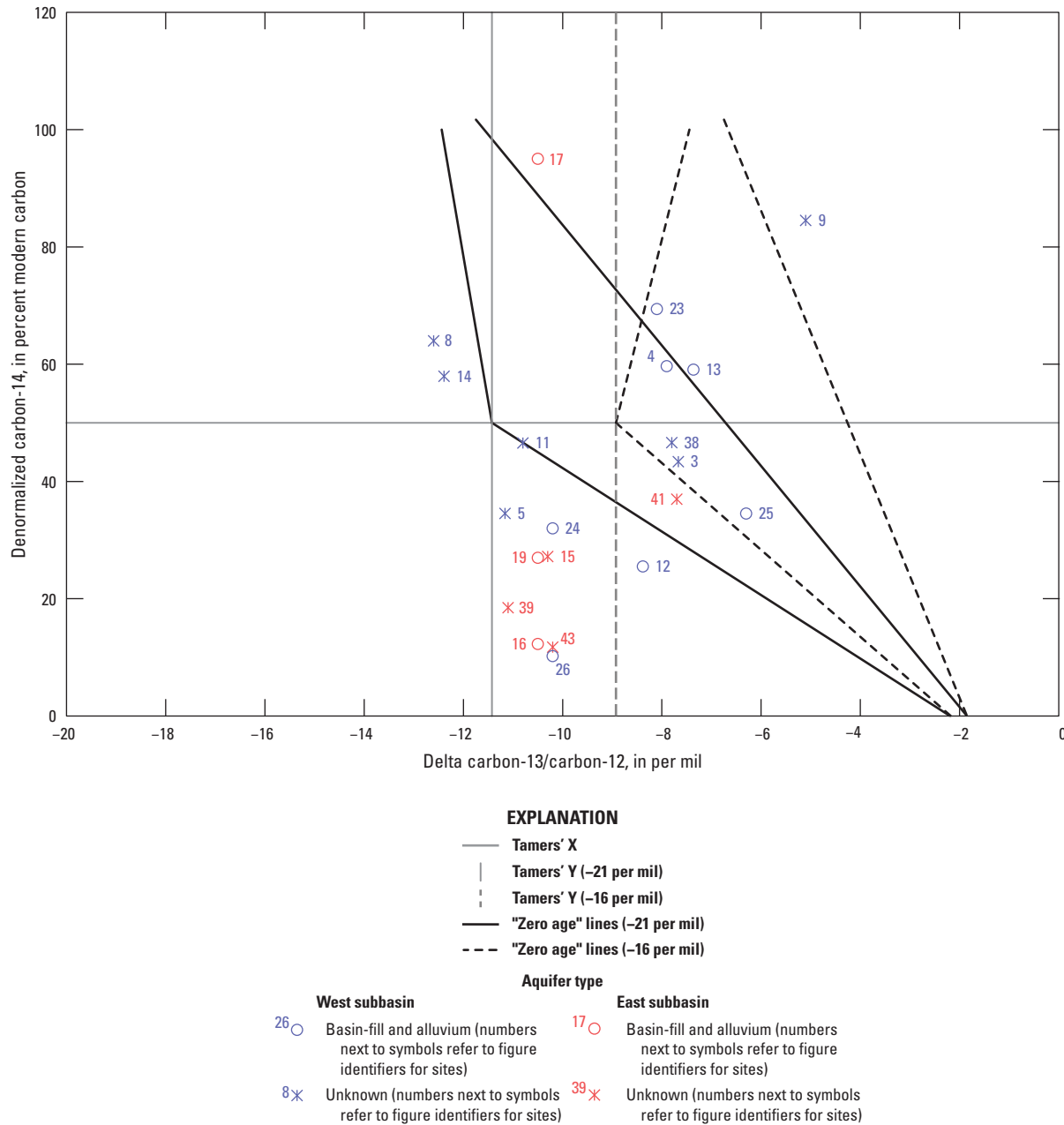
Figure 24. Denormalized carbon-14 compared to delta carbon-13/carbon-12 following Han and Plummer (2016) for groundwater samples collected in the San Agustin Basin, west-central New Mexico (2010–19). Figure identifiers correspond to those used in the tables of this report, and sites are plotted spatially in figure 4.

although evidence of modern (1953 and after) groundwater was minimal at sampled sites. This component of younger waters is likely recharge that enters the groundwater system in the highlands through mountain-block recharge and as focused recharge near the outlet of or within arroyos, whereas lowland recharge rates are generally low. The regional spatial distribution of groundwater age estimates indicates that faulting and the complex multigraben structure of the basin likely lead to variable regional groundwater flow rates and residence times.

Temporal consistency of lowland groundwater elevations suggests that regional groundwater dynamics have been more or less stable through time under current climate and development conditions, although median annual gradients indicate that groundwater elevations may have slightly declined on average between 1975 and 2019. Groundwater elevations are more dynamic in the highlands, where precipitation is more prevalent and relatively shallow depths to groundwater are more common.

Summary

The U.S. Geological Survey in cooperation with the Bureau of Land Management performed this study to improve the understanding of present-day (1975–2019) hydrogeology and groundwater quality of the San Agustin Basin (basin) in west-central New Mexico to support sustainable groundwater resource management. The basin hosts a relatively undeveloped basin-fill and alluvium aquifer system and is topographically divided into east and west subbasins by the McClure Hills. This work included the compilation and collection of groundwater chemistry (major ions, trace elements, stable isotopes, and groundwater age tracers) and groundwater elevation data along with the interpretation of these data in the context of groundwater flow and quality. The analyses included in this report considered groundwater chemistry data collected within the last decade (2010–19) and groundwater elevation data collected from 1975 through 2019; the longer timespan for groundwater elevation data was used in order to address sparsity in data collected over the last decade.

Groundwater elevation analyses included construction of a groundwater elevation map and assessment of the time dependence of groundwater elevations to estimate the dynamics of groundwater flow. The groundwater elevation map indicates that groundwater flows from the highlands towards the east-west central axis of the basin, where it then generally moves from east to west. Estimated groundwater elevation gradients were gentle (about 2 feet per mile) near the subbasin divide, thereby suggesting that groundwater slowly flows from the east subbasin into the west subbasin. Groundwater elevations were lowest in the southwestern portion of the west subbasin, where estimated groundwater flow directions suggest underflow through the local highlands into the northern East Fork Gila River watershed, which is further supported by historical groundwater elevation data from the northern East Fork Gila River watershed. Low groundwater elevations upgradient from this potential regional discharge area suggest that groundwater movement towards the northern East Fork Gila River watershed is likely at slow rates. Median annual gradients (groundwater elevation change over time) from 1975 through 2019 indicate that most groundwater elevations in the lowlands changed little (−0.2 to 0.2 foot per year), thereby also suggesting that lowland groundwater flow patterns have likely been more or less stable over time under current climate and development conditions. Groundwater elevations were more time sensitive in the highlands, where precipitation is more prevalent and relatively shallow depths to groundwater are more common. This contrast with the lowlands is evidence that most groundwater recharge takes place in the highlands, with minimal recharge in the lowlands. Median change for all sites was −0.05 foot per year, which indicates that groundwater elevations may have slightly declined on average between 1975 and 2019.

The general character and spatial variation of groundwater chemistry were also evaluated to further understand the quality and movement of basin groundwater. Waters were mainly bicarbonate-carbonate type with a broad distribution of cation chemistry across calcium, sodium, and potassium. Major ion chemistry showed minimal dependence on aquifer type, suggesting that the aquifers are generally well connected. Major ion chemistry was also similar in both the east and west subbasins. Subbasin chemistry results for 2010 through 2019 were quantitatively compared to one another by using Wilcoxon tests, where probability values (p-values) less than 0.05 were assumed to indicate statistically distinct chemistry between subbasins. Of the constituents considered, only potassium (p-value = 0.04) and temperature (p-value = 0.04) yielded statistically significant p-values. Thus, with these two slight exceptions, the geochemistry data did not demonstrate a statistically significant difference between subbasins.

Groundwater quality was generally good throughout the basin in comparison with U.S. Environmental Protection Agency (EPA) drinking water standards. Total dissolved solids (TDS) concentrations had a median of 211 milligrams per liter (mg/L) and ranged from 154 to 572 mg/L, with only one sampled site in excess of the EPA secondary maximum contaminant level of 500 mg/L for TDS. A prominent gap in recent TDS data exists for the lowest elevations of the west subbasin because of a lack of wells with existing groundwater pumps to allow practical sampling. Historical data and anecdotal accounts indicated poor water quality within the lacustrine and playa deposits in this area, with TDS, as estimated from specific conductance data, exceeding 25,000 mg/L. Overall, exceedances of EPA drinking water standards were rare and not extreme, thereby suggesting that water quality in the sampled wells is generally favorable for consumption.

Stable isotope analysis showed that most samples plotted along the local meteoric water line for the Middle Rio Grande Basin, with no clear dependence on aquifer type or subbasin. Despite minimal quantitative distinction between east and west subbasin stable isotope values, the most isotopically depleted (most negative) values were more common in the eastern portion of the basin. This pattern may be influenced by recharge at higher elevations and (or) colder temperatures.

Principal component analysis was performed on select constituents to further compare east and west subbasin groundwater chemistry. The first two principal components accounted for 52.2 percent of total dataset variance, had loading vectors that were generally similar in length, and showed no systematic point separation by subbasin when plotted. These results further indicate that groundwater chemistry is largely similar in the two subbasins.

Corrected carbon-14 groundwater age estimates in the basin ranged from 232 to 13,916 years before present with a median of 5,409 years. These results indicate that a wide range of groundwater ages is present in the basin with waters commonly being thousands of years old, thereby suggesting that regional groundwater movement is generally slow. A component of relatively young groundwater, for which estimated ages could not be accurately computed, is also present in the basin, and it may commonly mix with older waters. The spatial distribution of categorical and quantitative groundwater

ages indicates that most recharge likely occurs in the highlands through mountain-block recharge and as focused recharge within arroyos, although evidence of modern (1953 and after) groundwater from tritium analysis was minimal at sampled sites. A group of sites with relatively old groundwater is bisected by the subbasin divide, thereby further supporting hydrologic connectivity of the subbasins through the McClure Hills. Despite evidenced subbasin connectivity and regional east to west estimated groundwater flow patterns, a systematic east to west groundwater evolution in water chemistry was not observed, and groundwater chemistry in the subbasins was generally similar. These findings suggest that groundwater mixing is regionally prevalent, sediment reactivity is low and variable, and (or) recharge conditions are comparable in both subbasins. Relatively young groundwater age estimates near the potential discharge area towards the northern East Fork Gila River watershed suggest that groundwater mixes with local recharge in this area. The regional spatial distribution of groundwater age estimates indicates that faulting and the complex multigraben structure of the basin likely lead to variable regional groundwater flow rates and residence times.

References Cited

Basabilvazo, G.T., 1997, Ground-water resources of Catron County, New Mexico: U.S. Geological Survey Water-Resources Investigations Report 96–4258, 141 p.

Bethke, C.M., Farrell, B., and Yeakel, S., 2019, The Geochemist's Workbench release 12.0—GWB essentials reference manual: Urbana, Illinois, University of Illinois, 131 p., accessed April 15, 2020, at https://www.gwb.com/pdf/GWB12/GWBreference.pdf.

Blodgett, D.D., and Titus, F.B., 1973, Hydrogeology of the San Augustin Plains, New Mexico: New Mexico Bureau of Geology and Mineral Resources Open File Report 51, 55 p.

Chapin, C.E., Wilks, M., and McIntosh, W.C., 2004, Space-time patterns of Late Cretaceous to present magmatism in New Mexico—Comparison with Andean volcanism and potential for future volcanism: New Mexico Bureau of Geology and Mineral Resources Bulletin, v. 160, p. 13–40.

Craig, H., 1961, Isotopic variations in meteoric waters: Science, v. 133, no. 3465, p. 1702–1703.

Cunningham, W.L., and Schalk, C.W., comps., 2011, Groundwater technical procedures of the U.S. Geological Survey: U.S. Geological Survey Techniques and Methods, book 1, chap. A1, 151 p., accessed December 22, 2021, at https://pubs.usgs.gov/tm/1a1/.

Everitt, B.S., Landau, S., Leese, M., and Stahl, D., 2011, Cluster analysis (5th ed.): West Sussex, United Kingdom, John Wiley & Sons, Ltd., 330 p.

Faure, G., 1986, Principles of isotope geology: New York, Wiley, 589 p.

Fisher, J.C., 2013, Optimization of water-level monitoring networks in the eastern Snake River Plain aquifer using a kriging-based genetic algorithm method: U.S. Geological Survey Scientific Investigations Report 2013–5120, 74 p., accessed December 22, 2021, at https://doi.org/10.3133/sir20135120.

Fishman, M.J., ed., 1993, Methods of analysis by the U.S. Geological Survey National Water Quality Laboratory—Determination of inorganic and organic constituents in water and fluvial sediments: U.S. Geological Survey Open-File Report 93–125, 217 p.

Fishman, M.J., and Friedman, L.C., 1989, Methods for determination of inorganic substances in water and fluvial sediments: U.S. Geological Survey Techniques of Water-Resources Investigations, book 5, chap. A1, 545 p.

Garbarino, J.R., 1999, Methods of analysis by the U.S. Geological Survey National Water Quality Laboratory—Determination of dissolved arsenic, boron, lithium, selenium, strontium, thallium, and vanadium using inductively coupled plasma-mass spectrometry: U.S. Geological Survey Open-File Report 99–093, 31 p.

Garbarino, J.R., Kanagy, L.K., and Cree, M.E., 2005, Determination of elements in natural-water, biota, sediment and soil samples using collision/reaction cell inductively coupled plasma-mass spectrometry: U.S. Geological Survey Techniques and Methods, book 5, chap. B1, 88 p.

Ghosh, D., and Vogt, A., 2012, Outliers—An evaluation of methodologies, in Section on Survey Research Methods of Joint Statistical Meeting Conference, July 28–August 2, 2012, Proceedings: San Diego, California, Joint Statistical Meetings Program, p. 3455–3460.

Han, L.-F., and Plummer, L.N., 2013, Revision of Fontes & Garnier's model for the initial ^{14}C content of dissolved inorganic carbon used in groundwater dating: Chemical Geology, v. 351, p. 105–114.

Han, L.-F., and Plummer, L.N., 2016, A review of single sample-based models and other approaches for radiocarbon dating of dissolved inorganic carbon in groundwater: Earth-Science Reviews, v. 152, p. 119–142.

Hastie, T., Tibshirani, R., and Friedman, J., 2009, The elements of statistical learning—Data mining, inference, and prediction (2d ed.): New York, Springer Science+Business Media, LLC, 745 p.

Helsel, D.R., Hirsch, R.M., Ryberg, K.R., Archfield, S.A., and Gilroy, E.J., 2020, Statistical methods in water resources: U.S. Geological Survey Techniques and Methods, book 4, chap. A3, 458 p., accessed December 22, 2021, at https://doi.org/10.3133/tm4A3. [Supersedes USGS Techniques of Water-Resources Investigations, book 4, chap. A3, version 1.1.]

Homer, C., Dewitz, J., Jin, S., Xian, G., Costello, C., Danielson, P., Gass, L., Funk, M., Wickham, J., Stehman, S., Auch, R., and Riitters, K., 2020, Conterminous United States land cover change patterns 2001–2016 from the 2016 National Land Cover Database: ISPRS Journal of Photogrammetry and Remote Sensing, v. 162, p. 184–199.

Huth, T.E., Cerling, T.E., Marchetti, D.W., Bowling, D.R., Ellwein, A.L., and Passey, B.H., 2019, Seasonal bias in soil carbonate formation and its implications for interpreting high-resolution paleoarchives—Evidence from southern Utah: Journal of Geophysical Research, Biogeosciences, v. 124, no. 3, p. 616–632.

Iglewicz, B., and Hoaglin, D.C., 1993, How to detect and handle outliers, v. 16 of ASQC basic references in quality control: Milwaukee, Wisconsin, ASQC Quality Press, 87 p.

Ingebritsen, S., Sanford, W., and Neuzil, C., 2006, Groundwater in geologic processes (2d ed): Cambridge, University Press, 536 p.

Intergovernmental Panel on Climate Change, 2014, Climate change 2014—Synthesis report: Geneva, Intergovernmental Panel on Climate Change, 151 p.

James, G., Witten, D., Hastie, T., and Tibshirani, R., 2013, An introduction to statistical learning with applications in R: New York, Springer Science+Business Media, 426 p.

Kelley, R., 2015, New Mexico geothermal play fairway analysis: Los Alamos National Laboratory Geothermal Data Repository web page, accessed April 29, 2021, at https://gdr.openei.org/submissions/597.

Kendall, C., Sklash, M.G., and Bullen, T.D., 1995, Isotope tracers of water and solute sources in catchments, in Trudgill, S.T., ed., Solute modelling in catchment systems: New York, Wiley, p. 261–303.

Lee, L., 2020, Package 'NADA'—Nondetects and data analysis for environmental data (ver. 1.6–1.1): Comprehensive R Archive Network (CRAN) software release, accessed March 3, 2021, at https://cran.r-project.org/web/packages/NADA/NADA.pdf.

Lindsey, B.D., Jurgens, B.C., and Belitz, K., 2019, Tritium as an indicator of modern, mixed, and premodern groundwater age: U.S. Geological Survey Scientific Investigations Report 2019–5090, 18 p.

Lucas, L.L., and Unterweger, M.P., 2000, Comprehensive review and critical evaluation of the half-life of tritium: Journal of Research of the National Institute of Standards and Technology, v. 105, no. 4, p. 541–549.

Maechler, M., Rousseeuw, P., Struyf, A., Hubert, M., Hornik, K., Studer, M., and Roudier, P., 2019, Package 'cluster'—Finding groups in data: Comprehensive R Archive Network (CRAN) software release, accessed June 6, 2019, at https://cran.r-project.org/web/packages/cluster/cluster.pdf.

Magnuson, M.L., Valdez, J.M., Lawler, C.R., Nelson, M., and Petronis, L., 2019, New Mexico water use by categories 2015: New Mexico State Engineer Office, Technical Report 55, May 2019, 142 p.

Michel, R.L., Jurgens, B.C., and Young, M.B., 2018, Tritium deposition in precipitation in the United States, 1953–2012: U.S. Geological Survey Scientific Investigations Report 2018–5086, 11 p., accessed December 22, 2021, at https://doi.org/10.3133/sir20185086.

Motzer, W.E., 2008, Age dating groundwater: Alameda, California, Todd Engineers, 4 p.

Muller, A.B., and Mayo, A.L., 1986, 13C variation in limestone on an aquifer-wide scale and its effects on groundwater 14C dating models: Radiocarbon, v. 28, no. 3, p. 1041–1054.

Myers, R.G., Everheart, J.T., and Wilson, C.A., 1994, Geohydrology of the San Agustin Basin, Alamosa Creek Basin upstream from Monticello Box, and upper Gila Basin in parts of Catron, Socorro, and Sierra Counties, New Mexico: U.S. Geological Survey Water-Resources Investigations Report 94–4125, 70 p.

New Mexico Bureau of Geology and Mineral Resources, 2003, Geologic map of New Mexico: New Mexico Bureau of Geology and Mineral Resources, 2 sheets, scale 1:500,000.

New Mexico Climate Center, 2020, Augustine 2E weather station data: Las Cruces, New Mexico, New Mexico State University, New Mexico Climate Center web page, accessed December 30, 2020, at https://weather.nmsu.edu/coop/request/station/290640/data/.

New Mexico Office of the State Engineer, 2020, Aquifer test index—December 2016: New Mexico Office of the State Engineer, Hydrology Bureau web page, accessed April 30, 2020, at https://www.ose.state.nm.us/Hydrology/aquifer.php.

Nishikawa, T., Izbicki, J.A., Hevesi, J.A., Stamos, C.L., and Martin, P., 2004, Evaluation of geohydrologic framework, recharge estimates, and ground-water flow of the Joshua Tree area, San Bernardino County, California: U.S. Geological Survey Scientific Investigations Report 2004–5267, 115 p.

Parkhurst, D.L., and Charlton, S.R., 2008, NetpathXL—An Excel interface to the program NETPATH: U.S. Geological Survey Techniques and Methods, book 6, chap. A26, 11 p.

Pebesma, E., and Graeler, B., 2019, Package 'gstat'—Spatial and spatio-temporal geostatistical modelling, prediction and simulation: Comprehensive R Archive Network (CRAN) software release, accessed May 30, 2020, at https://cran.r-project.org/web/packages/gstat/gstat.pdf.

Phillips, F.M., Campbell, A.R., Kruger, C., Johnson, P., Roberts, R., and Keyes, E., 1992, A reconstruction of the response of the water balance in western United States lake basins to climatic change: New Mexico Water Resources Research Institute Report, v. 1, 167 p.

Plummer, L.N., Bexfield, L.M., Anderholm, S.K., Sanford, W.E., and Busenberg, E., 2012, Geochemical characterization of ground-water flow in the Santa Fe Group aquifer system, Middle Rio Grande Basin, New Mexico (ver. 1.2, November 20, 2012): U.S. Geological Survey Water-Resources Investigations Report 03–4131, 395 p.

Potter, L.D., 1957, Phytosociological study of San Augustin Plains, New Mexico: Ecological Monographs, v. 27, no. 2, p. 113–136.

R Core Team, 2019, R—A language and environment for statistical computing: Vienna, Austria, R Foundation for Statistical Computing, accessed May 12, 2020, at https://www.r-project.org/.

Reed, J.C., and Bush, C.A., 2007, About the geologic map in the National Atlas of the United States of America: U.S. Geological Survey Circular 1300, 52 p., accessed December 22, 2021, at https://doi.org/10.3133/cir1300.

Révész, K., and Coplen, T.B., 2008a, Determination of the $\delta(^2H/^1H)$ of water—RSIL lab code 1574, chap. C1 *of* Révész, K., and Coplen, T.B., eds., Methods of the Reston Stable Isotope Laboratory: U.S. Geological Survey Techniques and Methods, book 10, chap. C1, 27 p.

Révész, K., and Coplen, T.B., 2008b, Determination of the $\delta(^{18}O/^{16}O)$ of water—RSIL lab code 489, chap. C2 *of* Révész, K., and Coplen, T. B., eds., Methods of the Reston Stable Isotope Laboratory: U.S. Geological Survey Techniques and Methods, book 10, chap. C2, 28 p.

Rinehart, A., Koning, D., and Timmons, S., 2017, Hydrogeology of the San Agustin Plains, *in* New Mexico Water Conference, 62d, Socorro, New Mexico, August 16, 2017: New Mexico Bureau of Geology and Mineral Resources, 36 p., accessed November 26, 2019, at https://geoinfo.nmt.edu/geoscience/research/documents/37/D2_07_Alex_Rinehart.pdf.

Thatcher, L.L., Janzer, V.J., and Edwards, K.W., 1977, Methods for determination of radioactive substances in water and fluvial sediments: U.S. Geological Survey Techniques of Water-Resources Investigations, book 5, chap. A5, 95 p.

Timmons, S. S., Land, L., Newton, B. T., and Frey, B., 2013, Aquifer Mapping Program technical document—Water sampling procedures, analysis and systematics: New Mexico Tech, New Mexico Bureau of Geology and Mineral Resources Open-File Report 558, 14 p.

Tukey, J.W., 1977, Exploratory data analysis: London, Pearson, 712 p.

Turner, S., 2019, Decision denying water permit appealed: Albuquerque Journal, September 23, 2019, accessed December 29, 2020, at https://www.abqjournal.com/1370059/decision-denying-water-permit-appealed.html.

U.S. Environmental Protection Agency [EPA], 2020a, National Primary Drinking Water Regulations: U.S. Environmental Protection Agency online database, accessed February 13, 2020, at https://www.epa.gov/ground-water-and-drinking-water/national-primary-drinking-water-regulations.

U.S. Environmental Protection Agency [EPA], 2020b, Secondary Drinking Water Standards—Guidance for nuisance chemicals, table of secondary standards: U.S. Environmental Protection Agency [EPA] web page, accessed February 13, 2020, at https://www.epa.gov/sdwa/secondary-drinking-water-standards-guidance-nuisance-chemicals#table.

U.S. Geological Survey [USGS], 1999, Hydrologic unit: U.S. Geological Survey Information Sheet (February 1999), 1 p., accessed December 22, 2021, at https://pubs.usgs.gov/gip/hydrologic_units/pdf/hydrologic_units.pdf.

U.S. Geological Survey [USGS], 2021, USGS water data for the Nation: U.S. Geological Survey National Water Information System database, accessed January 8, 2021, at https://doi.org/10.5066/F7P55KJN.

U.S. Geological Survey [USGS], [variously dated], National field manual for the collection of water-quality data: U.S. Geological Survey Techniques of Water-Resources Investigations, book 9, chaps. A1–A10. [Also available at https://pubs.water.usgs.gov/twri9A.]

Vu, V.Q., 2011, ggbiplot—A ggplot2 based biplot: GitHub web page, accessed May 15, 2020, at https://github.com/vqv/ggbiplot.

Weber, R.H., 1994, Pluvial lakes of the Plains of San Agustin, *in* Chamberlin, R.M., Kues, B.S., Cather, S.M., Barker, J.M., and McIntosh, W.C., eds., Mogollon Slope, west-central New Mexico—New Mexico Geological Society, 45th Annual Field Conference, Guidebook: Socorro, New Mexico, New Mexico Geological Society, p. 9–11.

Wickham, H., 2016, ggplot2—Elegant graphics for data analysis: New York, Springer-Verlag web page, accessed May 14, 2020, at https://ggplot2.tidyverse.org.

Appendixes 1–4

Appendix 1.   Compiled Water Level Data

Appendix 1 presents a table of water level data compiled from the U.S. Geological Survey (USGS) National Water Information System (USGS, 2021) on January 8, 2021, for the San Agustin Basin, west-central New Mexico; table 1.1 is available at https://doi.org/10.3133/sir20225029. The area considered for data compilation is limited to a rectangle defined by the following North American Datum of 1983 decimal degree coordinates: 34.4° N., −107.4° W.; 33.3° N., −108.6° W. All reported water quality data have a USGS water level approval status of "approved." Horizontal coordinates are relative to the North American Datum of 1983; elevations are relative to the North American Vertical Datum of 1988.

Reference Cited

U.S. Geological Survey [USGS], 2021, USGS water data for the Nation: U.S. Geological Survey National Water Information System database, accessed January 8, 2021, at https://doi.org/10.5066/F7P55KJN.

Appendix 2.   Chemistry Data Analyzed in This Study

Appendix 2 presents a table of U.S. Geological Survey (USGS) and New Mexico Bureau of Geology and Mineral Resources (NMBGMR) groundwater chemistry data measured in the San Agustin Basin, west-central New Mexico, from 2010 through 2019 that were analyzed in this report; table 2.1 is available at https://doi.org/10.3133/sir20225029. USGS-collected data were compiled from the USGS National Water Information System (USGS, 2020), whereas the NMBGMR provided data that they collected (Rinehart and others, 2017). Horizontal coordinates are relative to the North American Datum of 1983.

References Cited

Rinehart, A., Koning, D., and Timmons, S., 2017, Hydrogeology of the San Agustin Plains, *in* New Mexico Water Conference, 62d, Socorro, New Mexico, August 16, 2017: New Mexico Bureau of Geology and Mineral Resources, 36 p., accessed November 26, 2019, at https://geoinfo.nmt.edu/geoscience/research/documents/37/D2_07_Alex_Rinehart.pdf.

U.S. Geological Survey [USGS], 2020, USGS water data for the Nation: U.S. Geological Survey National Water Information System database, accessed January 9, 2020, at https://doi.org/10.5066/F7P55KJN.

Appendix 3.   Compiled Chemistry Data

Appendix 3 presents a table of chemistry data compiled from the U.S. Geological Survey (USGS) National Water Information System (USGS, 2020) on January 9, 2020, for the San Agustin Basin, west-central New Mexico; table 3.1 is available at https://doi.org/10.3133/sir20225029. Modifications were made to the aquifer codes of sites 335032108184501 and 340547107464401 on May 5, 2020. The area considered for data compilation is limited to a rectangle defined by the following North American Datum of 1983 decimal degree coordinates: 34.4° N., −107.4° W.;

33.3° N., −108.6° W. All reported water quality data have a USGS water level approval status of "approved." Horizontal coordinates are relative to the North American Datum of 1983.

Reference Cited

U.S. Geological Survey [USGS], 2020, USGS water data for the Nation: U.S. Geological Survey National Water Information System database, accessed January 9, 2020, at https://doi.org/10.5066/F7P55KJN.

Appendix 4.   Field Blank and Replicate Chemistry Data

Table 4.1.   Field blank sample results for site 11 in the San Agustin Basin, west-central New Mexico.

[Sample collected on April 2, 2019; site location shown on figure 4 in report. Analyzed data from the U.S. Geological Survey (USGS) National Water Information System (USGS, 2020). µg/L, microgram per liter; <, less than detection limit; mg/L, milligram per liter; SiO_2, silicon dioxide; µS/cm, microsiemens per centimeter]

Constituent	Unit	Value
Aluminum	µg/L	<3
Antimony	µg/L	<0.060
Arsenic	µg/L	<0.10
Barium	µg/L	<0.10
Beryllium	µg/L	<0.010
Boron	µg/L	<5
Bromide	mg/L	<0.010
Cadmium	µg/L	<0.030
Calcium	mg/L	<0.022
Chloride	mg/L	<0.02
Chromium	µg/L	<0.50
Cobalt	µg/L	0.045
Copper	µg/L	<0.40
Fluoride	mg/L	<0.01
Iron	µg/L	<10.0
Lead	µg/L	<0.020
Lithium	µg/L	<0.15
Magnesium	mg/L	<0.011
Manganese	µg/L	<0.40
Molybdenum	µg/L	<0.050
Nickel	µg/L	<0.20
Potassium	mg/L	<0.30
Selenium	µg/L	<0.05
Silica	mg/L as SiO_2	<0.050
Silver	µg/L	<1.00
Sodium	mg/L	<0.40
Specific conductance (lab)	µS/cm	<5
Strontium	µg/L	<0.50
Sulfate	mg/L	<0.02
Thallium	µg/L	<0.040
Uranium	µg/L	<0.030
Vanadium	µg/L	0.11
Zinc	µg/L	<2.0

Table 4.2.   Replicate sample results for site 11 in the San Agustin Basin, west-central New Mexico.

[Sample collected on April 2, 2019; site location shown on figure 4 in report. Analyzed data from the U.S. Geological Survey (USGS) National Water Information System (USGS, 2020). μS/cm, microsiemens per centimeter; mg/L, milligram per liter; $CaCO_3$, calcium carbonate; SiO_2; silicon dioxide; μg/L, microgram per liter; <, less than detection limit; C, results are consistent, but a difference cannot be calculated; pCi/L, picocurie per liter; R, reported tritium value is less than the reporting level; NA, not available because one value is censored; pM, absolute percent modern]

Constituent	Unit	Environmental value	Replicate value	Difference	Absolute relative percent difference
Specific conductance (lab)	μS/cm	287.90	287.91	0.01	0.0
pH (lab)	standard units	8.41	8.41	0	0.0
Alkalinity (lab), fixed endpoint	mg/L as $CaCO_3$	133.4	133.5	0.1	0.1
Alkalinity (field), inflection point	mg/L as $CaCO_3$	144.2	134.0	−10.2	7.3
Calcium	mg/L	19.28	19.50	0.22	1.1
Magnesium	mg/L	6.802	6.839	0.04	0.5
Sodium	mg/L	33.76	34.04	0.28	0.8
Potassium	mg/L	2.841	2.833	−0.008	0.3
Bromide	mg/L	0.0908	0.0904	−0.0004	0.4
Chloride	mg/L	7.141	7.110	−0.031	0.4
Sulfate	mg/L	5.905	5.885	−0.02	0.3
Fluoride	mg/L	0.614	0.620	0.006	1.0
Silica	mg/L as SiO_2	24.67	24.92	0.25	1.0
Arsenic	μg/L	1.9699	1.9794	0.0095	0.5
Barium	μg/L	2.0492	2.0668	0.0176	0.9
Beryllium	μg/L	<0.010	<0.010	C	C
Boron	μg/L	32.8021	32.4238	−0.3783	1.2
Cadmium	μg/L	<0.030	<0.030	C	C
Chromium	μg/L	5.471	5.183	−0.289	5.4
Cobalt	μg/L	<0.030	<0.030	C	C
Copper	μg/L	1.0297	1.0122	−0.0175	1.7
Iron	μg/L	<10.0	<10.0	C	C
Lead	μg/L	0.0673	0.0519	−0.0154	25.8
Manganese	μg/L	<0.40	<0.40	C	C
Thallium	μg/L	<0.040	<0.040	C	C
Molybdenum	μg/L	0.9451	0.9534	0.0083	0.9
Nickel	μg/L	<0.20	<0.20	C	C
Silver	μg/L	<1.00	<1.00	C	C
Strontium	μg/L	53.3517	53.8582	0.5065	0.9
Vanadium	μg/L	14.5720	14.3954	−0.1766	1.2
Zinc	μg/L	15.7591	16.1991	0.44	2.8
Antimony	μg/L	<0.060	<0.060	C	C
Aluminum	μg/L	<3	<3	C	C
Lithium	μg/L	11.1995	10.9401	−0.2594	2.3
Selenium	μg/L	1.0609	1.0631	0.0022	0.2
Tritium	pCi/L	0.29	R −0.04	NA	NA
Uranium	μg/L	1.8251	1.8175	−0.0076	0.4
Carbon-14	pM	45.60	45.67	0.07	0.2
Delta carbon-13/carbon 12	per mil	−10.80	−10.78	0.02	0.2
Delta hydrogen-2/hydrogen-1	per mil	−72.3	−73.4	−1.1	1.5
Delta oxygen-18/oxygen-16	per mil	−10.13	−10.12	0.01	0.1

Reference Cited

U.S. Geological Survey [USGS], 2020, USGS water data for the Nation: U.S. Geological Survey National Water Information System database, accessed January 9, 2020, at https://doi.org/10.5066/F7P55KJN.